

## ABSTRACT

CHEN, JUSTIN. A Model Long Acting Sentinel Gel for Early Management of Tumor Recurrence. (Under the direction of Yevgeny Brudno).

Tumor recurrence is a common problem in the clinical treatment of cancer and can cause further complications if not addressed promptly. Current methods mostly aim to prevent tumor recurrence through the complete eradication of the tumor in the initial treatment and do not seek to directly address the tumor recurrence event. The few studies that do directly address tumor recurrence suffer from non-specific release of the payload which is not ideal for a long-term device. Therefore, this dissertation seeks to demonstrate the feasibility of such a long-term device by using the prostate specific antigen (PSA) sensitive peptide amino acid sequence RSSYYSLC to create a model device capable of achieving tumor specific release. The peptide linker were used as pendant linkers to anchor Cyanine5.5 (Cy5) fluorescent molecule onto an alginate hydrogel and demonstrated good stability in vivo in normal mice. However, slow in vivo release was observed in mice bearing a PSA expressing tumor. The results do support the potential for a sentinel gel for long term monitoring of local tumor recurrence, but further work would need to be done to realize this goal.

A Model Long Acting Sentinel Gel for Early Management of Tumor Recurrence

by  
Justin Chen

A thesis submitted to the Graduate Faculty of  
North Carolina State University  
in partial fulfillment of the  
requirements for the Degree of  
Master of Science

Biomedical Engineering

Raleigh, North Carolina

2019

APPROVED BY:

---

Dr. Rahima Behabbour

---

Dr. Ashley Brown

---

Dr. Yevgeny Brudno  
Chair of Advisory Committee

## **BIOGRAPHY**

Justin Chen was born March 16, 1995 in Holmdel New Jersey where he stayed before heading to Rutgers University for his undergraduate degree. Growing up, he could not figure out what he wanted to do for a living, having even considered applying for Business School for his undergraduate studies. The only thing he knew was that he liked problem solving and thus, decided to join the Biomedical Engineering Department. While maintaining an interest in industry, he decided to apply for a PhD to experience the academic side of the field but got quickly overwhelmed by the open-endedness of academia. Today, Justin works as a research assistant working to finish with a Master's degree.

## ACKNOWLEDGEMENTS

I would like to give special thanks to my advisor, Dr. Yevgeny Brudno, for the support and care given to guide me despite my lack of experience. While I may not currently fully adhere to what he has taught me, I will always remember his lessons and slowly integrate them into my work in days to come.

Next, I would like to thank my advisory committee for taking time out of their busy schedule to serve on my committee.

I would like to thank John, my collaborator from the Menegatti Lab, for help in the peptide synthesis.

I would finally like to thank my lab mates for the helpful discussions and help in the lab. Particularly Chris who has extensively helped me with the alginate gels.

## TABLE OF CONTENTS

<b>List of Tables</b> .....	<b>vi</b>
<b>List of Figures</b> .....	<b>vii</b>
<b>Chapter 1: Introduction</b> .....	<b>1</b>
1.1. Recurrence Overview .....	1
1.2. Stimuli Responsive Materials.....	1
1.2.1. pH Responsive Materials.....	2
1.2.2. Redox Responsive Materials .....	4
1.2.3. Enzyme Responsive Materials .....	5
1.3. Peptides in Drug Delivery .....	7
1.4. Click Chemistry Based Hydrogels .....	10
1.5. Objectives.....	11
1.6. References .....	14
<b>Chapter 2: Materials and Methodology</b> .....	<b>25</b>
2.1. Materials.....	25
2.2. Methods .....	26
<b>Chapter 3: Preliminary Testing with Peptide</b> .....	<b>41</b>
3.1. Results/Discussion .....	41
3.2. References .....	60
<b>Chapter 4: Peptide + Alginate Analysis</b> .....	<b>61</b>
4.1. Results/Discussion .....	61
4.2. References .....	78
<b>Chapter 5: Conclusion</b> .....	<b>79</b>
5.1. Conclusion.....	79

<b>Appendices</b> .....	<b>81</b>
Appendix A: List of Abbreviations .....	82
Appendix B: Matlab Code for Comparison of Kinetics Between RSSYYSL and HSSKLQ.....	83

## LIST OF TABLES

<b>Table 1:</b> Expected mass fragments for the LCMS-MS Analysis of RSSYYLX and RSYYSLX .....	43
--	----

## LIST OF FIGURES

<b>Figure 1.2.3.1</b>	Image depicting peptide bond formation [43] .....	7
<b>Figure 1.2.4.1</b>	Graphical abstract of proposed device. Protease sensitive peptide linkers anchor the drug on to the azide-modified hydrogel, where activity of the targeted protease results in cleavage of the peptide to release the drug into the surrounding space .....	12
<b>Figure 3.1</b>	The chemical structure of the peptide RSSYYSLX. Cleavage of the peptide occurs between the tyrosine and serine as depicted by the dashed line .....	41
<b>Figure 3.2</b>	An HPLC Chromatogram of the 1 <sup>st</sup> synthesis attempt for RSSYYSLX depicting the purity of the sample after peptide synthesis. The blue, green, and red chromatograms are the measured signals at 210, 280, and 254 nm respectively. The peptide peak is the predominant peak with a retention time of 4.3 minutes.....	42
<b>Figure 3.3</b>	LCMS of the 1 <sup>st</sup> synthesis attempt for RSSYYSLX shows an unexpected mass at 881 m/z in the negative mode which corresponds to a serine deletion in the peptide sequence. ....	42
<b>Figure 3.4</b>	LCMS-MS data (measured by NCSU Mass Spectrometry Facility) showing cleavage fragments that correspond to both serine deletion possibilities (Table 1).....	44
<b>Figure 3.5</b>	HPLC chromatogram for the 2 <sup>nd</sup> synthesis attempt for RSSYYSLX before purification at 280 nm shows potential product peak at 7.3-minute retention time with a difficult to separate side product. ....	45
<b>Figure 3.6</b>	Chromatogram at 280 nm of the purification and fraction collection of crude RSSYYSLX on the preparatory HPLC using a peak based method at 280 nm for tyrosine detection. Peak at 8-minute retention time was collected. ....	45
<b>Figure 3.7</b>	LCMS of the 2 <sup>nd</sup> synthesis attempt for RSSYYSLX after Prep-HPLC purification shows the expected mass in the positive mode ( $969 + [H]^+$ ) confirming the peptide product. However, the 875 m/z suggests a RSSYYSL side product with no propargylglycine. Both ESI modes are shown where top is positive mode and bottom is negative mode. ....	46
<b>Figure 3.8</b>	HPLC chromatogram at 280 nm of the incubation of RSSYYSLX with 23.7 nM of PSA. Left chromatogram shows the stability of peptide in PBS while the right chromatogram depicts the cleavage over time with the addition of PSA in PBS.....	47
<b>Figure 3.9</b>	(Top) Schematic of the CuAAC reaction between FITC-azide and excess RSSYYSLX with TBTA in 4:1 DMSO:H <sub>2</sub> O with 12 mM ascorbate buffer.	

	(Bottom) HPLC analysis of the CuAAC reaction at 280 nm (left) and 450 nm (right) shows possible product with 8.3-minute retention time where the new peak shows up at both 280 nm and 450 nm while having a retention time between the FITC-azide and Peptide references.....	47
<b>Figure 3.10</b>	Chromatogram at 450 nm of the purification and fraction collection of the RSSYYSLX-FITC CuAAC reaction on the preparatory HPLC using a peak based method at 450 nm for FITC detection. Peak at 11.1-minute retention time was collected.....	48
<b>Figure 3.11</b>	LCMS after purification of the RSSYYSLX-FITC sample shows successful collection of the RSSYYSLX-FITC molecule in the negative mode (1427 – [H] <sup>+</sup> ). Both ESI modes are shown where top is the positive mode and bottom is the negative mode. ....	48
<b>Figure 3.12</b>	LCMS after purification of the RSSYYSLX-FITC sample shows a likely TBTA impurity in the positive mode (530 + [H] <sup>+</sup> ). Both ESI modes are shown where top is the positive mode and bottom is the negative mode.....	49
<b>Figure 3.13</b>	Representative Images of LNCaP (B) and Du145 (A) cell cultures .....	50
<b>Figure 3.14</b>	Schematic for the commercial fluorogenic PSA substrate. Cleavage of the aryl-amide bond by PSA releases free AFC which can be then detected through fluorescence in contrast to the weak and qualitatively different fluorescence in the intact HSKLQ-AFC molecule. ....	51
<b>Figure 3.15</b>	Incubation of HSKLQ-AFC with LNCaP shows increasingly high fluorescence measurements with respect to time, in contrast to that of the RPMI control, confirming PSA expression by LNCaP cells.....	51
<b>Figure 3.16</b>	Schematic for the Peptide Specificity Experiment. Cell culture media supernatant were collected and incubated with the peptide of interest at 37°C. Time points were stored at -80C and thawed together at room temperature after collection of the last time point. The sample was then acetone precipitated and the supernatant analyzed on analytical HPLC.....	52
<b>Figure 3.17</b>	HPLC chromatogram of the peptide specificity experiment shows that cleavage of RSSYYSLX-FITC occurs during incubation of RSSYYSLX-FITC with both LNCaP and Du145. The picture is zoomed in to the peak of interest at 280 nm and shows a decrease in the peptide peak (5.95-minute retention time) with an increase in signal of a side peak (6.17-minute retention time) over time, where the latter is likely a cleavage product.....	52
<b>Figure 3.18</b>	HPLC chromatogram of the peptide specificity experiment shows that cleavage of RSSYYSLX-FITC also occurs during incubation with RPMI cell culture media control. The picture is zoomed in on the peak of interest at 280 nm and shows a decrease in the peptide peak (5.95-minute retention	

	time) with an increase in signal of a side peak (6.17-minute retention time) over time, where the latter is likely a cleavage product.....	53
<b>Figure 3.19</b>	Incubation of RSSYYSLX peptide with no serum RPMI (left) shows no cleavage within 24 hours, whereas incubation with RPMI with FBS serum (right) shows significant cleavage of the peptide after 24 hours as seen by the decrease in the peak height with increasing time, thus confirming cleavage of RSSYYSLX by FBS containing RPMI. ....	53
<b>Figure 3.20</b>	HPLC chromatogram at 378 nm for the Peptide Specificity Experiment with HSSKLQ-AFC where incubation of the peptide fluorophore with LNCaP (PSA positive) shows cleavage with a decrease in the Peptide-AFC peak (right) and an increase in a new peak (left) with respect to time.....	55
<b>Figure 3.21</b>	HPLC chromatogram at 378 nm for the Peptide Specificity Experiment with HSSKLQ-AFC where incubation of the peptide fluorophore with Du145 (PSA negative) also shows cleavage with a decrease in the Peptide-AFC peak (right) and an increase in a new peak (left) with respect to time. ....	55
<b>Figure 3.22</b>	(Left) Chromatogram of the Peptide Specificity Experiment shows that incubation of serum containing RPMI with HSSKLQ-AFC results in cleavage of the peptide, similar to what was observed in the LNCaP and Du145 groups. (Right) Shows the comparison of the incubation of RSYYSLX between LNCaP and RPMI at the 73-hour time point. The comparison of chromatograms suggests comparable extent of cleavage where the suspected AFC peak for RPMI + Peptide-AFC has a comparable peak height to that of the LNCaP + Peptide-AFC. ....	56
<b>Figure 3.23</b>	HPLC chromatogram of AFC at 378 nm before (red) and after (blue) acetone precipitation suggests that significant amount of AFC is lost during the precipitation process. ....	57
<b>Figure 3.24</b>	Comparison of the trends in signal between AFC standard, Suspected AFC peak, and Uncleaved Peptide-AFC show that the trend in signal is similar between the Suspected AFC peak and the Uncleaved Peptide-AFC (338 nm > 378 nm signal) but different from the AFC standard (378 nm > 337 nm signal).....	58
<b>Figure 3.25</b>	Comparison of kinetics between RSSYYSL [4] and HSSKLQ [5] using simple Michaelis-Menten kinetics and literature reported kinetic parameters shows that RSSYYSL is cleaved significantly faster than HSSKLQ at 45 nM of PSA. Matlab code found in Appendix B. ....	59
<b>Figure 4.1</b>	Synthesis plan for DBCO-RSSYYSLX-Cy7. CuAAC will be first used to conjugate the sCy7 while on the other side, the N-terminus will be conjugated with DBCO using NHS chemistry. ....	61

<b>Figure 4.2</b>	LCMS of the RSSYYSLX-Cy7 after preparatory HPLC purification shows successful collection of my molecule in both positive (1013 m/z) and negative (1011 m/z) modes. Both ESI modes are shown in the LCMS where top is the positive mode and the bottom is the negative mode. ....62
<b>Figure 4.3</b>	LCMS analysis of the DBCO-RSSYYSLX-Cy7 reaction shows a small peak of the expected product mass in the negative mode with a slight deviation (DBCO-RSSYYSLX-Cy7 M/2 = 1169.435). Both ESI modes are shown in the LCMS where top is the positive mode and the bottom is the negative mode.....62
<b>Figure 4.4</b>	Strategy for the synthesis of DBCO-RSSYYSLC-sCy5. Thiol-Maleimide chemistry will be first used to attach sCy5 onto the C-terminal end while the N-terminal amine will be conjugated to DBCO using NHS chemistry. ....63
<b>Figure 4.5</b>	Chromatogram of the purification and fraction collection of DBCO-RSSYYSLC-sCy5 using preparatory HPLC using a peak based method at 648 nm. The peak with 11-minute retention time was collected. ....64
<b>Figure 4.6</b>	LCMS analysis of DPC after purification shows successful collection and relative purity of the molecule in both the positive and negative mode. Both ESI modes are shown in the LCMS where top is the positive mode and the bottom is the negative mode. ....64
<b>Figure 4.7</b>	Solubility for DPC measured at PBS:DMSO (9:1) using a method based on the shake flask method yielded a solubility of 51.04 $\mu$ M .....65
<b>Figure 4.8</b>	Schematic of the modification of alginate with azide-amine through EDC/NHS chemistry by targeting the carboxylic acid groups on the alginate strands. ....66
<b>Figure 4.9</b>	Schematic for the Peptide Specificity Experiment with crosslinked DPC preloaded alginate hydrogel. Cell culture media supernatant were collected and incubated with the crosslinked DPC preloaded alginate hydrogel at 37°C. The supernatant was collected at time points and were stored at -80C. Samples were thawed together at room temperature after collection of the last time point, whereupon the sample was precipitated with DMSO and the fluorescence of the supernatant measured on the micro well plate reader. ....66
<b>Figure 4.10</b>	Peptide Specificity Experiment results with preloaded calcium crosslinked hydrogels show significant cleavage by LNCaP cell culture supernatant during incubation with the preloaded hydrogels. The difference between Du145 and LNCaP groups were statistically significant ( $p \ll 0.05$ ). The difference between Du145 and RPMI was also statistically significant ( $p \ll 0.05$ ), suggesting that the Du145 is cleaving the peptide linkers to release Cy5, albeit at a much slower rate compared to LNCaP. ....67
<b>Figure 4.11</b>	Schematic for the measurement of the loading efficiency. Alginate was loaded onto the alginate strands for 24 hours before DMSO precipitation and

	subsequent analysis of the fluorescence in the supernatant. The calculated value was subtracted from the added amount to calculate the amount of DPC loaded onto the alginate. ....	68
<b>Figure 4.12</b>	Summary of the loading efficiency measurements show about 60% loading efficiency at different concentrations. The control unmodified alginate measured about 3% loading efficiency which was deemed insignificant. Error bars represent the standard deviation of the samples.....	68
<b>Figure 4.13</b>	Fluorescent measurements for the In vivo stability experiment with preloaded calcium crosslinked gels (n=2). Alginate were preloaded with DPC for 24 hours before crosslinking with calcium followed by subcutaneous injection into the subcutaneous space in male CD1 mice. The fluorescence measurement results show instability of the device in vivo for both DPC and DCy5 preloaded gels.....	69
<b>Figure 4.14</b>	Schematic for T-BCN crosslinking of azide-modified alginate strands to create a hydrogel.....	70
<b>Figure 4.15</b>	Chromatogram at 210 nm for the preparatory HPLC purification and fraction collection of T-BCN using a peak based method at 210 nm. Peak with 10.9-minute retention time was collected. ....	71
<b>Figure 4.16</b>	LCMS of the preparatory HPLC purified T-BCN shows successful collection of the product with detection of 1222 m/z in the positive mode ( $1221 + [H]^+$ m/z). Both ESI modes are shown in the LCMS where top is the positive mode and the bottom is the negative mode.....	71
<b>Figure 4.17</b>	In vivo stability experiment repeated with preloaded T-BCN crosslinked alginate gels (n=2). Alginate gels were preloaded with DPC for 24 hours before crosslinking with T-BCN for 30 minutes, followed by subcutaneous injection into male CD1 mice. The fluorescence measurements show higher stability with both DPC and DCy5 compared to that of the calcium crosslinked counterpart. ....	72
<b>Figure 4.18</b>	Peptide Specificity Experiment results with DPC preloaded T-BCN crosslinked alginate gels. DPC preloaded gels were crosslinked with T-BCN overnight before addition of cell culture media. Fluorescence measurements of the supernatant show inconclusive results that were very different from the calcium crosslinked version (Figure 4.10).....	73
<b>Figure 4.19</b>	Michaelis Menten Kinetics Equation. With the assumption that $K_m \gg [S]$ , we can easily measure $k_{cat}/K_m$ .....	75
<b>Figure 4.20</b>	Result from the kinetics experiment after 7 hours reaction of the DPC preloaded T-BCN crosslinked alginate gel. The fluorescence of the supernatant was measured and the reaction velocity (mol/s) was calculated	

using a standard curve. The slope was used to calculate a  $k_{cat}/K_m$  value of  $160 \text{ s}^{-1}\text{M}^{-1}$  .....75

**Figure 4.21** Result from In Vivo Tumor Experiment with DPC preloaded T-BCN crosslinked alginate gels (n=2). Alginate gels were preloaded with DPC for 24 hours before 30 minutes of T-BCN crosslinking followed by co-injection of the gel and the LNCaP tumor cells in Matrigel (3 million cells). The preliminary results suggest increased reduction in signal by the PSA (+) LNCaP tumor starting at around 15 days. Calculated p-value = 0.0558 at the last time point. The error bars are standard error mean. ....76

**Figure 4.22** Results from the LNCaP Tumor + Depot Experiment (n=3). Alginate were preloaded with DPC or DCy5 for 24 hours before 30-minute crosslinking with T-BCN. The gel was then injected subcutaneously with either Matrigel or the LNCaP tumor cell mixture (3 million cells). The resulting measurements show inconclusive results (pvalue = 0.1568 at Day 30 between DPC + LNCaP and DPC + Matrigel) with large variability within the tumor containing groups. The error bars are standard error mean. ....77

## **Chapter 1: Introduction**

### **1.1. Tumor Recurrence**

Tumor recurrence refers to the reappearance of a tumor following treatment, predominantly due to the inability to fully eliminate the tumor. Tumors can generally recur locally around the original tumor location or at a distant metastatic site. Generally, distant recurrence has a worse prognostic outlook compared to that of local recurrence due to the implication of a higher stage, metastatic tumor. Local recurrence events have mixed prognosis depending on the cancer type. Some cancer types, such as breast cancer [1], hepatocellular carcinoma [2,3], or osteosarcoma [4] have been found to have no link between local recurrence events and the prognosis. However, other cancer types including melanoma [5], soft tissue sarcoma [6,7], and colorectal cancer [8], have been reported to be linked with poor prognosis. Generally, local recurrence causes complications in the treatment of cancer and is associated with decreasing survival rates due to the clinical progression of cancer. Therefore, it is important to detect and manage local recurrence early before the survival rate decreases through clinical progression of the tumor. In that regard, it would be ideal to have a stimuli responsive device that can sit and wait for long periods of time before reacting to the reappearance of a tumor.

### **1.2. Stimuli Responsive Materials**

Stimuli responsive biomaterials are materials that can respond to changes in the environment through a conformational or chemical change. Inefficient drug release is a large barrier in systemic routes of administration and can be solved using stimuli responsive modes of release to selectively target the diseased site. In terms of cancer, stimuli responsive materials

have allowed us to deliver drugs to the tumor with higher specificity [9]. There are many different modes of release within the stimuli responsive materials field [10]. However, for controlled release with endogenous stimuli in cancer applications, pH, redox, and enzymes are often used [11].

### **1.2.1. pH-Responsive Materials**

pH-sensitive materials have attracted interest due to the acidic environment present in both the endosome (pH 4.5-6.5) following endocytosis, as well the tumor microenvironment (pH ~6.7-7.1) [12], maintained through a combination of H<sup>+</sup> efflux [13], carbonic anhydrase [14], and the Warburg effect [15]. With reference to a normal physiological pH of ~7.4 in the extracellular space, one can use pH-responsive materials to selectively achieve release in either the endosome or the tumor microenvironment. There are typically two types of mechanisms in pH-responsive release: acid-labile linkers and ionization. Acid-labile linkers have been used extensively in drug delivery to achieve controlled release [16]. In systemic delivery, acid-labile linkers are often used to conjugate the drug to the vehicle, resulting in drug release upon reaching the target acidic environment. Etrych et al. have demonstrated such a mechanism using N-(2-hydroxypropyl)methacrylamide (HPMA) copolymers as a carrier for doxorubicin (Dox) by attaching the drug to the polymer backbone, using a stable oligopeptide spacer together with a pH-sensitive hydrazide linker [17]. The resulting HPMA-Dox drug conjugate demonstrated up to 85% release in 48 hours at pH 5 compared to ~8% release at pH 7 and showed promising results in vivo in an EL4 T-lymphoma model. Acid-labile linkers can also be used to decompose the drug vehicle, exposing the payload to the target environment. For example, Poon et al. has used the pH-dependent iminobiotin-neutravidin to hold together a poly-L-lysine (PLL) and polyethylene glycol (PEG) based carrier [18]. Upon interaction with the tumor in the

extracellular space, the PEG layer is released through the cleavage of the iminobiotin-neutravidin bond, resulting in a PLL-coated nanoparticle where the PLL helps enhance uptake of the nanoparticle into the tumor cell. Using the MDA-MB-435 tumor model, the authors showed that the iminobiotin-neutravidin carrier resulted in a much higher cellular uptake in tumor cells compared to that of the pH-insensitive biotin-neutravidin control. Acid-labile linkers have also shown use in hydrogels for treatment of tumors. Li et al. used polyaspartylhydrazide hydrogel containing pH-sensitive acylhydrazone linkers to release Dox through the degradation of the hydrogel [19]. These hydrogels were shown to release ~42% of the loaded Dox at pH 6.0 and showed significant increase in tumor growth suppression compared to that of the free Dox control in a fibrosarcoma model.

pH-responsive release can also be achieved through ionization of charged functional groups, causing an electrostatic repulsion between the groups to destabilize the drug vehicle. Liang et al. has used such a system to create pH-responsive micelles, self-assembled by amphiphilic peptides to release Dox in the endosomal compartment [20]. The peptide carries a lysine group which, upon ionization at low pH, results in disassembly of the micelles via electrostatic repulsion. While hydrogels can also exhibit such a mode of release [21, 22, 23], not much work has been translated to in vivo due to their restriction to the extracellular space. Indeed, targeting aimed at the extracellular pH of tumors is generally a difficult task due to the narrow pH range (6.7-7.4) and has therefore not been extensively utilized. Much work related to this strategy have seen some success in vitro [24, 25, 26], but few if any work has been successfully translated in vivo. Difficulties imposed by the narrow pH range result in high non-specific release in extracellular pH-mediated release, with ~20% release after 48 hours at

physiological pH being one of the more successful attempts [19]. Thus, the current state of extracellular pH-responsive strategies isn't suitable for single dosage long term therapies.

### **1.2.2. Redox-Responsive Materials**

Redox reactions are oxidation-reduction reactions that involve the transfer of electrons between two species. This interaction is often used in drug delivery due to the uniquely reductive environment in tumor cells. Many types of tumors overexpress glutathione, which promotes proliferation and provides protection from oxidative stress [27]. Thus, as a reducing agent, glutathione creates a much more reductive environment in cancer cells compared to that of normal cells allowing for selective release in tumor cells. Low off target toxicity with this strategy can be achieved due to the difference in extracellular (2-20  $\mu\text{M}$ ) and intracellular (10  $\text{mM}$ ) concentrations of glutathione in normal tissues, as well as the fact that intracellular concentrations of glutathione in tumors are at least 4-fold higher than that of normal cells [28]. Most redox responsive materials in cancer therapy revolve around glutathione cleaving a redox-sensitive bond to release the drug. The most common redox-sensitive moiety used in these systems is the disulfide bond. For example, Yin et al. used hyaluronic acid-Paclitaxel drug conjugate directly linked through a disulfide bond to create micelles that showed significant in vivo tumor reduction in hepatic carcinoma cells [29]. Disulfide bonds have been similarly used to crosslink the drug carrier to achieve glutathione-mediated disassembly of the carrier to release drug. Shi et al. showed such a system with star-shaped micelles self-assembled from a 4-arm poly( $\epsilon$ -caprolactone)-poly(ethylene glycol) copolymer with folic acid ends for active tumor targeting to show significant tumor suppression results in vivo on 4T1 tumor bearing mice [30]. Hydrophilic and hydrophobic segments were connected using disulfide bonds, whereupon cleavage by glutathione resulted in the disassembly of the micelle to release the encapsulated

Dox. Besides disulfide bonds, diselenide bonds have also been explored with a potentially more sensitive redox response, but this strategy is limited by low solubility and stability during synthesis [31, 32]. While these drug delivery systems show great promise, they are limited to the intracellular space and are unlikely to find use in the extracellular space without additional functional moieties.

### **1.2.3. Enzyme-Responsive Materials**

Proteases are the main area of research within the class of enzyme-mediated release with other enzymes either lacking investigation or having mixed in vivo results [33,34]. Proteases are enzymes that catalyze the hydrolysis of proteins into smaller fragments. They are involved with a wide variety of physiological processes and are often dysregulated in a wide variety of diseases, including cancer. The disruption of the existing balance of the protease expression and activity can result in an abnormal increase or decrease on protease function and activity. Abnormally enhanced protease activity can be exploited to achieve release specific to the disease causing this abnormality.

Many such proteases have been explored for use in cancer drug delivery including matrix metalloproteinase (MMP), PSA, and Cathepsins being the more popular targets. Indeed, these proteases have many publications dedicated on elucidating substrate recognition by these proteases [35, 36, 37]. Thus, much work has been done in the field to explore their potential against cancer. Many different peptide substrates have been used to achieve protease-responsive release to target cancer with a wide variety of protease targets. Chau and coworkers have conjugated dextran and methotrexate onto the peptide amino acid sequence PVGLIG to target tumors from systemic circulation through MMP-mediated cleavage of the peptide, releasing the methotrexate drug [38]. Similarly, Schmid et al. used a repeating peptide amino acid sequence of

ALAL to create an albumin-binding prodrug that releases either Dox or camptothecin in the presence of Cathepsin B [39]. A lot of similar work have been done with a focus on systemic administration of the molecule [40], but while there have been quite a few studies done with hydrogels, not many of them are able to translate to in vivo. This is in large part due to the poor long-term sustainability or stability of the device due to nonspecific release. For example, Tauro et al. used the MMP-sensitive sequence CGLDD to complex cisplatin onto poly(ethylene glycol) diacrylate hydrogel wafers. However, the in vitro release of cisplatin in presence of MMP-2 was comparable to the release in absence of MMP at about 70% and 60% release respectively [41]. Similarly, Wade et al. has introduced protease-degradable electrospun nanofibers that degrade in response to MMP-2 [42]. In vivo hydrogel degradation was measured by covalently conjugating Cyanine7.5 dye onto the polymer. The results in absence of MMP-2 showed about 65% signal after 6 weeks with the decrease in signal seemingly accelerating as time goes on. Hence, passive release in the absence of the target protease is one of the greatest challenges in achieving tumor-specific release through proteases. The biological environment contains many nonspecific-proteases that can cause unintended degradation of the peptide sequence, resulting in passive release in absence of the tumor. Most studies choose to avoid addressing this issue due to the short-term nature of their device but for a long-term device to remain stable for months, this issue is unavoidable.

### 1.3. Peptides in Drug Delivery

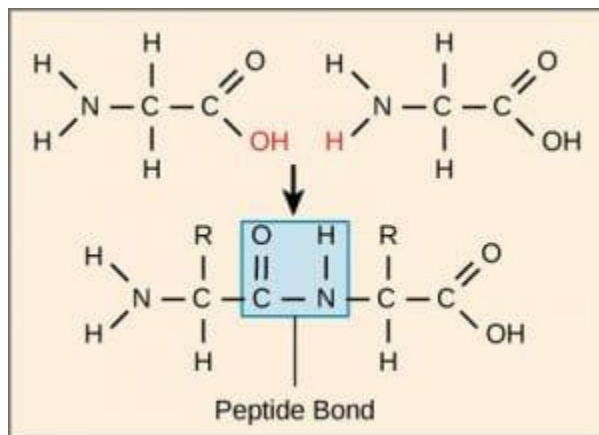


Figure 1.2.3.1: Image depicting peptide bond formation. [43]

Peptides are short chains of amino acids linked together by peptide bonds. The peptide bond is formed via dehydration reaction between a carboxyl group and amino group from the adjacent amino acid. Peptide notation is generally read from left to right with the left most amino acid representing the N-terminus containing an amino group, and the right most amino acid containing a carboxylic acid group known as the C-terminus. The specific amino acids in the chain determine the functional groups present on the peptide which is the main determinant of the peptide's properties. Peptides differ from proteins based on size where peptides are typically considered proteins when there are more than 50 amino acids present in the sequence.

Peptides are a major building block of nature and are associated with a large variety of biological processes. Different functions include hormones, antimicrobial agents, growth factors, and structural building blocks. With a wide variety of possibilities, peptides have been extensively used in drug delivery. In general, peptides have high efficacy, are safe, and easy to synthesize. However, peptides have major difficulties with in vivo stability with short half-lives and degradation by proteases. In fact, due to these difficulties, naturally occurring peptides are rarely suitable for use in drug delivery [44]. Peptides also have the tendency to aggregate mainly

due to long stretches of hydrophobic amino acids in the peptide sequence [45]. Hence, careful design is needed for successful application of peptides in drug delivery. Nevertheless, peptides have found a wide variety of use as therapeutics [45].

Antimicrobial peptides are an important part of the innate immune system [46] involved with direct killing of bacteria through lysis of the bacterial membrane or through modulation of the immune response. Antimicrobial peptides have seen a wide variety of use as therapeutics due to their cytotoxic action against both gram-negative [47] and gram-positive bacteria [48]. Peptides have also been used as antagonists which effectively inhibit the function of a receptor by occupying the receptor binding space. One well known example is CTCE-9908 which is a clinically approved peptide that acts as an antagonist by competitively binding CXCR4 which results in tumor size reduction [49]. Carfilzomib (Kyprolis) is another clinically approved peptide therapeutic for the treatment of multiple myeloma. Carfilzomib delays proliferation and induces apoptosis in tumors through the binding and irreversible inhibition of the 20S and 26S proteasome [50]. On the other hand, peptide therapeutics have also seen use as agonists as shown by Pasireotide (Signifor), a clinically approved somatostatin receptor agonist which binds to activate the somatostatin receptor to inhibit secretion of corticotropin in Cushing's disease [51]. Overall, peptide therapeutics have found successful use in a wide variety of applications and show much promise.

In addition to therapeutics, peptides have also found further use as auxiliary materials to aid in drug delivery. Amphiphilic peptides can self-assemble into micelles which have been used extensively in vaccine delivery due to their ability to activate an immune response [52]. Peptides have also been used to self-assemble into hydrogels for use as a drug depot [53] or scaffold in regenerative medicine [54]. Peptide-based hydrogels have advantages in their synthetic nature;

minimizing risk of carrying biological pathogens in contrast to animal-derived materials, as well as the ability to control the interactions inside the hydrogel, through modification of the peptide sequence and functional groups [55]. Besides being used as vehicles, peptides have also found prominent use as a targeting modality. For example, peptide substrates have been used to design protease-responsive prodrugs [39] and hydrogels [41] with varying degrees of success. Peptides have also been used to target receptors on the cell membrane. One prominent example is the use of the Arg-Gly-Asp (RGD) peptide amino acid sequence to target  $\alpha_v\beta_3$  integrin which is an adhesion receptor expressed by multiple types of cancer cells. For example, Janssen et al. used radiolabeled dimeric cyclic RGDfK and showed increased tumor suppression compared to that of the scrambled RGKfD, suggesting an enhanced efficacy as a result of the better tumor targeting from RGD [56]. Peptides have also been used to bind other structures associated with tumors to enhance tumor targeting. For example, Chung et al. attached the fibrin binding peptide amino acid sequence Cys-Arg-Glu-Lys-Ala (CREKA) to Cyanine7-labeled micelles to target fibrin deposition in glioblastoma. Micelles with CREKA resulted in 3-4 fold higher signal compared to that of micelles without, demonstrating increased retention with the addition of the peptide sequence [57]. In addition to targeting, peptides have been used to facilitate entry of therapeutics into cells. One such example is cell penetrating peptides, which are short peptide sequences that can penetrate the cell membrane without the help of receptors, with little damage sustained by the cell membrane. In doing so, they can be used to effectively transport electrostatically or covalently bound macromolecules across the cellular membrane [58]. There are many studies that utilize this strategy to help ferry across drugs in drug resistant tumors [59] or hydrophilic molecules that have trouble crossing the cell membrane [60]. In conclusion, peptides are a hot

topic with extensive application in the drug delivery field due to their flexible properties and high potential.

#### **1.4. Click Chemistry based Hydrogels**

Hydrogels are a macromolecular network of crosslinked polymer chains that can retain a significant fraction of water. The crosslinking between the polymers allow the hydrogel to not dissolve in water while the hydrophilic groups located in the polymer network allow the hydrogel to retain water. Hydrogels are a large class of materials, containing many different types from natural to synthetic. Of these hydrogels, click chemistry-based hydrogels is a rapidly growing field [61]. Click chemistry is a concept introduced by Sharpless et al. [62] describing fast, specific, high yielding reactions. These reactions have been applied to hydrogels to synthesize a wide variety of new synthetic hydrogel materials. There have been various of cases reporting the synthesis of new hydrogels via click chemistry as a mediator for crosslinking [63, 64, 65]. Of significant interest is the application towards functionalization of hydrogels. For example, He et al. used copper catalyzed click chemistry to attach azide modified bone morphogenetic protein (BMP) onto the propargyl groups on the hydrogel, while RGD was attached through a reaction between acrylamide and fumarate [66]. Moreover, the introduction of strain promoted azide-alkyne cycloaddition (SPAAC) allowed for more possibilities, particularly with in vivo applications. SPAAC describes the spontaneous reaction between an azide and a strained alkyne to form a stable triazole ring. Brudno et al. utilized this reaction to capture systemically circulating prodrugs using an azide-modified alginate hydrogel [67]. This interaction enabled successful refill of the alginate drug depot through a systemic injection,

whereupon the drugs are slowly released in the surrounding space. Altogether, the ease of functionalization, high specificity, and quick yields opens a plethora of possibilities for this click chemistry-based hydrogels.

## **1.5. Objectives**

There are currently few attempts being made to specifically address tumor recurrence. Due to the generality of tumor recurrence events, most studies choose to indirectly address tumor recurrence through a more effective therapy aimed towards fully eliminating the tumor with the initial treatment. Indeed, since tumor recurrence is a result of a partially ineffective treatment, most strategies focus on fully eradicating the tumor in one go with prevention of tumor recurrence as a consequential result. While there are many papers that focus on reducing tumor recurrence, the strategy they employ is to essentially fully eliminate the tumor without targeting the recurrence event itself as previously mentioned. For example, Zhang and coworkers used a cisplatin-loaded, multilayered polylactide electrospun nanofibers for prolonged cisplatin release applied after surgical resection [68]. While they successfully reduced the number of recurrence events, it is hard to say that their strategy directly addressed recurrence as it focused on using ubiquitous release of cisplatin from the implant to help enhance tumor death; reduced tumor recurrence was simply a consequential event. Indeed, there are many similar papers that reduce recurrence through more effective therapies but do not look at the recurrence event itself [69,70,71]. In order to directly target a recurrence event, one would need to use stimuli responsive class of materials that can respond selectively to the presence of a tumor. A material with tumor specific release would allow one to achieve functionality over longer periods of time, increased cytotoxic potential, less side effects, and the possibility for a diagnostic towards early

detection of recurrence. There has been much work done in the stimuli responsive biomaterials field, of which, pH [72], enzyme [73], and redox activity [74] have been commonly used to achieve varying degrees of tumor specific release through endogenous stimuli. However, there have been few, if any, report of a material that is highly sensitive to tumors with negligible release over a period of months.

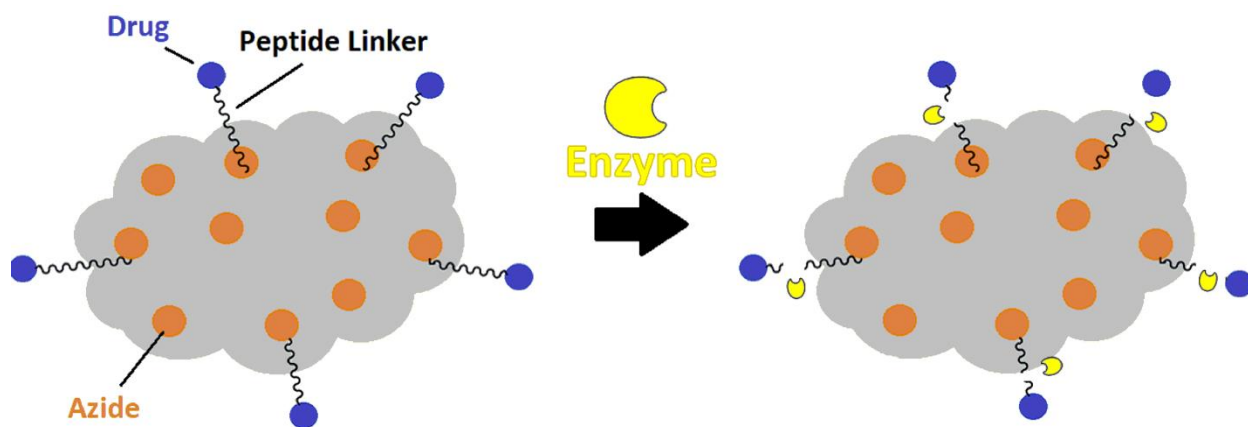


**Figure 1.2.4.1:** Graphical abstract of proposed device. Protease sensitive peptide linkers anchor the drug on to the azide-modified hydrogel, where activity of the targeted protease results in cleavage of the peptide to release the drug into the surrounding space.

My goal is to create a sentinel gel that will quietly wait at the tumor resection site for local tumor recurrence which, when detected, will result in the release of its cargo. Such a long-term device would require high stability, high sensitivity, and high selectivity, with release only in presence of a tumor. Hence, I aim to create a proof of concept to show the possibility of such a device. I have chosen to use protease to mediate the tumor-responsive release. Protease-mediated release is a very popular field with a large assortment of literature and extracellular targets to choose from. A significant advantage in working with proteases lies in the relative ease of synthesis of the peptide substrates. The peptide synthesis process has been streamlined and with equipment like automated peptide synthesizers, the process has become much cheaper and faster. With proper site selection for modification, peptide molecules can also be easily customizable without compromising the peptide's functionality. Of the available proteases, I have chosen to

work with PSA which is a serine protease that breaks down proteins in the seminal coagulum and is often overexpressed in cancer. The protease itself has been extensively researched with studies assessing substrate specificity patterns [39] and 3d models being simulated [75]. One study used the heptapeptide amino acid sequence Arg-Ser-Ser-Tyr-Tyr-Ser-Leu (RSSYYSL) attached to Dox through a self-immolative linker to create prodrugs that achieved rapid release of active Dox in the presence of PSA [76]. Notably, the sequence seemed to show high specificity towards PSA, where incubation of the peptide with Du145, a non-PSA expressing cell line, resulted in no significant cleavage on the high-performance liquid chromatography (HPLC) chromatogram. Thus, I have chosen to use this peptide sequence and will combine it with a hydrogel to make my device. Click chemistry-based hydrogels have shown easy and flexible modification of hydrogels using SPAAC to attach functional groups onto the hydrogel. This design not only allows for easy incorporation of multiple active agents but also allows one to easily switch peptide sequences, without a need for drastic change in protocol. Of note, the resulting triazole bond is also very inert which helps limit nonspecific release [77]. In previous work, Brudno et al. has shown such a system with the use of azide-functionalized alginate hydrogels [67]. This work aims to adapt this design with the addition of the PSA sensitive RSSYYSL sequence attached to the hydrogel as pendant chains to anchor the active agent. Altogether, the goal of this dissertation is to develop a device that can remain stable for months in vivo but also demonstrate fast release in presence of a tumor.

## 1.6. References

- 1) Kyndi, M., Overgaard, M., Nielsen, H. M., Sørensen, F. B., Knudsen, H., & Overgaard, J. (2009). High local recurrence risk is not associated with large survival reduction after postmastectomy radiotherapy in high-risk breast cancer: A subgroup analysis of DBCG 82 b&c. *Radiotherapy and Oncology*, 90(1), 74-79. doi:10.1016/j.radonc.2008.04.014
- 2) Lam, V. W., Ng, K. K., Chok, K. S., Cheung, T., Yuen, J., Tung, H., . . . Poon, R. T. (2008). Risk Factors and Prognostic Factors of Local Recurrence after Radiofrequency Ablation of Hepatocellular Carcinoma. *Journal of the American College of Surgeons*, 207(1), 20-29. doi:10.1016/j.jamcollsurg.2008.01.020
- 3) Liang, P., Dong, B., Yu, X., Yu, D., Wang, Y., Feng, L., & Xiao, Q. (2005). Prognostic Factors for Survival in Patients with Hepatocellular Carcinoma after Percutaneous Microwave Ablation. *Radiology*, 235(1), 299-307. doi:10.1148/radiol.2351031944
- 4) Kong, C., Song, W. S., Cho, W. H., Oh, J. M., & Jeon, D. (2011). Local Recurrence has only a Small Effect on Survival in High-risk Extremity Osteosarcoma. *Clinical Orthopaedics and Related Research®*, 470(5), 1482-1490. doi:10.1007/s11999-011-2137-y
- 5) Dong, X. D., Tyler, D., Johnson, J. L., Dematos, P., & Seigler, H. F. (2000). Analysis of prognosis and disease progression after local recurrence of melanoma. *Cancer*, 88(5), 1063-1071. doi:10.1002/(sici)1097-0142(20000301)88:53.0.co;2-e
- 6) Lewis, J. J., Leung, D., Heslin, M., Woodruff, J. M., & Brennan, M. F. (1997). Association of local recurrence with subsequent survival in extremity soft tissue sarcoma. *Journal of Clinical Oncology*, 15(2), 646-652. doi:10.1200/jco.1997.15.2.646

- 7) Emrich, L. J., Ruka, W., Driscoll, D. L., & Karakousis, C. P. (1989). The effect of local recurrence on survival time in adult high-grade soft tissue sarcomas. *Journal of Clinical Epidemiology*, 42(2), 105-110. doi:10.1016/0895-4356(89)90083-8
- 8) Ryuk, J. P., Choi, G., Park, J. S., Kim, H. J., Park, S. Y., Yoon, G. S., . . . Kwon, Y. C. (2014). Predictive factors and the prognosis of recurrence of colorectal cancer within 2 years after curative resection. *Annals of Surgical Treatment and Research*, 86(3), 143. doi:10.4174/astr.2014.86.3.143
- 9) Macewan, S. R., Callahan, D. J., & Chilkoti, A. (2010). Stimulus-responsive macromolecules and nanoparticles for cancer drug delivery. *Nanomedicine*, 5(5), 793-806. doi:10.2217/nnm.10.50
- 10) Roy, D., Cambre, J. N., & Sumerlin, B. S. (2010). Future perspectives and recent advances in stimuli-responsive materials. *Progress in Polymer Science*, 35(1-2), 278-301. doi:10.1016/j.progpolymsci.2009.10.008
- 11) Mura, S., Nicolas, J., & Couvreur, P. (2013). Stimuli-responsive nanocarriers for drug delivery. *Nature Materials*. Doi:<https://doi-org.prox.lib.ncsu.edu/10.1038/nmat3776>
- 12) Gallagher, F. A., Kettunen, M. I., Day, S. E., Hu, D., Ardenkjær-Larsen, J. H., Zandt, R. I., . . . Brindle, K. M. (2008). Magnetic resonance imaging of pH in vivo using hyperpolarized <sup>13</sup>C-labelled bicarbonate. *Nature*, 453(7197), 940-943. doi:10.1038/nature07017
- 13) Sennoune, S. R., Luo, D., & Martínez-Zaguilán, R. (2004). Plasmalemmal Vacuolar-Type H<sup>+</sup>-ATPase in Cancer Biology. *Cell Biochemistry and Biophysics*, 40(2), 185-206. doi:10.1385/cbb:40:2:185

- 14) Wykoff, C. C., Beasley, N. J., Watson, P. H., Turner, K. J., Pastorek, J., Sibtain, A., . . . Harris, A. L. (2000). Hypoxia-inducible Expression of Tumor-associated Carbonic Anhydrases. *Tumor Biology*, 60(24).
- 15) Alfarouk, K. O., Verduzco, D., Rauch, C., Muddathir, A. K., Bashir, A. H., Elhassan, G. O., . . . Harguindey, S. (2014). Glycolysis, tumor metabolism, cancer growth and dissemination. A new pH-based etiopathogenic perspective and therapeutic approach to an old cancer question. *Oncoscience*, 1, 777. doi:10.18632/oncoscience.109
- 16) Gao, W., Chan, J., & Farokhzad, O. C. (2010). PH-responsive Nanoparticles for Drug Delivery. *Molecular Pharmaceutics*. doi:10.1021/mp100253e
- 17) Etrych, T., Jelínková, M., Říhová, B., & Ulbrich, K. (2001). New HPMA copolymers containing doxorubicin bound via pH-sensitive linkage: Synthesis and preliminary in vitro and in vivo biological properties. *Journal of Controlled Release*, 73(1), 89-102. doi:10.1016/s0168-3659(01)00281-4
- 18) Poon, Z., Chang, D., Zhao, X., & Hammond, P. T. (2011). Layer-by-Layer Nanoparticles with a pH-Sheddable Layer for in Vivo Targeting of Tumor Hypoxia. *ACS Nano*, 5(6), 4284-4292. doi:10.1021/nn200876f
- 19) Li, L., Gu, J., Zhang, J., Xie, Z., Lu, Y., Shen, L., . . . Wang, Y. (2015). Injectable and Biodegradable pH-Responsive Hydrogels for Localized and Sustained Treatment of Human Fibrosarcoma. *ACS Applied Materials & Interfaces*, 7(15), 8033-8040. doi:10.1021/acsami.5b00389
- 20) Liang, J., Wu, W., Xu, X., Zhuo, R., & Zhang, X. (2014). PH Responsive micelle self-assembled from a new amphiphilic peptide as anti-tumor drug carrier. *Colloids and Surfaces B: Biointerfaces*, 114, 398-403. doi:10.1016/j.colsurfb.2013.10.037

- 21) Dadsetan, M., Taylor, K. E., Yong, C., Bajzer, Ž, Lu, L., & Yaszemski, M. J. (2013). Controlled release of doxorubicin from pH-responsive microgels. *Acta Biomaterialia*, 9(3), 5438-5446. doi:10.1016/j.actbio.2012.09.019
- 22) Chen, H., & Hsieh, Y. (2004). Ultrafine hydrogel fibers with dual temperature- and pH-responsive swelling behaviors. *Journal of Polymer Science Part A: Polymer Chemistry*, 42(24), 6331-6339. doi:10.1002/pola.20461
- 23) Zhou, S., Matsumoto, S., Tian, H., Yamane, H., Ojida, A., Kiyonaka, S., & Hamachi, I. (2005). PH-Responsive Shrinkage/Swelling of a Supramolecular Hydrogel Composed of Two Small Amphiphilic Molecules. *Chemistry - A European Journal*, 11(4), 1130-1136. doi:10.1002/chem.200400677
- 24) Li, F., Wu, H., Zhang, H., Li, F., Gu, C., & Yang, Q. (2009). Antitumor drug Paclitaxel-loaded pH-sensitive nanoparticles targeting tumor extracellular pH. *Carbohydrate Polymers*, 77(4), 773-778. doi:10.1016/j.carbpol.2009.02.029
- 25) Na, K., & Bae, Y. H. (2002). Self-Assembled Hydrogel Nanoparticles Responsive to Tumor Extracellular pH from Pullulan Derivative/Sulfonamide Conjugate: Characterization, Aggregation, and Adriamycin Release in Vitro. *Pharmaceutical Research*. doi:https://doi.org/10.1023/A:1015370532543
- 26) Na, K., Lee, E. S., & Bae, Y. H. (2007). Self-Organized Nanogels Responding to Tumor Extracellular pH: pH-Dependent Drug Release and in Vitro Cytotoxicity against MCF-7 Cells. *Bioconjugate Chemistry*, 18(5), 1568-1574. doi:10.1021/bc070052e
- 27) Traverso, N., Ricciarelli, R., Nitti, M., Marengo, B., Furfaro, A. L., Pronzato, M. A., . . . Domenicotti, C. (2013). Role of Glutathione in Cancer Progression and Chemoresistance. *Oxidative Medicine and Cellular Longevity*, 2013, 1-10. doi:10.1155/2013/972913

- 28) Guo, X., Cheng, Y., Zhao, X., Luo, Y., Chen, J., & Yuan, W. (2018). Advances in redox-responsive drug delivery systems of tumor microenvironment. *Journal of Nanobiotechnology*, 16(1). doi:10.1186/s12951-018-0398-2
- 29) Yin, S., Huai, J., Chen, X., Yang, Y., Zhang, X., Gan, Y., . . . Li, J. (2015). Intracellular delivery and antitumor effects of a redox-responsive polymeric paclitaxel conjugate based on hyaluronic acid. *Acta Biomaterialia*, 26, 274-285. doi:10.1016/j.actbio.2015.08.029
- 30) Shi, C., Guo, X., Qu, Q., Tang, Z., Wang, Y., & Zhou, S. (2014). Actively targeted delivery of anticancer drug to tumor cells by redox-responsive star-shaped micelles. *Biomaterials*, 35(30), 8711-8722. doi:10.1016/j.biomaterials.2014.06.036
- 31) Huo, M., Yuan, J., Tao, L., & Wei, Y. (2014). Redox-responsive polymers for drug delivery: From molecular design to applications. *Polym. Chem.*, 5(5), 1519-1528. doi:10.1039/c3py01192e
- 32) Guo, X., Cheng, Y., Zhao, X., Luo, Y., Chen, J., & Yuan, W. (2018). Advances in redox-responsive drug delivery systems of tumor microenvironment. *Journal of Nanobiotechnology*, 16(1). doi:10.1186/s12951-018-0398-2
- 33) Jin, Y., Yang, F., & Du, L. (2013). Nanoassemblies containing a fluorouracil/zidovudine glyceryl prodrug with phospholipase A2-triggered drug release for cancer treatment. *Colloids and Surfaces B: Biointerfaces*, 112, 421-428. doi:10.1016/j.colsurfb.2013.08.021
- 34) Pourhassan, H., Clergeaud, G., Hansen, A. E., Østrem, R. G., Fliedner, F. P., Melander, F., . . . Andresen, T. L. (2017). Revisiting the use of sPLA 2 -sensitive liposomes in cancer therapy. *Journal of Controlled Release*, 261, 163-173. doi:10.1016/j.jconrel.2017.06.024

- 35) Krupa, J. C., Hasnain, S., Nägler, D. K., Ménard, R., & Mort, J. S. (2002). S'2 substrate specificity and the role of His110 and His111 in the exopeptidase activity of human cathepsin B. *Biochemical Journal*, 361(3), 613-619. doi:10.1042/bj3610613
- 36) Chen, E. I., Kridel, S. J., Howard, E. W., Li, W., Godzik, A., & Smith, J. W. (2001). A Unique Substrate Recognition Profile for Matrix Metalloproteinase-2. *Journal of Biological Chemistry*, 277(6), 4485-4491. doi:10.1074/jbc.m109469200
- 37) Coombs, G. S., Bergstrom, R. C., Pellequer, J. L., Baker, S. I., Navre, M., Smith M. M., Tainer J. A., Madison E. L., Corey, David. R. (1998). Substrate specificity of prostate-specific antigen (PSA). *Cell Chemical Biology*, 5(9), 475-488.  
doi:[https://doi.org/10.1016/S1074-5521\(98\)90004-7](https://doi.org/10.1016/S1074-5521(98)90004-7)
- 38) Chau, Y., Tan, F. E., & Langer, R. (2004). Synthesis and Characterization of Dextran–Peptide–Methotrexate Conjugates for Tumor Targeting via Mediation by Matrix Metalloproteinase II and Matrix Metalloproteinase IX. *Bioconjugate Chemistry*, 15(4), 931-941. doi:10.1021/bc0499174
- 39) Schmid, B., Chung, D., Warnecke, A., Fichtner, I., & Kratz, F. (2007). Albumin-Binding Prodrugs of Camptothecin and Doxorubicin with an Ala-Leu-Ala-Leu-Linker That Are Cleaved by Cathepsin B: Synthesis and Antitumor Efficacy. *Bioconjugate Chemistry*, 18(3), 702-716. doi:10.1021/bc0602735
- 40) Hu, Q., Katti, P. S., & Gu, Z. (2014). Enzyme-responsive nanomaterials for controlled drug delivery. *Nanoscale*, 6(21), 12273-12286. doi:10.1039/c4nr04249b
- 41) Tauro, J. R., & Gemeinhart, R. A. (2005). Matrix Metalloprotease Triggered Delivery of Cancer Chemotherapeutics from Hydrogel Matrixes. *Bioconjugate Chemistry*, 16(5), 1133-1139. doi:10.1021/bc0501303

- 42) Wade, R. J., Bassin, E. J., Rodell, C. B., & Burdick, J. A. (2015). Protease-degradable electrospun fibrous hydrogels. *Nature Communications*, 6(1). doi:10.1038/ncomms7639
- 43) Editors. (2017, April 29). Peptide Bond. Retrieved from <https://biologydictionary.net/peptide-bond/>
- 44) Böttger, R., Hoffmann, R., & Knappe, D. (2017). Differential stability of therapeutic peptides with different proteolytic cleavage sites in blood, plasma and serum. *Plos One*, 12(6). doi:10.1371/journal.pone.0178943
- 45) Fosgerau, K., & Hoffmann, T. (2015). Peptide therapeutics: Current status and future directions. *Drug Discovery Today*, 20(1), 122-128. doi:10.1016/j.drudis.2014.10.003
- 46) Hancock, R. E., & Diamond, G. (2000). The role of cationic antimicrobial peptides in innate host defences. *Trends in Microbiology*, 8(9), 402-410. doi:10.1016/s0966-842x(00)01823-0
- 47) Lam, S. J., O'Brien-Simpson, N. M., Pantarat, N., Sulistio, A., Wong, E. H., Chen, Y., . . . Qiao, G. G. (2016). Combating multidrug-resistant Gram-negative bacteria with structurally nanoengineered antimicrobial peptide polymers. *Nature Microbiology*, 1(11). doi:10.1038/nmicrobiol.2016.162
- 48) Friedrich, C. L., Moyles, D., Beveridge, T. J., & Hancock, R. E. (2000). Antibacterial Action of Structurally Diverse Cationic Peptides on Gram-Positive Bacteria. *Antimicrobial Agents and Chemotherapy*, 44(8), 2086-2092. doi:10.1128/aac.44.8.2086-2092.2000
- 49) Hassan, S., Buchanan, M., Jahan, K., Aguilar-Mahecha, A., Gaboury, L., Muller, W. J., . . . Basik, M. (2010). CXCR4 peptide antagonist inhibits primary breast tumor growth, metastasis and enhances the efficacy of anti-VEGF treatment or docetaxel in a transgenic mouse model. *International Journal of Cancer*, 129(1), 225-232. doi:10.1002/ijc.25665

- 50) Perel G., Bliss J., Thomas C.M. (2016). Carfilzomib (Kyprolis): a novel proteasome inhibitor for relapsed and/or refractory multiple myeloma. P T.
- 51) Kaspar, A. A., & Reichert, J. M. (2013). Future directions for peptide therapeutics development. *Drug Discovery Today*, 18(17-18), 807-817. doi:10.1016/j.drudis.2013.05.011
- 52) Barrett, J. C., & Tirrell, M. V. (2018). Peptide Amphiphile Micelles for Vaccine Delivery. *Methods in Molecular Biology Protein Scaffolds*, 277-292. doi:10.1007/978-1-4939-7893-9\_21
- 53) Altunbas, A., Lee, S. J., Rajasekaran, S. A., Schneider, J. P., & Pochan, D. J. (2011). Encapsulation of curcumin in self-assembling peptide hydrogels as injectable drug delivery vehicles. *Biomaterials*, 32(25), 5906-5914. doi:10.1016/j.biomaterials.2011.04.069
- 54) Kisiday, J., Jin, M., Kurz, B., Hung, H., Semino, C., Zhang, S., & Grodzinsky, A. J. (2002). Self-assembling peptide hydrogel fosters chondrocyte extracellular matrix production and cell division: Implications for cartilage tissue repair. *Proceedings of the National Academy of Sciences*, 99(15), 9996-10001. doi:10.1073/pnas.142309999
- 55) Marini, D. M., Hwang, W., Lauffenburger, D. A., Zhang, S., & Kamm, R. D. (2002). Left-Handed Helical Ribbon Intermediates in the Self-Assembly of a  $\beta$ -Sheet Peptide. *Nano Letters*, 2(4), 295-299. doi:10.1021/nl015697g
- 56) Janssen, M. L. et al. Tumor targeting with radiolabeled  $\alpha v \beta 3$  integrin binding peptides in a nude mouse model. (2002) *Cancer Res*.
- 57) Chung, E. J., Cheng, Y., Morshed, R., Nord, K., Han, Y., Wegscheid, M. L., . . . Tirrell, M. V. (2014). Fibrin-binding, peptide amphiphile micelles for targeting glioblastoma. *Biomaterials*, 35(4), 1249-1256. doi:10.1016/j.biomaterials.2013.10.064

- 58) Nasrollahi, S. A., Taghibiglou, C., Azizi, E., & Farboud, E. S. (2012). Cell-penetrating Peptides as a Novel Transdermal Drug Delivery System. *Chemical Biology & Drug Design*, 80(5), 639-646. doi:10.1111/cbdd.12008
- 59) Lindgren, M., Rosenthal-Aizman, K., Saar, K., Eiríksdóttir, E., Jiang, Y., Sassian, M., . . . Langel, Ü. (2006). Overcoming methotrexate resistance in breast cancer tumour cells by the use of a new cell-penetrating peptide. *Biochemical Pharmacology*, 71(4), 416-425. doi:10.1016/j.bcp.2005.10.048
- 60) Mae, M., & Langel, U. (2006). Cell-penetrating peptides as vectors for peptide, protein and oligonucleotide delivery. *Current Opinion in Pharmacology*, 6(5), 509-514. doi:10.1016/j.coph.2006.04.004
- 61) Jiang, Y., Chen, J., Deng, C., Suuronen, E. J., & Zhong, Z. (2014). Click hydrogels, microgels and nanogels: Emerging platforms for drug delivery and tissue engineering. *Biomaterials*, 35(18), 4969-4985. doi:10.1016/j.biomaterials.2014.03.001
- 62) Kolb, H. C., Finn, M. G., & Sharpless, K. B. (2001). Click Chemistry: Diverse Chemical Function from a Few Good Reactions. *Angewandte Chemie International Edition*, 40(11), 2004-2021. doi:10.1002/1521-3773(20010601)40:113.0.co;2-5
- 63) Yigit, S., Sanyal, R., & Sanyal, A. (2011). Fabrication and Functionalization of Hydrogels through “Click” Chemistry. *Chemistry - An Asian Journal*, 6(10), 2648-2659. doi:10.1002/asia.201100440
- 64) Gopinathan, J., & Noh, I. (2018). Click Chemistry-Based Injectable Hydrogels and Bioprinting Inks for Tissue Engineering Applications. *Tissue Engineering and Regenerative Medicine*, 15(5), 531-546. doi:10.1007/s13770-018-0152-8

- 65) Golas, P. L., & Matyjaszewski, K. (2010). Marrying click chemistry with polymerization: Expanding the scope of polymeric materials. *Chem. Soc. Rev.*, 39(4), 1338-1354.  
doi:10.1039/b901978m
- 66) He, X., Ma, J., & Jabbari, E. (2008). Effect of Grafting RGD and BMP-2 Protein-Derived Peptides to a Hydrogel Substrate on Osteogenic Differentiation of Marrow Stromal Cells. *Langmuir*, 24(21), 12508-12516. doi:10.1021/la802447v
- 67) Brudno, Y., Desai, R. M., Kwee, B. J., Joshi, N. S., Aizenberg, M., & Mooney, D. J. (2015). In Vivo Targeting through Click Chemistry. *ChemMedChem*, 10(4), 617-620.  
doi:10.1002/cmdc.201402527
- 68) Zhang, Y., Liu, S., Wang, X., Zhang, Z., Jing, X., Zhang, P., & Xie, Z. (2014). Prevention of local liver cancer recurrence after surgery using multilayered cisplatin-loaded polylactide electrospun nanofibers. *Chinese Journal of Polymer Science*, 32(8), 1111-1118.  
doi:10.1007/s10118-014-1491-0
- 69) Lei, N., Gong, C., Qian, Z., Luo, F., Wang, C., Wang, H., & Wei, Y. (2012). Therapeutic application of injectable thermosensitive hydrogel in preventing local breast cancer recurrence and improving incision wound healing in a mouse model. *Nanoscale*, 4(18), 5686.  
doi:10.1039/c2nr30731f
- 70) Fisher, B., Bryant, J., Dignam, J. J., Wickerham, D. L., Mamounas, E. P., Fisher, E. R., . . . Wolmark, N. (2002). Tamoxifen, Radiation Therapy, or Both for Prevention of Ipsilateral Breast Tumor Recurrence After Lumpectomy in Women With Invasive Breast Cancers of One Centimeter or Less. *Journal of Clinical Oncology*, 20(20), 4141-4149.  
doi:10.1200/jco.2002.11.101

- 71) Kaplan, J. A., Liu, R., Freedman, J. D., Padera, R., Schwartz, J., Colson, Y. L., & Grinstaff, M. W. (2016). Prevention of lung cancer recurrence using cisplatin-loaded superhydrophobic nanofiber meshes. *Biomaterials*, 76, 273-281. doi:10.1016/j.biomaterials.2015.10.060
- 72) Kanamala, M., Wilson, W. R., Yang, M., Palmer, B. D., & Wu, Z. (2016). Mechanisms and biomaterials in pH-responsive tumour targeted drug delivery: A review. *Biomaterials*, 85, 152-167. doi:10.1016/j.biomaterials.2016.01.061
- 73) Deonarain, M., & Epenetos, A. (1994). Targeting enzymes for cancer therapy: Old enzymes in new roles. *British Journal of Cancer*, 70(5), 786-794. doi:10.1038/bjc.1994.400
- 74) Trachootham, D., Alexandre, J., & Huang, P. (2009). Targeting cancer cells by ROS-mediated mechanisms: A radical therapeutic approach? *Nature Reviews Drug Discovery*, 8(7), 579-591. doi:10.1038/nrd2803
- 75) Villoutreix, B., Getzoff, E., & Griffin, J. (1995). A Structural Model For The Prostate Disease Marker, Prostate Specific Antigen. doi:10.2210/pdb1pfa/pdb
- 76) Elsadek, B., Graeser, R., Warnecke, A., Unger, C., Saleem, T., El-Melegy, N., . . . Kratz, F. (2010). Optimization of an Albumin-Binding Prodrug of Doxorubicin That Is Cleaved by Prostate-Specific Antigen. *ACS Medicinal Chemistry Letters*, 1(5), 234-238. doi:10.1021/ml100060m
- 77) Lin, Y., & Wang, Q. (2012). Unlocking the 1,2,3-Triazole Ring Using Mechanical Force. *Angewandte Chemie International Edition*, 51(9), 2006-2007. doi:10.1002/anie.201108044

## Chapter 2: Materials and Methods

### 2.1. Materials

All protected amino acids, CuSO<sub>4</sub> pentahydrate, N-methylpyrrolidone (NMP), ethanedithiol, N,N-Diisopropylethylamine (DIPEA), and HCTU were purchased from ChemImpex. Matrigel, HPLC grade methanol, and HPLC grade acetonitrile (ACN), dichloromethane (DCM), dimethylformamide (DMF), methyl tert-butyl ether (MTBE) was purchased from VWR. All other cell culture supplies were purchased from Gibco. Enzymatically active prostate specific antigen and fluorogenic PSA substrate were purchased from Millipore. PAMAM dendrimer ethylenediamine core generation 0.0 solution, Hydroxylamine, sulfo N-hydroxysuccinimide (sNHS) amine, azide-amine, triisopropyl silane (TIS), thiolanisole, anisole and trifluoroacetic acid were all purchased from Sigma. 6-fam (FITC)-azide and dibenzocyclooctyne (DBCO)- N-hydroxysuccinimide (NHS) ester were purchased from Lumiprobe. Sulfo-Cyanine5.5 (sCy5)-Maleimide and DBCO-sNHS were purchased from Broadpharm. DBCO-amine was purchased from click chemistry tools. 1-ethyl-3-(3-dimethylaminopropyl)carbodiimide (EDC) was purchased from Oakwood Chemical. Pronova UP MVP Alginate was purchased from Nova Matrix. Bicyclo[6.1.0]nonyne (BCN)-NHS was purchased from Berry and Associates. Sulfo-Cyanine7 (sCy7)-azide was purchased from Jena Bioscience. Tris(benzyltriazolylmethyl)amine (TBTA) was purchased from Cayman Chemical. RSSYYSLC was custom synthesized by Genscript. CD1 mice were purchased from Charles River and J:Nu nude mice were purchased from Jax Laboratory.

## 2.2. Methods

### 1. Peptide Synthesis of RSSYYSLX

Peptides were synthesized with help by the Menegatti Lab (North Carolina State University, Biomedical Engineering Department). Peptides were synthesized following established Fluorenylmethyloxycarbonyl (Fmoc) based solid phase peptide synthesis protocols. Briefly, the peptide was synthesized on a Biotage Initiator+ using a rink amide polystyrene resin, loading 0.5 - 1 mmol/g. Coupling reactions utilized 5eq of Fmoc-protected amino acid, 4.95eq HCTU in DMF, and 10eq of base DIPEA in NMP. The coupling reaction proceeded for 5 min at 75°C under microwave irradiation. After each amino acid coupling, the Fmoc-protecting group was removed via a two-step reaction using 20% piperidine, for 3 minutes and 12 minutes. The resin was then washed 3 times with DCM and dried before being subjected to the deprotection/cleavage cocktail, TFA/Thioanisole/Ethanedithiol/Anisole (90/5/3/2 v/v). The cocktail was added in a 10-fold volume to mass (mL to g). The cleavage reaction then proceeded for 2 hours after which the solution was added dropwise to an ice-cold MTBE solution at a 10:1 v/v ratio. The precipitate formed was then washed thrice with the MTBE solution. The precipitate was dried, then dissolved in H<sub>2</sub>O/ACN (50:50 v/v), and lyophilized.

Samples were analyzed on an analytical HPLC (Agilent 1290 Infinity) through a C18 Zorbax Eclipse Plus C18 Rapid Resolution HD 1.8-micron column. Mobile phase (A) contained water with 0.1% (v/v) TFA solution while mobile phase (B) contained a methanol solution with 0.1% (v/v) TFA. The gradient was started at 5% solvent B to 58% solvent B over 14 minutes at a flow rate of 0.5 mL/min. Samples were then purified on a preparatory HPLC (Agilent 1100 Series) through a XBridge Prep C18 5µm OBD column. A simple gradient was started at 5% Solvent B to 95% solvent B over 15 minutes at a flow rate of 20 mL/min. Fractions were

collected based on 280 nm detector with the automated fractionator collecting based on a peak based method. The peak at 8-minute retention time was collected and then then rotovapped for about 15 minutes at 45°C at 150 rpm before freezing at -80°C and lyophilizing overnight.

Samples were analyzed on an LCMS (Shimadzu LC-20AD Prominence) on a C18 Kinetex 2.6mm column. Mobile phase (A) contained water with 0.1% (v/v) formic acid and mobile phase (B) contained acetonitrile with 0.1% (v/v) formic acid. A simple gradient was started at 5% Solvent B to 100% Solvent B over 3.5 minutes at a flowrate of 0.75 mL/min.

## 2. Synthesis of RSSYYSLX-FITC or RSSYYSLX-sCy7

Ascorbic acid and sodium bicarbonate were dissolved in DI H<sub>2</sub>O and then mixed together in a 1:1 molar ratio to create a fresh 0.375M Sodium Ascorbate stock solution. CuSO<sub>4</sub> stock (50 mM) was freshly made by dissolving Cu(II) Sulfate Pentahydrate (CuSO<sub>4</sub>) with DI H<sub>2</sub>O. TBTA stock (50 mM) was prepared in DMF and then combined with CuSO<sub>4</sub> stock in a 2:1 molar ratio TBTA:CuSO<sub>4</sub> with additional DI H<sub>2</sub>O being added to create a 1:1 DMF:H<sub>2</sub>O solution and then vortexed. RSSYYSLX (2.33 mg) was then dissolved in 767 μL of dimethyl sulfoxide (DMSO) followed by 135.4 μL of DI H<sub>2</sub>O. 0.396 μmol of FITC-azide or sCy7-azide was then added and solution was then bubbled with Nitrogen gas. After bubbling for about 5 minutes, ascorbate stock (31.8 μL) and Cu (copper):TBTA solution (66 μL) were quickly added. The solution was then bubbled with Nitrogen gas again for 20 minutes before quickly sealing the container and wrapping the container with aluminum foil before leaving the solution overnight at room temp.

Samples were analyzed on an analytical HPLC (Agilent 1290 Infinity) through a C18 Zorbax Eclipse Plus C18 Rapid Resolution HD 1.8-micron column. Mobile phase (A) contained water with 0.1% (v/v) TFA solution while mobile phase (B) contained a methanol solution with

0.1% (v/v) TFA. The gradient was started at 5% solvent B to 58% solvent B over 14 minutes at a flow rate of 0.5 mL/min. Samples were analyzed on an LCMS (Shimadzu LC-20AD Prominence) on a C18 Kinetex 2.6mm column. Mobile phase (A) contained water with 0.1% (v/v) formic acid and mobile phase (B) contained acetonitrile with 0.1% (v/v) formic acid. A simple gradient was started at 5% Solvent B to 100% Solvent B over 3.5 minutes at a flowrate of 0.75 mL/min. Samples were then purified on a preparatory HPLC (Agilent 1100 Series) through a XBridge Prep C18 5 $\mu$ m OBD column. Mobile phase (A) contained water with 0.1% (v/v) TFA solution while mobile phase (B) contained an ACN solution with 0.1% (v/v) TFA. A simple gradient was started at 5% Solvent B to 58% solvent B over 15 minutes at a flow rate of 20 mL/min. Fractions were collected based on the 450 nm (FITC) or 750 nm (sCy7) wavelength with the automated fractionator using a peak based method. The 11.1-minute (RSSYYSLX-FITC) and 9.1-minute (RSSYYSLX-sCy7) peak were collected respectively and the samples were then rotovapped for about 15 minutes at 45°C at 150 rpm before freezing at -80°C and lyophilizing overnight.

### 3. Synthesis of DBCO-RSSYYSLX-sCy7

Method 1: After the overnight reaction of RSSYYSLX-sCy7, for 100  $\mu$ L of the reaction solution, added 0.2376  $\mu$ mol of DBCO-NHS and Sodium Bicarbonate to create a 10 mM solution. The solution was then gently agitated overnight under aluminum foil.

Method 2: After purification of RSSYYSLX-sCy7, 0.2  $\mu$ mol of the purified RSSYYSLX-sCy7 was dissolved with 1  $\mu$ mol of DBCO-NHS Ester in 350  $\mu$ L of DMSO and 650  $\mu$ L of 10x

phosphate buffered saline (PBS). The solution was gently agitated for 4 hours under aluminum foil.

Samples were analyzed on an analytical HPLC (Agilent 1290 Infinity) through a C18 Zorbax Eclipse Plus C18 Rapid Resolution HD 1.8-micron column. Mobile phase (A) contained water with 0.1% (v/v) TFA solution while mobile phase (B) contained an ACN solution with 0.1% (v/v) TFA. The gradient was started at 5% solvent B to 100% solvent B over 15 minutes at a flow rate of 0.5 mL/min. Samples were then analyzed on an LCMS (Shimadzu LC-20AD Prominence) on a C18 Kinetex 2.6mm column. Mobile phase (A) contained water with 0.1% (v/v) formic acid and mobile phase (B) contained acetonitrile with 0.1% (v/v) formic acid. A simple gradient was started at 5% Solvent B to 100% Solvent B over 3.5 minutes at a flowrate of 0.75 mL/min.

#### 4. Synthesis of DBCO-RSSYYSLC-sCy5 (DPC)

RSSYYSLC (0.5 mg) was dissolved in 400  $\mu$ L of 4:1 5x PBS:DMSO solution followed by Sulfo-Cy5-Maleimide (10  $\mu$ L, 76.9 mM stock in DMSO). The reaction vessel was wrapped in aluminum foil and the solution was shook at room temperature for 4 hours. After the 4 hours, 2.06  $\mu$ mol of DBCO-sNHS and 30  $\mu$ L of DMSO was added, followed by another 400  $\mu$ L of 5x PBS:DMSO (4:1 v/v) solution. The reaction was then shook at room temperature for 2 hours.

Samples were analyzed on an analytical HPLC (Agilent 1290 Infinity) through a C18 Zorbax Eclipse Plus C18 Rapid Resolution HD 1.8-micron column. Mobile phase (A) contained water with 0.1% (v/v) TFA solution while mobile phase (B) contained an ACN solution with 0.1% (v/v) TFA. The gradient was started at 5% solvent B to 100% solvent B over 15 minutes at a flow rate of 0.5 mL/min. Samples were then purified on a preparatory HPLC (Agilent 1100

Series) through a XBridge Prep C18 5 $\mu$ m OBD column. A simple gradient was started at 5% Solvent B to 80% solvent B over 20 minutes at a flow rate of 20 mL/min. Fractions were collected based on 280 nm detector with the automated fractionator collecting based on a peak based method. The peak at 11-minute retention time was collected and the sample was rotovapped for about 15 minutes at 45°C at 150 rpm before freezing at -80°C and lyophilizing overnight. Samples were then analyzed on an LCMS (Shimadzu LC-20AD Prominence) on a C18 Kinetex 2.6mm column. Mobile phase (A) contained water with 0.1% (v/v) formic acid and mobile phase (B) contained acetonitrile with 0.1% (v/v) formic acid. A simple gradient was started at 5% Solvent B to 100% Solvent B over 3.5 minutes at a flowrate of 0.75 mL/min.

## 5. Alginate-Azide Hydrogel Coupling

For the coupling of azide onto alginate, 1 g of alginate was dissolved in 200 mL of 1x MES buffer. Separately, 2 mL of HCl was added to 2 mL of 1x MES buffer and 2 mmol of azide-amine. After 1 hour of stirring the alginate, the azide-amine solution was added. The solution was left to stir while the pH was maintained at 6.5. After at least 8 hours, 127.8 mg of EDC and 38.3 mg of sNHS was added. This step was repeated twice for a total of three times. 165 mg of hydroxylamine was then added and stirred for an hour. The solution was then dialyzed against decreased NaCl and PBS concentrations. After dialysis, the alginate was then vacuum filtered through a 0.2  $\mu$ m sterile filter. Then samples were then frozen and lyophilized.

Azide quantification was done by reacting DBCO-amine in excess with azide-alginate gels overnight on a thermoshaker at room temperature and 800 rpm. Afterwards, the absorbance was measured on a Nanodrop at 309 nm. Using an extinction coefficient of 12,000 M<sup>-1</sup> cm<sup>-1</sup>, the concentration of unreacted DBCO was measured and the number of azides was determined.

## 6. Tetra-BCN (T-BCN) Synthesis

T-BCN was synthesized by combining 20  $\mu\text{mol}$  of PAMAM with 80.4  $\mu\text{mol}$  of BCN-NHS and 100  $\mu\text{mol}$  of triethylamine in 392  $\mu\text{L}$  of DMSO followed by 392  $\mu\text{L}$  of Methanol. The reaction was left at room temperature for 20 minutes.

Samples were analyzed on an analytical HPLC (Agilent 1290 Infinity) through a C18 Zorbax Eclipse Plus C18 Rapid Resolution HD 1.8-micron column. Mobile phase (A) contained water with 0.1% (v/v) TFA solution while mobile phase (B) contained a methanol solution with 0.1% (v/v) TFA. The gradient was started at 0% solvent B to 100% solvent B over 10 minutes at a flow rate of 0.5 mL/min. Samples were then purified on a preparatory HPLC (Agilent 1100 Series) through a XBridge Prep C18 5 $\mu\text{m}$  OBD column. A simple gradient was started at 0% Solvent B to 100% solvent B over 12 minutes at a flow rate of 20 mL/min. Fractions were collected based on 210 nm detector with the automated fractionator collecting based on a peak based method. The peak at 10.9-minute retention time was collected and the samples were then analyzed on an LCMS (Shimadzu LC-20AD Prominence) on a C18 Kinetex 2.6mm column. Mobile phase (A) contained water with 0.1% (v/v) formic acid and mobile phase (B) contained acetonitrile with 0.1% (v/v) formic acid. A simple gradient was started at 5% Solvent B to 100% Solvent B over 3.5 minutes at a flowrate of 0.75 mL/min. After confirmation of the product, the samples were then rotovapped for about 15 minutes at 40°C at 150 rpm before freezing at -80°C and lyophilizing overnight.

## 7. Loading Efficiency Test

20 mg of lyophilized azide-alginate were dissolved in 900  $\mu\text{L}$  of 1x PBS. The sample was then set on the thermomixer for at least 5 hours set at 800 rpm at room temperature. Alginate was

then distributed into individual tubes in 45  $\mu\text{L}$  aliquot. Concentrations ranging between 2.7  $\mu\text{M}$  and 44.3  $\mu\text{M}$  of DPC were then prepared in 100% DMSO before adding 5  $\mu\text{L}$  of DPC solution to the corresponding gel. Samples were then vigorously vortexed for 40 seconds each before briefly centrifuging for 7 seconds on a micro centrifuge. The samples were then set on a thermomixer for 24 hours set at 800 rpm at room temperature. After the 24 hours, 150  $\mu\text{L}$  of DMSO was added to each sample and stored at  $-20^{\circ}\text{C}$  overnight after vortexing. The following day, samples were centrifuged down at  $14,000\times g$  at  $5^{\circ}\text{C}$  for 15 minutes. 50  $\mu\text{L}$  supernatant was carefully collected and transferred into a 96-well black plate and the fluorescence measured using a micro well plate reader (Glomax Multi Detection System) using the Cy5 preset setting. Concentration of DPC was calculated using a freshly prepared standard curve during the measurement. The % unbound DPC molecules were then calculated using the fluorescence data and the loading efficiency was then extrapolated.

## 8. Solubility Experiment

DBCO-RSSYYSLC-sCy5 was dissolved to make 21.4  $\mu\text{M}$ , 42.8  $\mu\text{M}$ , and 171.2  $\mu\text{M}$  solution in PBS:DMSO (9:1 v/v). Samples were then shook on a thermomixer for 24 hours at 900 rpm at room temp under aluminum foil, after which the samples were removed and left to sit at room temperature for 48 hours under aluminum foil. Samples were then centrifuged at  $12,000\times g$  for 10 minutes at room temperature. The supernatant was then diluted with PBS:DMSO (9:1 v/v) and transferred into a 96-well black plate and the fluorescence measured using a micro well plate reader (Glomax Multi Detection System) using the Cy5 preset setting. Concentration was calculated using a freshly prepared standard curve during the measurement.

## 9. Peptide Digestion Experiment

About 900  $\mu\text{M}$  solution of RSSYYSLX was prepared in 210  $\mu\text{L}$  of 1x PBS. Solutions were then added with 0.65  $\mu\text{L}$  of 0.2 g/L PSA stock to the experimental groups. 25  $\mu\text{L}$  aliquots were taken at  $T = 0, 24, 48, 72$  hours and stored at  $-20^\circ\text{C}$ . After freezing the last time point, the samples were taken out to thaw. The samples were then spun on a micro centrifuge for a couple of seconds before injecting the samples into the Analytical HPLC.

Samples were analyzed on an analytical HPLC (Agilent 1290 Infinity) through a C18 Zorbax Eclipse Plus C18 Rapid Resolution HD 1.8-micron column. Mobile phase (A) contained water with 0.1% (v/v) TFA solution while mobile phase (B) contained a methanol solution with 0.1% (v/v) TFA. The gradient was started at 5% solvent B to 95% solvent B over 10 minutes at a flow rate of 0.5 mL/min.

## 10. Kinetics Experiment

20 mg of lyophilized azide-alginate were dissolved in 900  $\mu\text{L}$  of 1x PBS. The sample was then set on the thermomixer for at least 5 hours set at 800 rpm at room temperature.

Concentrations ranging between 2.7  $\mu\text{M}$  and 44.3  $\mu\text{M}$  of DPC were then prepared in 100% DMSO before adding 100  $\mu\text{L}$  of DPC solution to the corresponding gel. Samples were then vigorously vortexed for 40 seconds each before briefly centrifuging for 7 seconds on a micro centrifuge. The samples were then set on thermomixer for 24 hours set at 800 rpm at room temperature. After the 24 hours 50  $\mu\text{L}$  aliquots were made with the preloaded alginate and 2  $\mu\text{L}$  of 10 mM T-BCN was added individually to each aliquot. The samples were all vortexed for 40 seconds each before briefly centrifuging for 7 seconds on the microcentrifuge. Solutions were washed twice with PBS:DMSO (9:1 v/v) and twice with 1x PBS for 30 minutes each. A final

concentration of 50 nM of PSA in PBS was then prepared in the sample. Samples were then stored in the cell incubator 37°C 5% CO<sub>2</sub> for 7 hours. At the 7-hour time point, 60 μL of the supernatant was taken out and stored at -80°C. The following day, 60 μL of DMSO was added and stored at -20°C for 2 hours, following which the samples were centrifuged at 14,000xg for 20 minutes at 5°C. 100 μL of the supernatant was then transferred to a 96-well black plate and the fluorescence measured using a micro well plate reader (Glomax Multi Detection System) using the Cy5 preset setting. Concentration was calculated using a freshly prepared standard curve during the measurement. The velocity of the reaction was calculated and graphed against concentration of prepared DPC, whereupon the slope was used to determine kcat/km.

#### 11. Cell Culture Protocol

LNCaP cells (P38) and Du145 cells (unknown passage) were kind gifts from the Lawrence Lab at University of North Carolina Chapel Hill (UNC). LNCaP and Du145 cells were grown as a monolayer in T-75 adherent flasks with phenol red RPMI 1640 containing 10% fetal bovine serum (FBS) and 1% 1x penstrep. Cells were cultured in the cell incubator at 37°C 5% CO<sub>2</sub>. Passaging was done using 0.05% trypsin/Ethylenediaminetetraacetic acid (EDTA), incubation for 5 minutes in the cell incubator, followed by centrifugation at 300xg for 5 minutes. The supernatant was aspirated followed by resuspension of the cells before cell counting and aliquot.

#### 12. PSA Detection Experiment in LNCaP

HSSKLQ-AFC (1 mg) was dissolved in 109.5 μL of DMSO. The resulting solution (22 μL) was then diluted with PBS (418 μL) to create a 400 μM solution. The dissolved peptide (100

$\mu\text{L}$ ) was then mixed with LNCaP media supernatant (100  $\mu\text{L}$ ), collected from LNCaP cells grown at approximately 80% confluency with phenol red free RPMI media with 10% FBS and 1% penstrep, in a black 96-well plate. Fluorescence was measured at 360 nm excitation and 590 nm emission on a Magellan microplate reader.

### 13. Peptide Specificity Experiment:

Method 1 (No Hydrogel): After cultured tumor cells were grown to ~80% confluency, the cell media supernatant was extracted. 500  $\mu\text{M}$  of peptide was prepared in DMSO, before diluting it 2-fold with 1x PBS. 70  $\mu\text{L}$  of the peptide solution was then added to 230  $\mu\text{L}$  of the LNCaP, Du145, RPMI, PSA control, and blank PBS control. 50  $\mu\text{L}$  Aliquots were collected at T = 0, 12, 24, 48 hours and stored at  $-80^{\circ}\text{C}$ . The day after freezing the last time point, samples were then thawed and precipitated with 200  $\mu\text{L}$  of ice-cold acetone and were kept at  $-20^{\circ}\text{C}$  for 1 hour. Samples were then spun at 12,000 rpm at  $5^{\circ}\text{C}$  for 20 minutes followed by collecting 215  $\mu\text{L}$  of the supernatant into a new container and dried under vacuum for at least 48 hours. Samples were then resuspended in 50  $\mu\text{L}$  of DI H<sub>2</sub>O and spun down using centrifugal filters for about 30 seconds per run. The flow through was collected and injected into the HPLC (Agilent 1290 infinity) through a C18 Zorbax Eclipse Plus C18 Rapid Resolution HD 1.8-micron column. Mobile phase (A) contained water with 0.1% (v/v) TFA solution while mobile phase (B) contained a methanol solution with 0.1% (v/v) TFA. The gradient was started at 5% solvent B to 90% solvent B over 13.5 minutes at a flow rate of 0.5 mL/min.

Method 2 (Calcium Crosslinked Hydrogel): Before starting, LNCaP and Du145 were cultured to ~80% confluency before aspirating the cell media and adding in no serum RPMI. After 24 hours,

the cell media supernatant was collected. Following centrifugation at 300xg, the supernatant was collected and stored at -80°C.

Alginate-azide (20 mg) was dissolved in PBS (900 µL) and mixed on the thermomixer at 900 rpm overnight at room temperature. DBCO-RSSYYSLC-sCy5 (100 µL, 11.1 µM stock in DMSO) was then vortexed vigorously for 40 seconds before briefly centrifuging for 7 short seconds on a mini centrifuge. The sample was then agitated for 24 hours on a thermoshaker at 900 rpm at room temperature. 50 µL aliquots were then distributed into individual Eppendorf tubes and 3.13 µL of 0.3 M calcium sulfate was physically mixed with a pipette tip. The samples were then left to gel overnight under aluminum foil. The following day, PSA was prepared in specially prepared PBS with 0.4 mM CaCl<sub>2</sub> to create a 502 nM solution of PSA. Hydrogel was then washed with 1x PBS and 100 µL of LNCaP, Du145, no serum RPMI, and PSA were added to the corresponding preloaded alginate hydrogels. 35 µL aliquots were taken out at T = 0, 2, 6, 12, 24, 48, 72, 120 hours where they are stored at -80°C after collection. The day after the final collection, the samples were thawed and 35 µL of DMSO was added to each solution. Samples were vortexed at 10,000 rpm and 50 µL of the supernatant was transferred to a 96-well black plate and the fluorescence measured using a micro well plate reader (Glomax Multi Detection System) using the Cy5 preset setting. Concentrations were calculated with a freshly prepared standard curve during each measurement and the % release was calculated.

Method 3 (T-BCN Crosslinked Hydrogel): Before starting, LNCaP and Du145 were cultured to ~80% confluency before aspirating the cell media and adding in no serum RPMI. After 24 hours, the cell media supernatant was collected. Following centrifugation at 300xg, the supernatant was collected and stored at -80°C.

Alginate-azide (20 mg) was dissolved in sterile filtered PBS (900  $\mu$ L) and mixed on the thermomixer at 900 rpm overnight at room temperature. DBCO-RSSYYSLC-sCy5 (100  $\mu$ L, 11.1  $\mu$ M stock in DMSO) was then vortexed vigorously for 40 seconds before briefly centrifuging for 7 short seconds on a mini centrifuge. The sample was then agitated for 24 hours on a thermoshaker at 900 rpm at room temperature. 50  $\mu$ L aliquots were then distributed into individual Eppendorf tubes and 2  $\mu$ L of T-BCN was added to each sample, followed by vigorous vortexing for 40 seconds and brief centrifugation for 7 seconds on the mini centrifuge. The samples were then left to gel for about 24 hours under aluminum foil. The following day, PSA was at a concentration of 502 nM solution of PSA. Hydrogel was then washed with 1x PBS and 100  $\mu$ L of LNCaP, Du145, no serum RPMI, and PSA were added to the corresponding preloaded alginate hydrogels. 35  $\mu$ L aliquots were taken out at T = 0, 2, 6, 12, 24, 48, 72, 120 hours where they are stored at -80°C after collection. The day after the final collection, the samples were thawed and 35  $\mu$ L of DMSO was added to each solution. Samples were vortexed at 10,000 rpm and 50  $\mu$ L of the supernatant was transferred into a 96-well black plate and the fluorescence measured using a micro well plate reader (Glomax Multi Detection System) using the Cy5 preset setting. Concentrations were calculated with a freshly prepared standard curve during each measurement and the % release was calculated.

#### 14. AFC Acetone Precipitation

AFC was dissolved in DI H<sub>2</sub>O in excess. After vigorous vortexing, the sample was centrifuged down using a centrifugal filter (0.2  $\mu$ M pore size). The run through was collected and 50  $\mu$ L aliquots were taken for both control and experimental groups. Both groups were further diluted with 50  $\mu$ L of DI H<sub>2</sub>O and vortexed vigorously. 400  $\mu$ L of ice-cold acetone was then

added to the experimental and was kept at -20°C for 1 hour. The sample was then centrifuged at 12,000 rpm at 5°C for 20 minutes followed by collection of 440 µL of the supernatant into a new container and dried under vacuum for at least 48 hours. The sample was then resuspended in 100 µL of DI H<sub>2</sub>O and both samples were injected into the HPLC (Agilent 1290 Infinity) through a C18 Zorbax Eclipse Plus C18 Rapid Resolution HD 1.8-micron column. Mobile phase (A) contained water with 0.1% (v/v) TFA solution while mobile phase (B) contained a methanol solution with 0.1% (v/v) TFA. The gradient was started at 5% solvent B to 90% solvent B over 13.5 minutes at a flow rate of 0.5 mL/min.

#### 15. Gel Stability Experiment

Method 1 (calcium): Alginate-azide (20 mg) was dissolved in sterile filtered PBS (900 µL) and mixed on the thermomixer at 900 rpm overnight at room temperature. DBCO-RSSYYSLC-sCy5 or DBCO-sCy5 (100 µL, 11.1 µM stock in DMSO) was then vortexed vigorously for 40 seconds before briefly centrifuging for 7 short seconds on a mini centrifuge. The sample was then agitated for 24 hours on a thermoshaker at 900 rpm at room temperature. The dissolved solution was then taken to the animal facility where 800 µL was transferred to a 3 mL syringe. 50 µL of 0.3M calcium sulfate was then added to a 1 mL syringe before locking the two syringes together with a luer lock coupler and vigorously mixing. The gel was then immediately injected into the mice subcutaneously on the right hind flank of 9-week old CD1 mice.

Method 2 (T-BCN): Alginate-azide (20 mg) was dissolved in sterile filtered PBS (900 µL) and mixed on the thermomixer at 900 rpm overnight at room temperature. DBCO-RSSYYSLC-sCy5 or DBCO-sCy5 (100 µL, 11.1 µM stock in DMSO) was then vortexed vigorously for 40 seconds

before briefly centrifuging for 7 short seconds on a mini centrifuge. The sample was then agitated for 24 hours on a thermoshaker at 900 rpm at room temperature. The dissolved solution was then taken to the animal facility where 800  $\mu$ L was transferred to a 3 mL syringe. T-BCN (32  $\mu$ L, 10 mM stock in DMSO) was also loaded into a 1 mL syringe before locking the two syringes together with a luer lock coupler and vigorously mixing. The syringes were then set aside for 30 minutes before subcutaneous injection of the preloaded alginate on the right flank of 9-week old CD1 mice.

## 16. Tumor Experiment

2 Days prior to the experiment, 20 mg of alginate was dissolved overnight with 900  $\mu$ L of sterile 1x PBS. The following day, 100  $\mu$ L of 11.1  $\mu$ M DPC or DCy5 solution in DMSO was added to the alginate and vortexed vigorously for 40 seconds followed by a short 7 second centrifugation on the micro centrifuge.

Matrigel were thawed overnight on ice at 4°C the day before the experiment. Cells were grown to about 80% confluency in an adherent T-75 flask before washing twice with 2 mL of PBS and trypsinizing with 2 mL of 0.05% Trypsin/EDTA. After 5 minutes of incubation at 37°C + 5% CO<sub>2</sub>, the cells were then transferred to a centrifuge tube and centrifuged for 5 minutes at 300xg. The samples were then aspirated and resuspended in serum free RPMI and spun down again at 300xg for 5 minutes. Cells were counted and a tumor cell suspension was prepared at 1.5 million cells per 100  $\mu$ L at 2:1 matrigel:no serum RPMI. The cells in the Matrigel:RPMI solution were then transported on ice to the animal facility.

Method 1 (Preliminary Experiment): On site, 800  $\mu\text{L}$  of the DPC solution was transferred to a 3 mL syringe. T-BCN (32  $\mu\text{L}$ , 10 mM stock in DMSO) was also loaded into a 1 mL syringe before locking the two syringes together with a luer lock coupler and vigorously mixing. The syringes were then set aside for 30 minutes. After 30 minutes, 200  $\mu\text{L}$  of the tumor cell suspension was injected subcutaneously on the right dorsal flank of J:NU nude mice. Right after inoculation, 50  $\mu\text{L}$  of the alginate gel was injected at the same spot, followed by an additional injection on the left dorsal flank in both mice

Method 2 (Main Experiment): After 30 minutes, 200  $\mu\text{L}$  of the tumor cell suspension or Matrigel control was injected subcutaneously on the right dorsal flank of J:NU nude mice and the tumor inoculation site was marked. 24 hours after inoculation, 800  $\mu\text{L}$  of the DPC or DCy5 solution was transferred to a 3 mL syringe. T-BCN (32  $\mu\text{L}$ , 10 mM stock in DMSO) was also loaded into a 1 mL syringe before locking the two syringes together with a luer lock coupler and vigorously mixing. After 30 minutes, 50  $\mu\text{L}$  of the alginate gel was injected at the same spot.

## Chapter 3: Preliminary Testing with Peptide

### 3.1. Results and Discussion

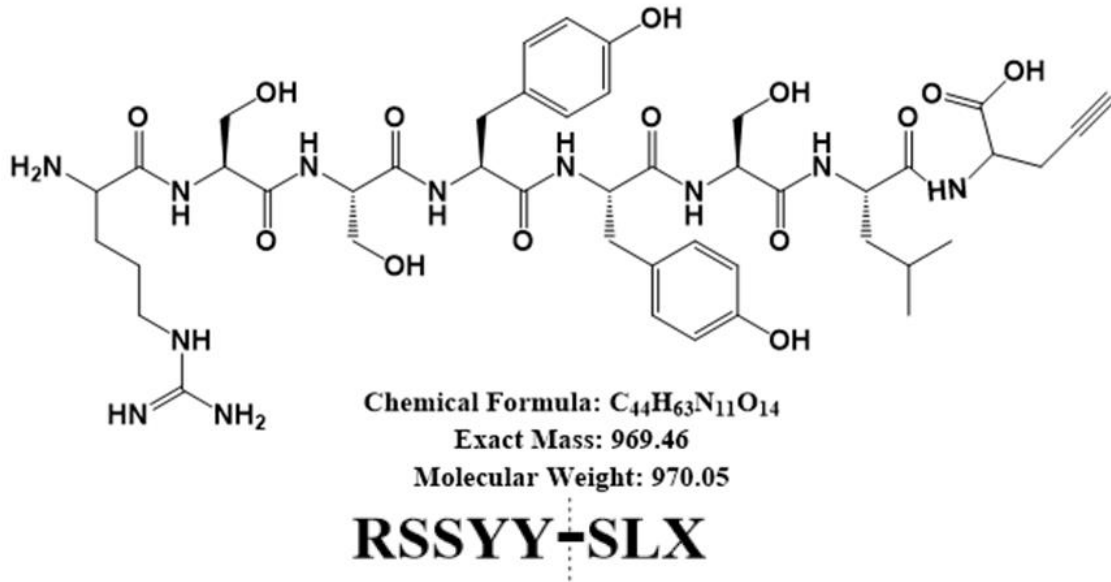


**Figure 3.1:** The chemical structure of the peptide RSSYYSLX. Cleavage of the peptide occurs between the tyrosine and serine as depicted by the dashed line.

The RSSYYSLX peptide was first synthesized for preliminary testing of the sequence. Propargylglycine (X) was added to the reference sequence (RSSYYSL) to allow for easy conjugation onto the C-terminus by targeting the alkyne, and to also help prevent steric hindrance of PSA cleavage by the molecule attached onto the C-terminus end of the peptide. The peptides were synthesized using standard Fmoc solid phase peptide synthesis protocols with help from the Menegatti Lab. After peptide synthesis, the peptides were then analyzed on the analytical HPLC. The HPLC showed a clear distinct peak at 4.3-minute retention time with a variety of smaller peaks, presumably the side products from the peptide synthesis (Figure 3.2). The peptide was then analyzed on the LCMS to confirm the product, but the main peak had an m/z value of 881 in the negative mode, contrary to the expected 968 m/z (Figure 3.3)

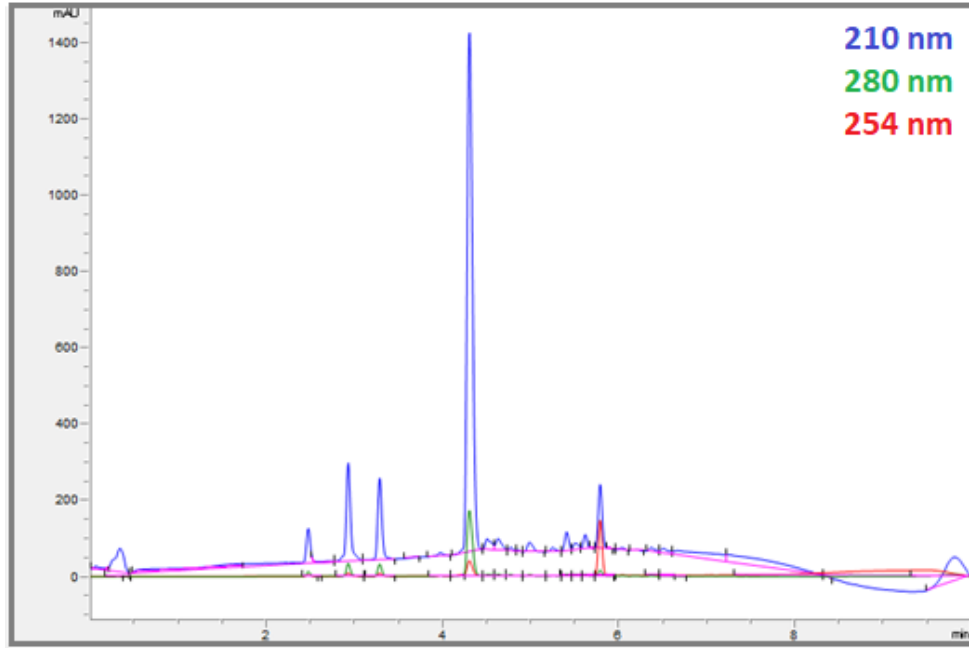


**Figure 3.2:** An HPLC Chromatogram of the 1<sup>st</sup> synthesis attempt for RSSYYSLX depicting the purity of the sample after peptide synthesis. The blue, green, and red chromatograms are the measured signals at 210, 280, and 254 nm respectively. The peptide peak is the predominant peak with a retention time of 4.3 minutes.

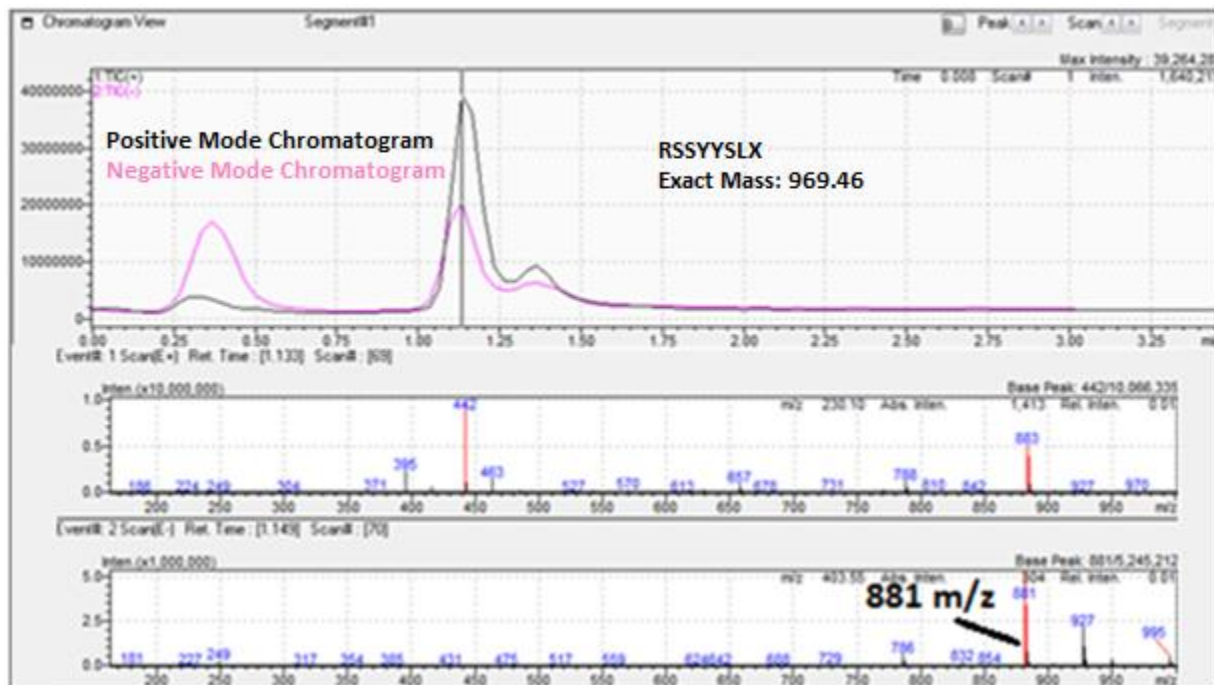


**Figure 3.3:** LCMS of the 1<sup>st</sup> synthesis attempt for RSSYYSLX shows an unexpected mass at 881 m/z in the negative mode which corresponds to a serine deletion in the peptide sequence.

This 881 m/z observed in the LCMS results suggests a serine deletion in the sequence, resulting in either RSYYSL or RSSYYL. In peptide chemistry, repeating serines are known to cause deletions during synthesis [1]. Thus, it is likely that the serine is missing in the repeating portion, resulting in RSYYSL. To verify this, the peptide was sent to the LCMS facility at North Carolina State University for LCMS-MS service and the results are shown (Figure 3.4). The expected mass fragments were calculated and displayed in Table 1. As shown, expected mass fragments were found for both serine deletion possibilities. Therefore, the only clear conclusion is that both RSSYYL and RSYYSL exist in the sample. Another peptide synthesis was then attempted with addition of double coupling on repeating amino acids. After synthesis, the peptide was analyzed on the analytical HPLC (Figure 3.5).

**Table 1:** Expected mass fragments for the LCMS-MS Analysis of RSSYYLX and RSYYSLX.

↓	157.11	<b>R</b>	882.42	↑	↓	157.11	<b>R</b>	882.42	↑
	244.14	<b>S</b>	725.31			244.14	<b>S</b>	725.31	
	331.17	<b>S</b>	638.28			407.2	<b>Y</b>	638.28	
	494.24	<b>Y</b>	551.25			570.27	<b>Y</b>	475.22	
	657.3	<b>Y</b>	388.19			657.3	<b>S</b>	312.16	
	770.38	<b>L</b>	225.12			770.38	<b>L</b>	225.12	
	882.42	<b>X</b>	112.04			882.42	<b>X</b>	112.04	

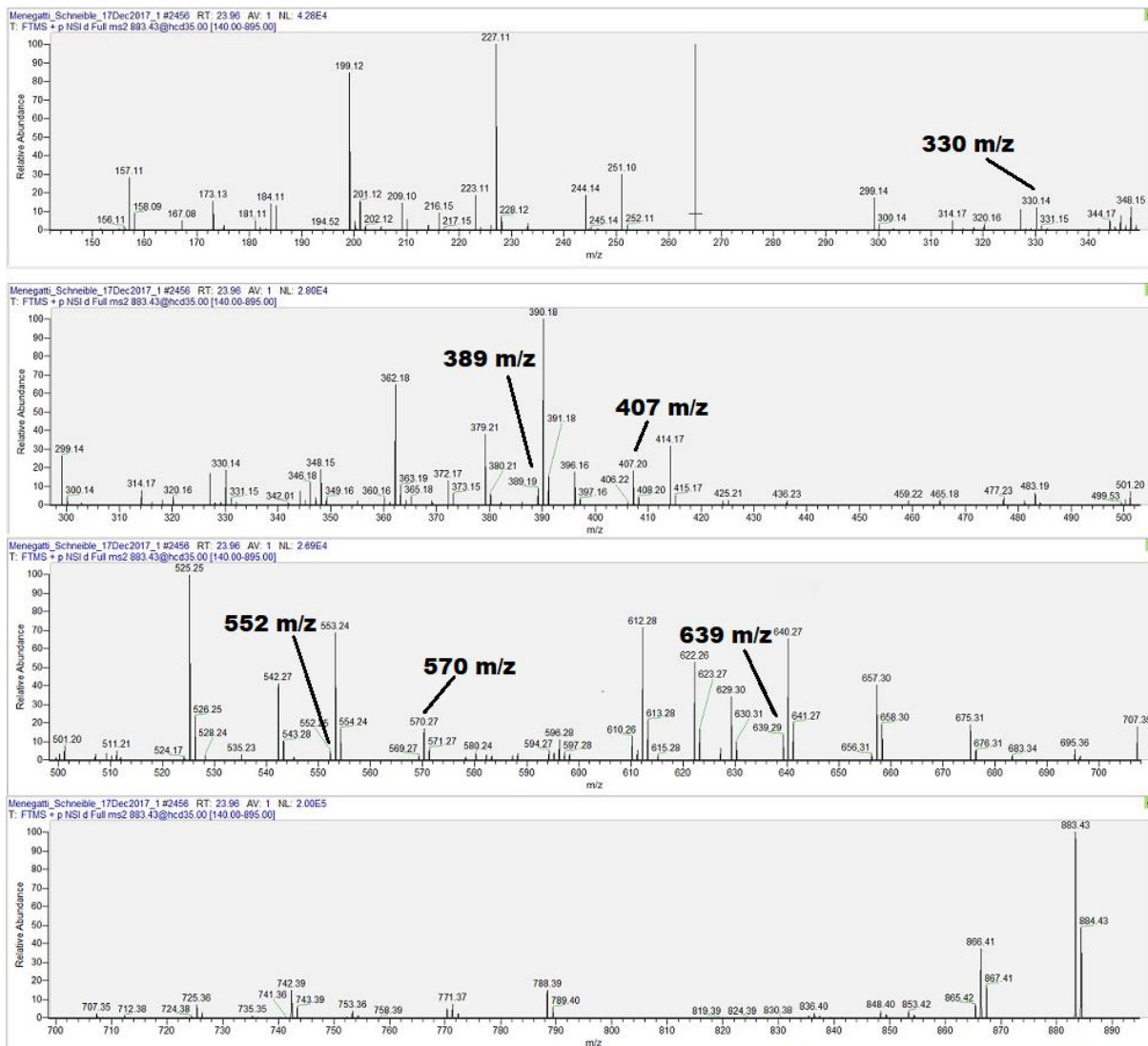


**Figure 3.4:** LCMS-MS data (measured by NCSU Mass Spectrometry Facility) showing cleavage fragments that correspond to both serine deletion possibilities (Table 1).

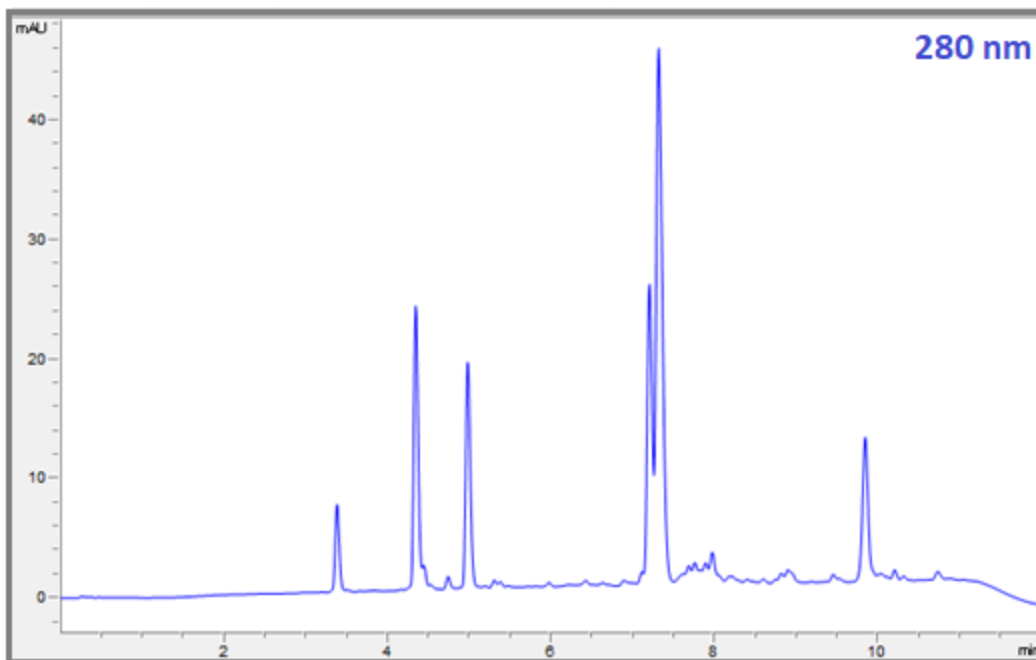


**Figure 3.5:** HPLC chromatogram for the 2<sup>nd</sup> synthesis attempt for RSSYYSLX before purification at 280 nm shows potential product peak at 7.3-minute retention time with a difficult to separate side product.

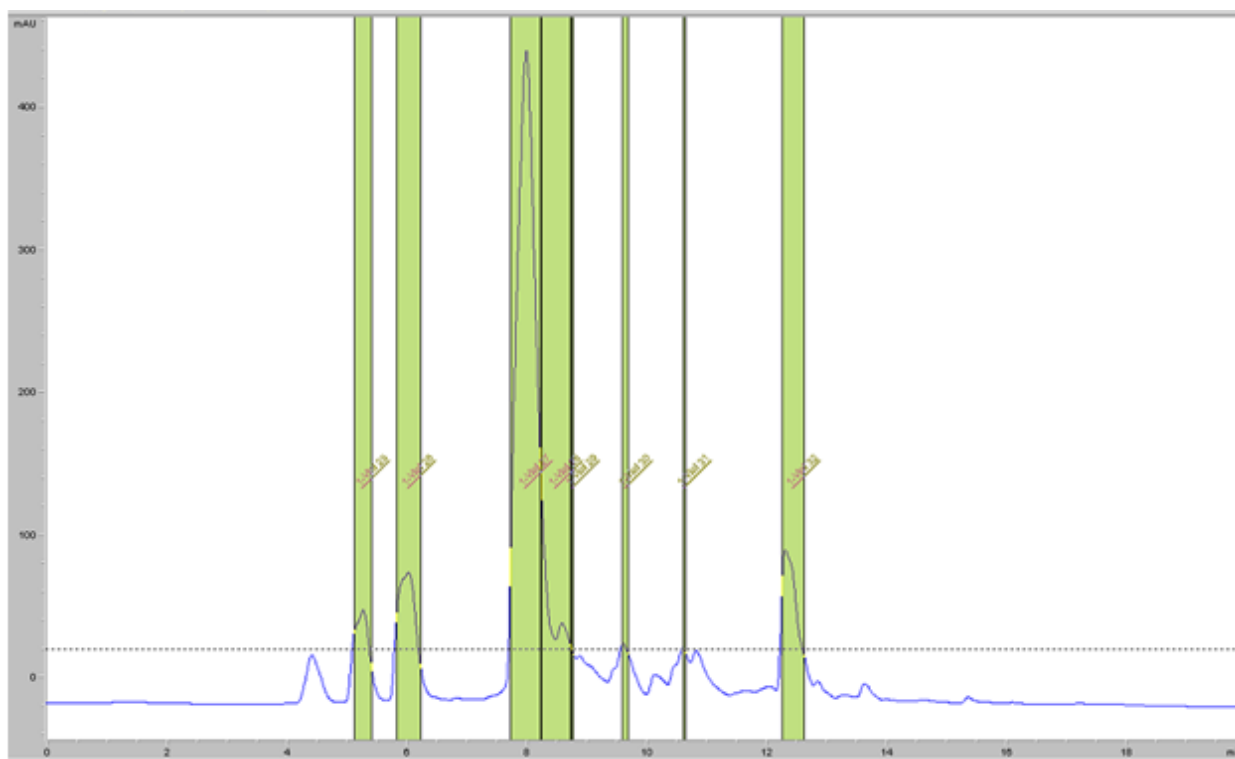


**Figure 3.6:** Chromatogram at 280 nm of the purification and fraction collection of crude RSSYYSLX on the preparatory HPLC using a peak based method at 280 nm for tyrosine detection. Peak at 8-minute retention time was collected.

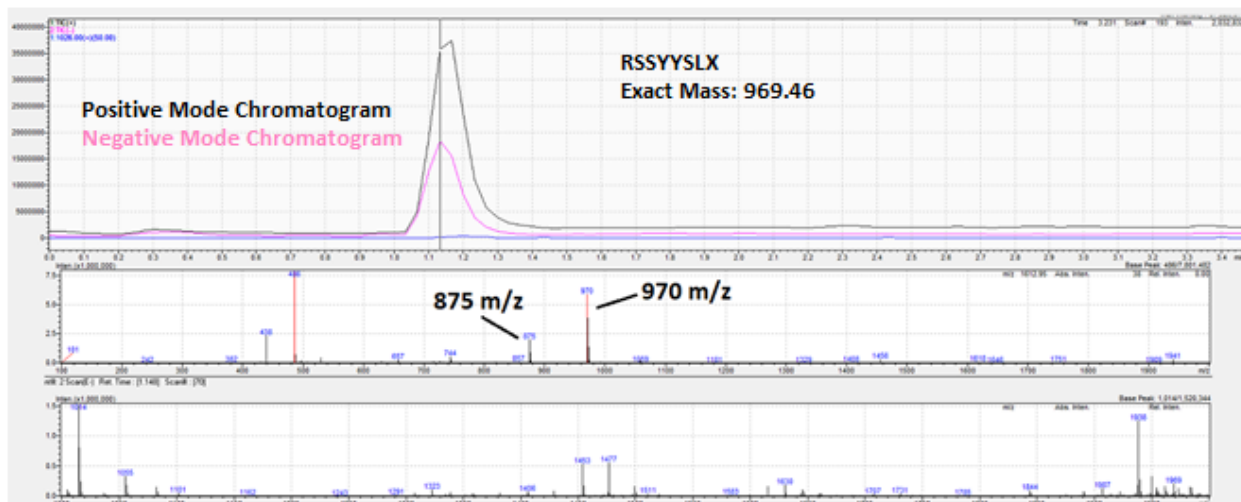


**Figure 3.7:** LCMS of the 2<sup>nd</sup> synthesis attempt for RSSYYSLX after Prep-HPLC purification shows the expected mass in the positive mode ( $969 + [H]^+$ ) confirming the peptide product. However, the 875 m/z suggests a RSSYYSL side product with no propargylglycine. Both ESI modes are shown where top is positive mode and bottom is negative mode.

The analytical HPLC shows a distinct peak at 7.3-minutes which is the suspected peptide, but the additional peak nearby suggests difficult purification. The sample was then purified on the preparatory HPLC and the peak at 8-minute retention time was collected and lyophilized (Figure 3.6). The sample was then analyzed on the LCMS the RSSYYSLX peptide was successfully collect but an impurity was observed with 875 m/z (Figure 3.7). The observed mass of the impurity corresponds to an RSSYYSL side product that is missing a propargylglycine (874.42 exact mass). However, this side product is not expected to affect subsequent synthesis due to the lack of the alkyne which will allow for easy purification after conjugation onto the alkyne. The peptide was then incubated with PSA to confirm cleavage (Figure 3.8).

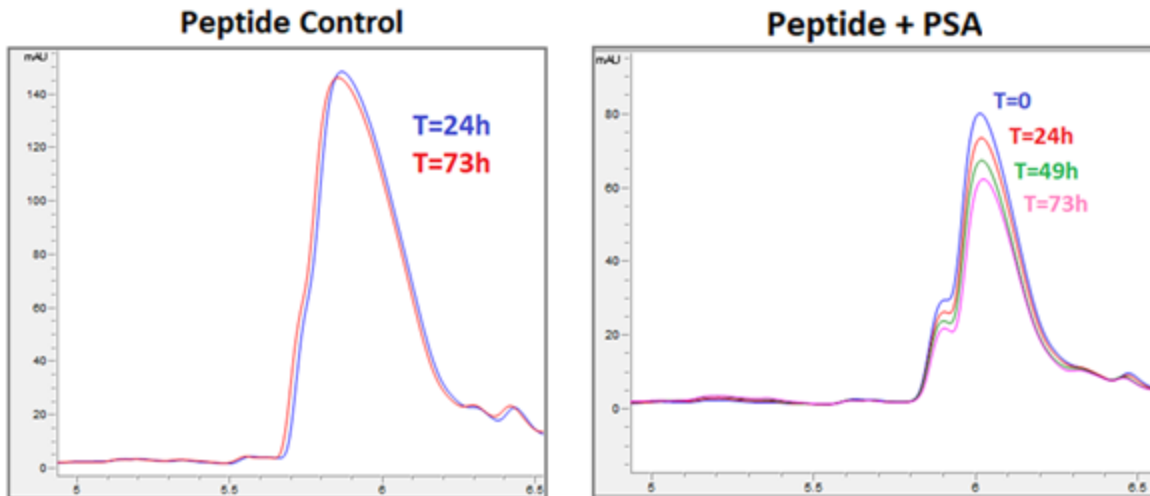


**Figure 3.8:** HPLC chromatogram at 280 nm of the incubation of RSSYYSYLX with 23.7 nM of PSA. Left chromatogram shows the stability of peptide in PBS while the right chromatogram depicts the cleavage over time with the addition of PSA in PBS.

After confirmation of cleavage, FITC was then conjugated onto the peptide through copper catalyzed azide-alkyne cycloaddition (CuAAC) between the alkyne on the propargylglycine (X) and the azide on FITC-azide (Figure 3.9). The FITC was added to allow easy identification of the cleavage product and to simulate the effect on PSA cleavage similar to what would be expected from other active agents.

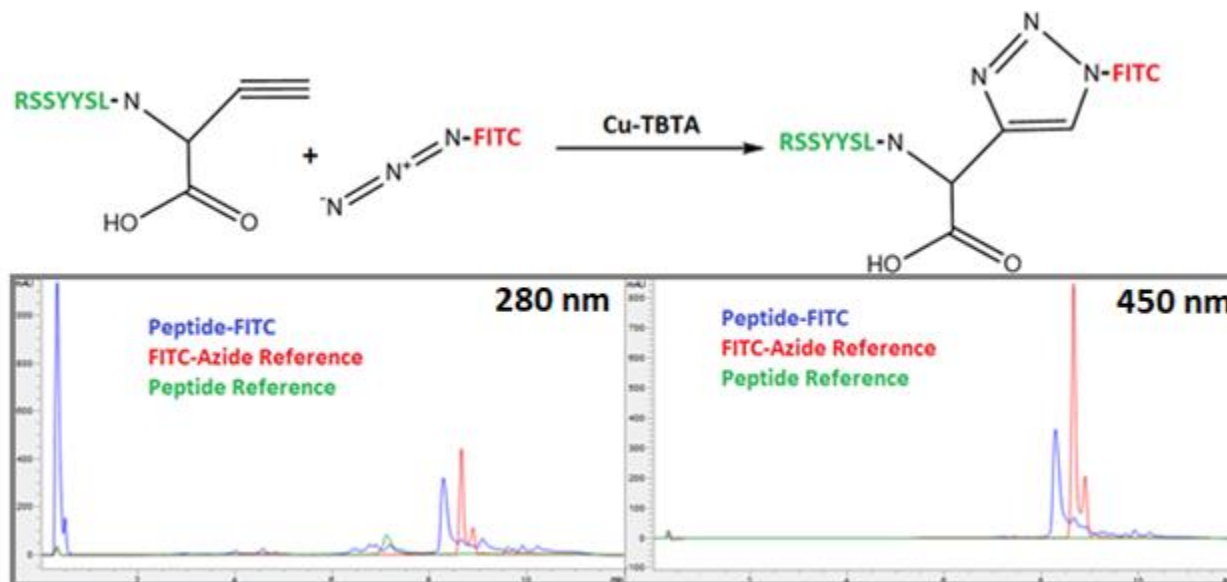


**Figure 3.9:** (Top) Schematic of the CuAAC reaction between FITC-azide and excess RSSYYSYLX with TBTA in 4:1 DMSO:H<sub>2</sub>O with 12 mM ascorbate buffer. (Bottom) HPLC analysis of the CuAAC reaction at 280 nm (left) and 450 nm (right) shows possible product with 8.3-minute retention time where the new peak shows up at both 280 nm and 450 nm while having a retention time between the FITC-azide and Peptide references.

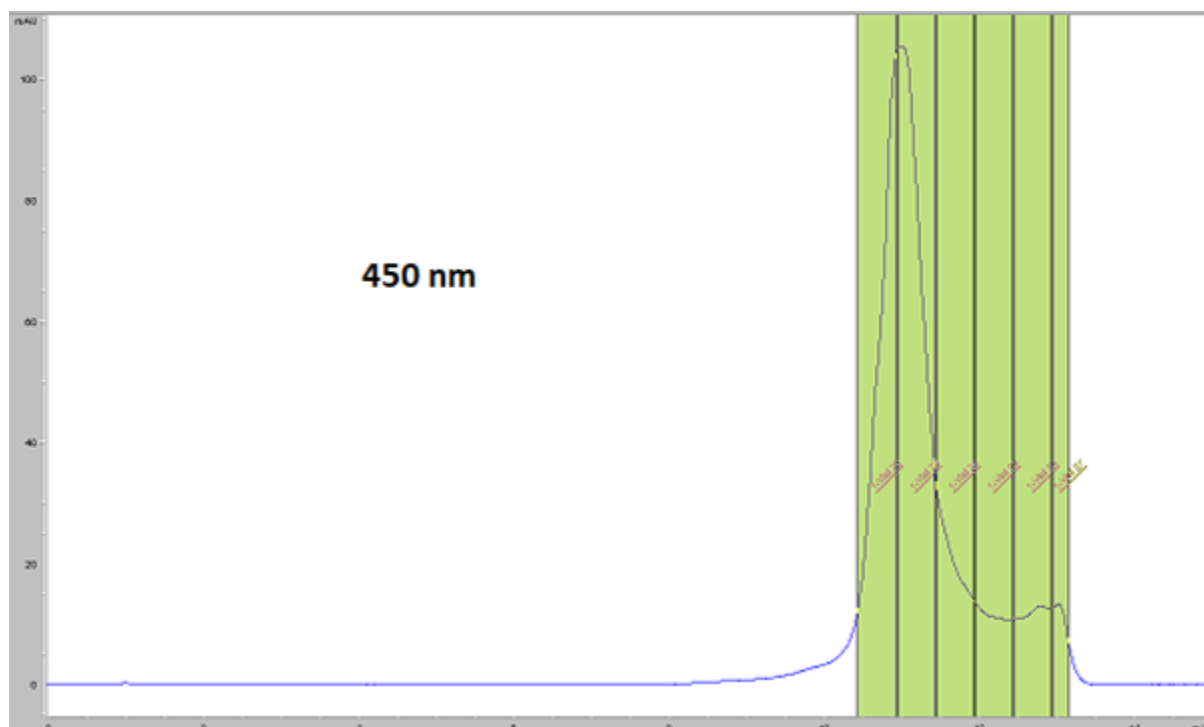


**Figure 3.10:** Chromatogram at 450 nm of the purification and fraction collection of the RSSYYS LX-FITC CuAAC reaction on the preparatory HPLC using a peak based method at 450 nm for FITC detection. Peak at 11.1-minute retention time was collected.

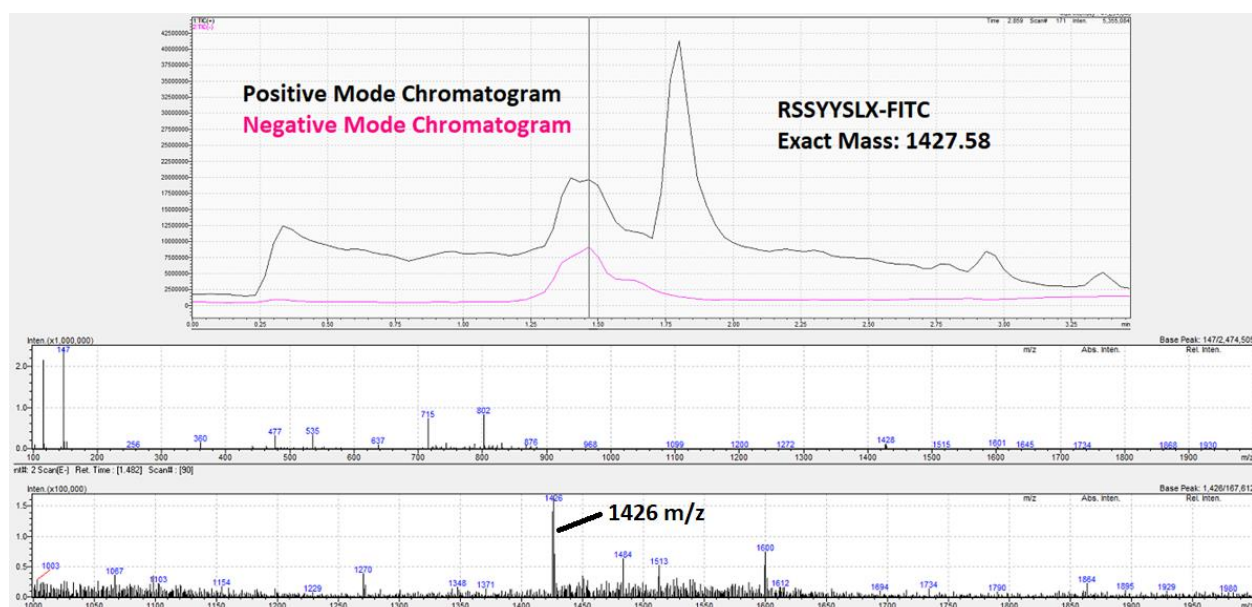


**Figure 3.11:** LCMS after purification of the RSSYYS LX-FITC sample shows successful collection of the RSSYYS LX-FITC molecule in the negative mode ( $1427 - [H]^+$ ). Both ESI modes are shown where top is the positive mode and bottom is the negative mode.

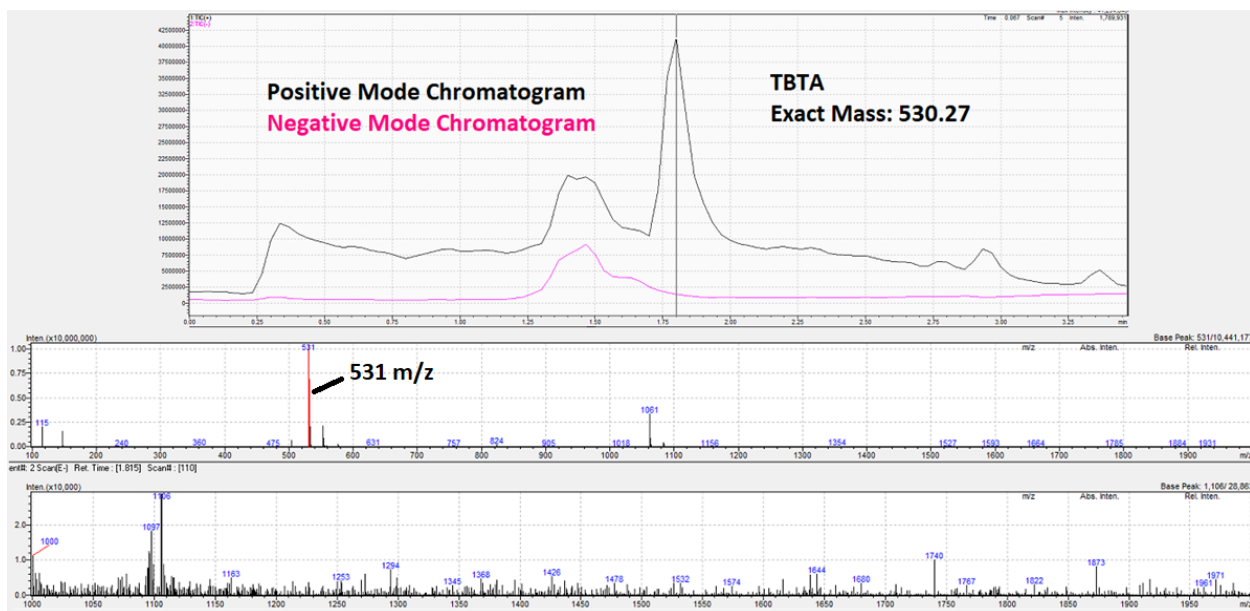


**Figure 3.12:** LCMS after purification of the RSSYYSLX-FITC sample shows a likely TBTA impurity in the positive mode ( $530 + [H]^+$ ). Both ESI modes are shown where top is the positive mode and bottom is the negative mode.

The HPLC shows a new peak with 8.3-minute retention time in the 450 nm chromatogram between the FITC-azide reference peak and the peptide reference peak, which is likely the product peak (Figure 3.9). The sample was then purified using the preparatory HPLC and the peak at 11.1-minute retention time was collected and lyophilized (Figure 3.10). The purified sample was then analyzed on the LCMS which showed successful collection of RSSYYSLX-FITC with a high yield of ~83% of RSSYYSLX-FITC as calculated on the nanodrop (Figure 3.11). However, the resulting sample was impure with the detection of a 531 m/z species in the positive mode on the LCMS (Figure 3.12). This mass is likely TBTA which has an exact mass of 530.27 which would correspond to the observed 531 m/z species in the positive mode. However, presence of TBTA should not pose an issue with the subsequent experiments because TBTA is extremely insoluble in aqueous solution. In addition, there have been no reports to my knowledge of TBTA affecting enzyme kinetics, presumably due to the precipitation of TBTA in aqueous solution. Hence, the sample was used to perform the subsequent experiments.

The RSSYYSLX-FITC molecule was then tested with the Peptide Specificity Experiment. The goal of this experiment was to show cleavage only during incubation with the extracellular secretions of the LNCaP cells in contrast to the PSA negative Du145 cell media. In doing so, one can conclude the specificity of the peptide substrate towards PSA. The PSA positive and PSA negative prostate cancer cell lines LNCaP and Du145 used in the experiments were kind gifts from the Lawrence Lab. The LNCaP and Du145 both have distinctive morphology as shown in Figure 3.13.

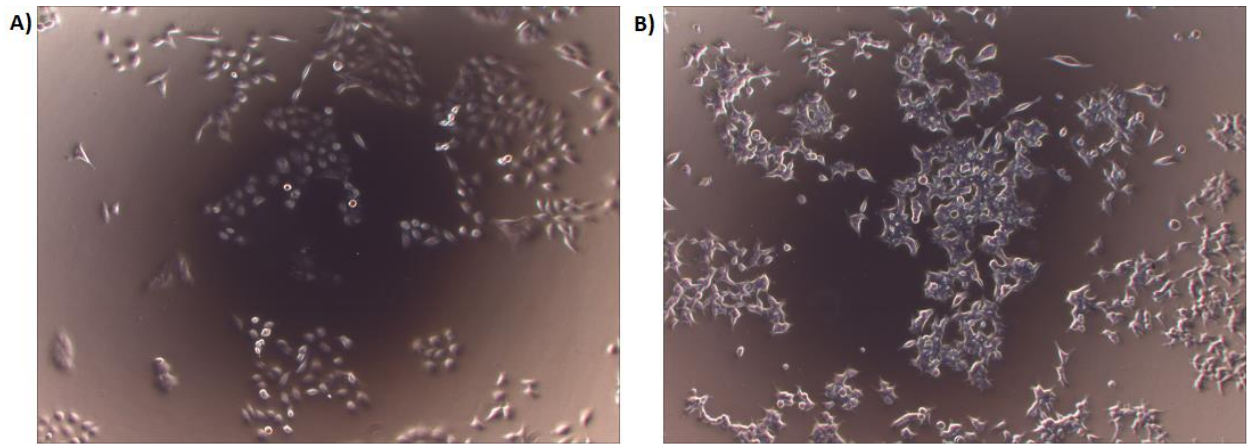


**Figure 3.13:** Representative Images of LNCaP (B) and Du145 (A) cell cultures.

The LNCaP cells were first tested to confirm secretion of PSA due to the relatively higher passage number of the received LNCaP cells (P38). The PSA Detection experiment was performed using a commercial PSA fluorogenic substrate based on the amino acid peptide sequence HSSKLQ. The substrate detects PSA through cleavage of the aryl-amide bond which releases free AFC, resulting in a shift and dramatic increase in fluorescence compared to the intact fluorogenic substrate (3.14) [2].

### Commercial Fluorogenic PSA Substrate (HSSKLQ-AFC) Schematic

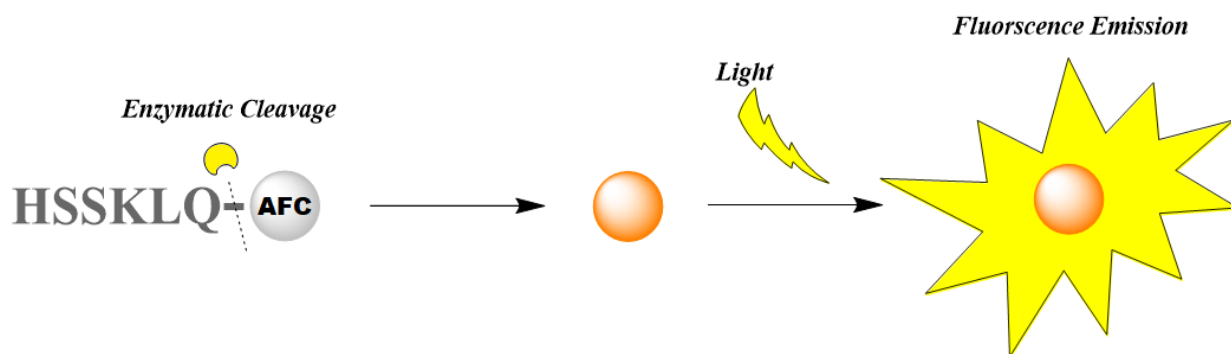


**Figure 3.14:** Schematic for the commercial fluorogenic PSA substrate. Cleavage of the aryl-amide bond by PSA releases free AFC which can be then detected through fluorescence in contrast to the weak and qualitatively different fluorescence in the intact HSSKLQ-AFC molecule.

The LNCaP cell culture media was incubated with the fluorogenic substrate and the fluorescence was measured over time. The results shown in Figure 3.15, show increasing fluorescence activity with respect to the RPMI control. This suggests that the LNCaP cells are expressing PSA and so, the cells were then used to test the specificity of RSSYYS LX-FITC towards PSA. This peptide specificity experiment was performed through incubation of the peptide molecule with cell culture media supernatant, followed by acetone precipitation after collection of each time point (Figure 3.16). The resulting supernatant was then analyzed on the analytical HPLC to determine cleavage.

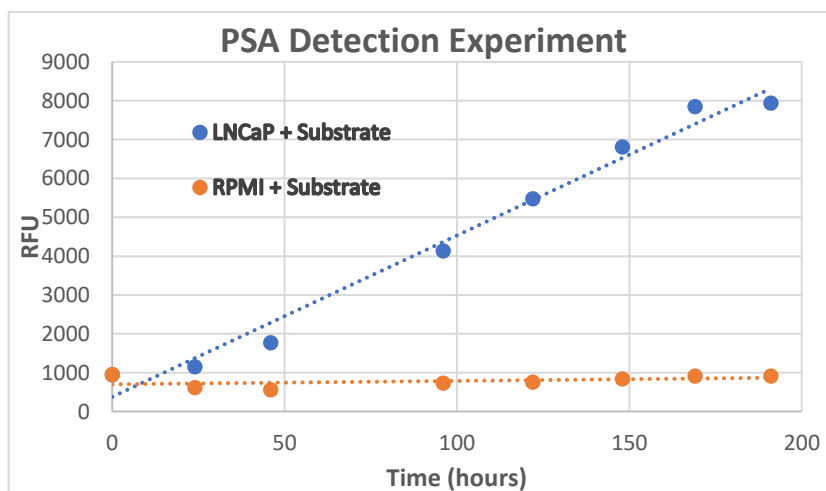


**Figure 3.15:** Incubation of HSSKLQ-AFC with LNCaP shows increasingly high fluorescence measurements with respect to time, in contrast to that of the RPMI control, confirming PSA expression by LNCaP cells.

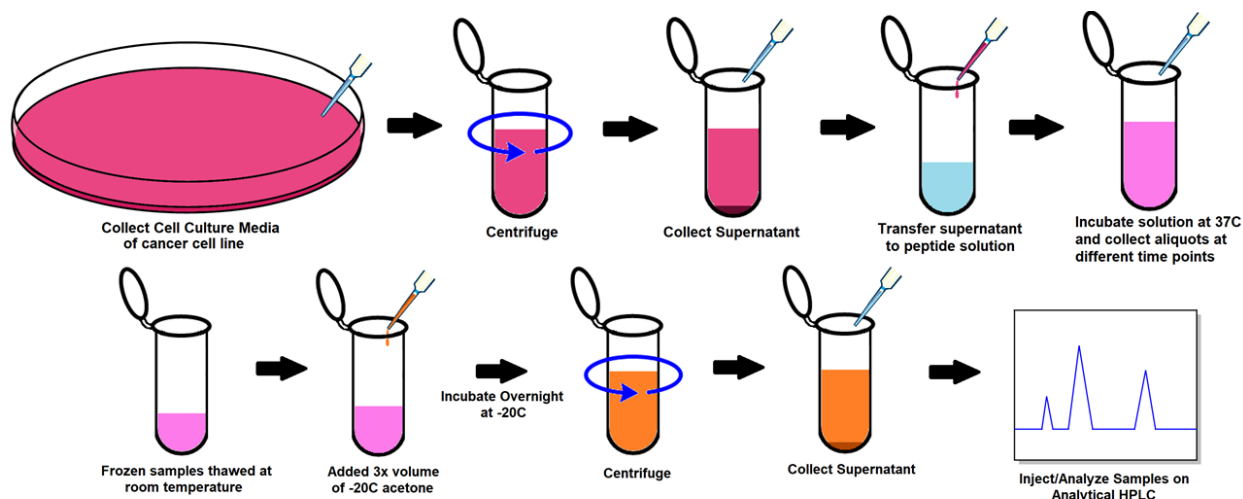


**Figure 3.16:** Schematic for the Peptide Specificity Experiment. Cell culture media supernatant were collected and incubated with the peptide of interest at 37°C. Time points were stored at -80°C and thawed together at room temperature after collection of the last time point. The sample was then acetone precipitated and the supernatant analyzed on analytical HPLC.

Unfortunately, cleavage was observed in both the Du145 and LNCaP groups where the RSSYYSLX-FITC peak with 5.95-min retention time decreases with respect to time while a new side peak, presumably the cleavage product, with 6.17-min retention time increases with time (Figure 3.17). Closer investigation in the media controls (Figure 3.18) suggest that the previous observation may be due to the cell culture media instead of the Du145 itself. Indeed, it is not too surprising for the cell culture media to cleave the peptide as serum often contain nonspecific proteases [3].

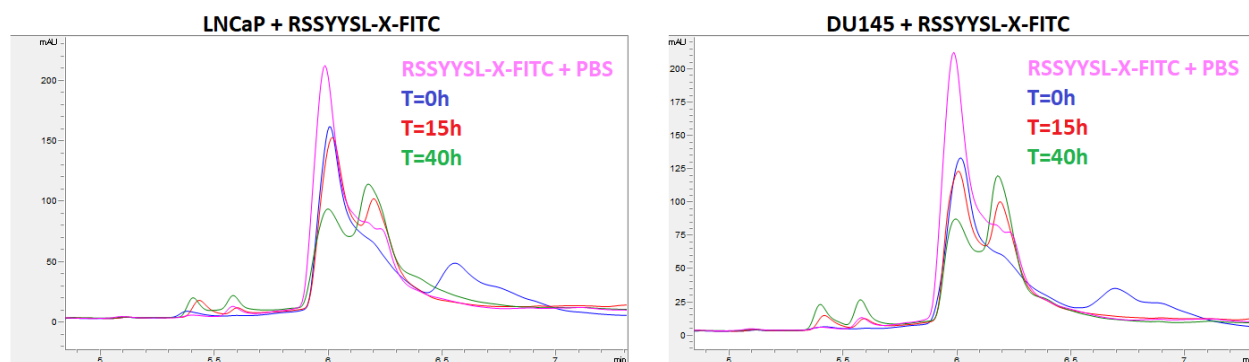


**Figure 3.17:** HPLC chromatogram of the peptide specificity experiment shows that cleavage of RSSYYSLX-FITC occurs during incubation of RSSYYSLX-FITC with both LNCaP and Du145. The picture is zoomed in to the peak of interest at 280 nm and shows a decrease in the peptide peak (5.95-minute retention time) with an increase in signal of a side peak (6.17-minute retention time) over time, where the latter is likely a cleavage product.

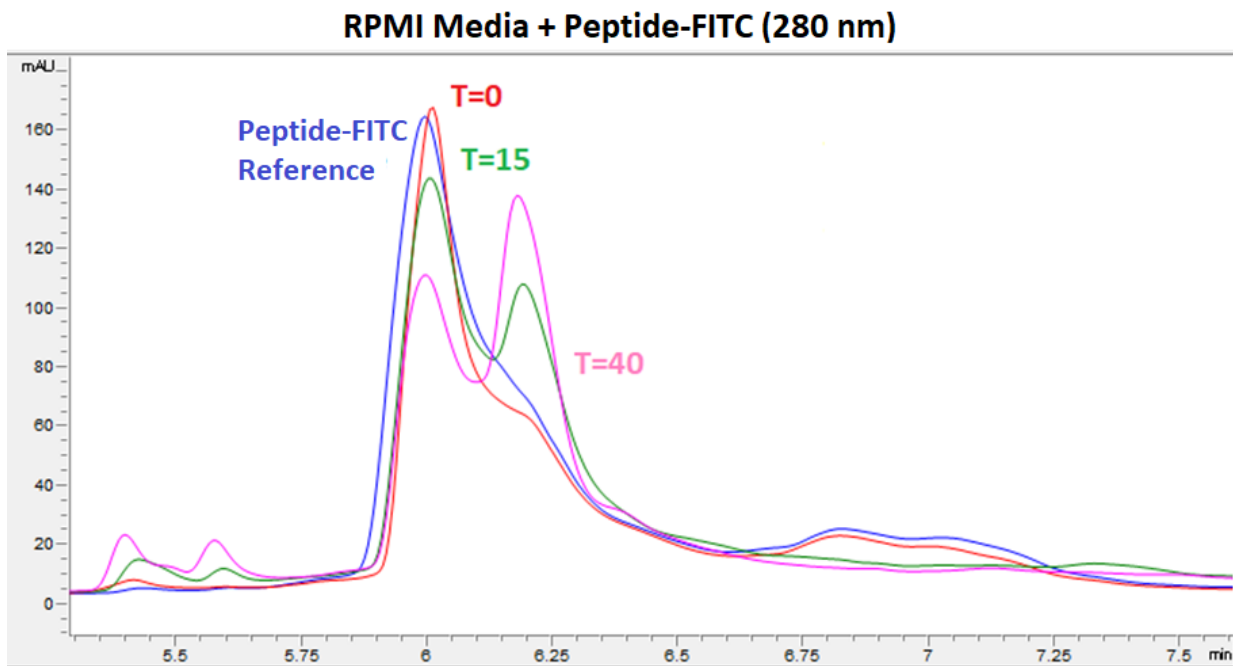


**Figure 3.18:** HPLC chromatogram of the peptide specificity experiment shows that cleavage of RSSYYSLX-FITC also occurs during incubation with RPMI cell culture media control. The picture is zoomed in on the peak of interest at 280 nm and shows a decrease in the peptide peak (5.95-minute retention time) with an increase in signal of a side peak (6.17-minute retention time) over time, where the latter is likely a cleavage product.

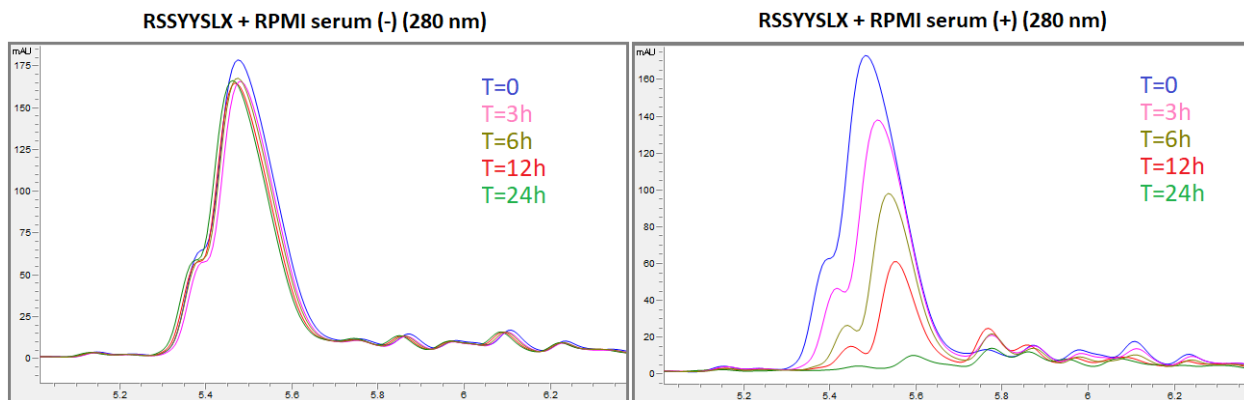


**Figure 3.19:** Incubation of RSSYYSLX peptide with no serum RPMI (left) shows no cleavage within 24 hours, whereas incubation with RPMI with FBS serum (right) shows significant cleavage of the peptide after 24 hours as seen by the decrease in the peak height with increasing time, thus confirming cleavage of RSSYYSLX by FBS containing RPMI.

To verify whether the FBS present in the RPMI cell culture media was cleaving the RSSYYSLX peptide, the peptide was incubated with FBS containing RPMI (Figure 3.19). Significant cleavage in the FBS containing RPMI experimental group was observed compared to the no serum RPMI control. Thus, it was certain that RSSYYSLX is cleaved by FBS. While this problem with the FBS can be remedied by culturing the cells in no serum media before collection, it does call into question about how specific RSSYYSLX is towards PSA. Therefore, I decided to move on to test whether my device can at least be stable in vivo in my intended application to see whether the sequence will work. In the meantime, I decided to also repeat the specificity experiment with the commercial PSA fluorogenic substrate (HSSKLQ). Going back to the initial PSA detection experiment with the LNCaP cells, the substrate has been used as a commercial fluorogenic PSA substrate to measure PSA activity and showed fluorescence only in the LNCaP cells compared to the serum containing RPMI control (Figure 3.15). The fact that the RPMI control showed little to no signal despite FBS being present, suggests that the sequence HSSKLQ may be a better option. Thus, the peptide specificity experiment was repeated with the commercial fluorogenic PSA substrate HSSKLQ-AFC instead of RSSYYSLX-FITC.

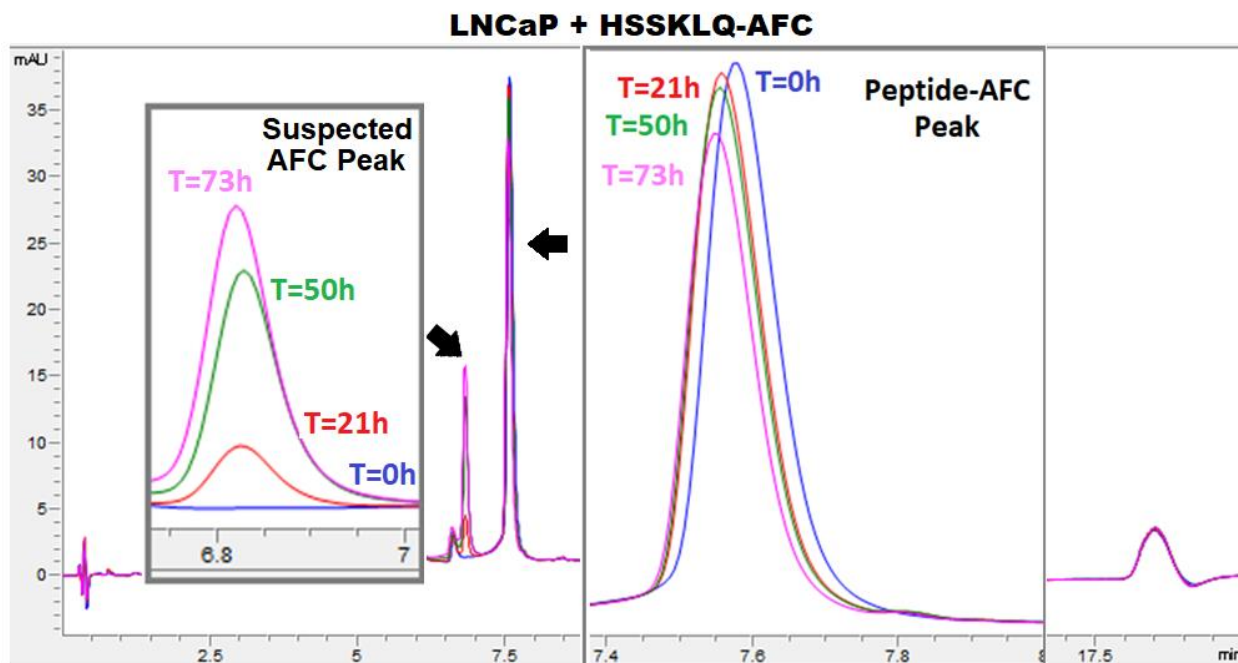


**Figure 3.20:** HPLC chromatogram at 378 nm for the Peptide Specificity Experiment with HSSKLQ-AFC where incubation of the peptide fluorophore with LNCaP (PSA positive) shows cleavage with a decrease in the Peptide-AFC peak (right) and an increase in a new peak (left) with respect to time.

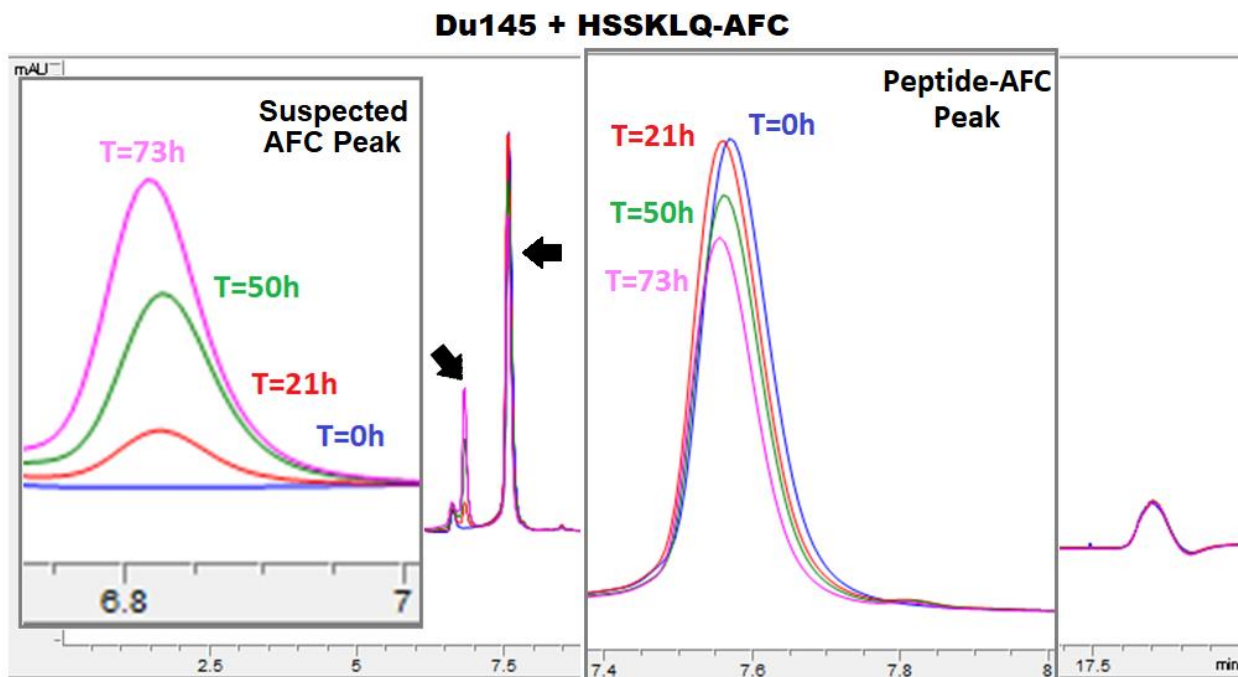


**Figure 3.21:** HPLC chromatogram at 378 nm for the Peptide Specificity Experiment with HSSKLQ-AFC where incubation of the peptide fluorophore with Du145 (PSA negative) also shows cleavage with a decrease in the Peptide-AFC peak (right) and an increase in a new peak (left) with respect to time.

The results of the Peptide Specificity Experiment with HSSKLQ-AFC suggest that cleavage of the peptide occurs in both LNCaP and Du145 (Figure 3.20 and 3.21). Incubation of HSSKLQ-AFC in both cell lines resulted in the intact peptide peak at 7.57-minute retention time decreasing as a function of time while a new peak, presumably free AFC, at 6.8-minute retention time appearing at 378 nm which continues to increase over time.

On the other hand, the RPMI media control also showed cleavage, similar to what is seen in the LNCaP and Du145 groups (Figure 3.22). This suggests that FBS is also cleaving the HSSKLQ-AFC molecule. This however is strange given the fact that the FBS containing RPMI control in the PSA detection experiment showed no fluorescence upon incubation with the HSSKLQ-AFC molecule (Figure 3.15)

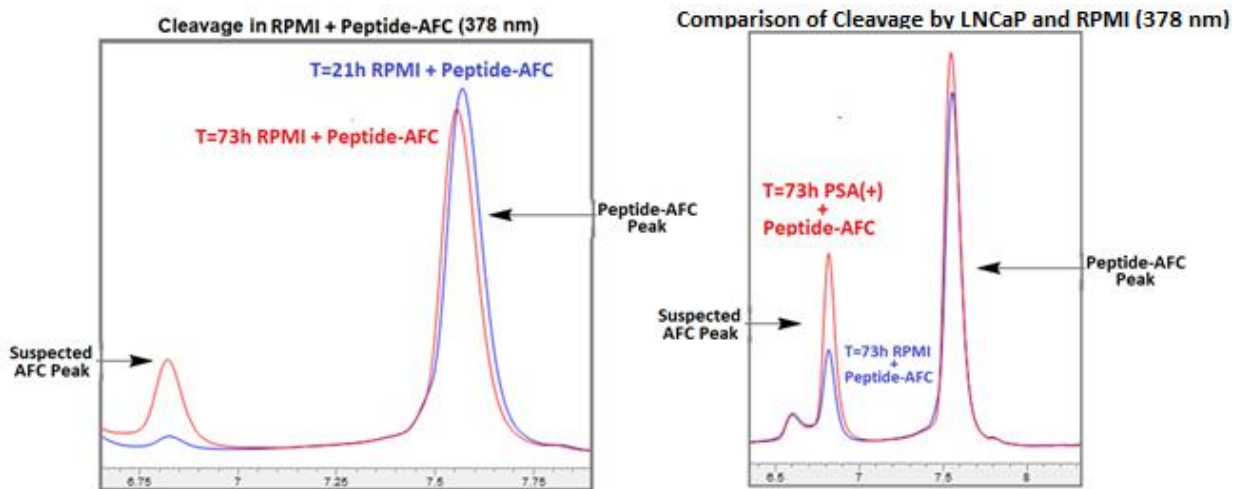


**Figure 3.22:** (Left) Chromatogram of the Peptide Specificity Experiment shows that incubation of serum containing RPMI with HSSKLQ-AFC results in cleavage of the peptide, similar to what was observed in the LNCaP and Du145 groups. (Right) Shows the comparison of the incubation of RSYYSLX between LNCaP and RPMI at the 73-hour time point. The comparison of chromatograms suggests comparable extent of cleavage where the suspected AFC peak for RPMI + Peptide-AFC has a comparable peak height to that of the LNCaP + Peptide-AFC.

Free AFC was first subjected to acetone precipitation to test for the possibility of AFC loss during the experimental procedure. As shown in Figure 3.23, the control had a much peak height compared to that of the acetone precipitated sample, suggesting that a significant amount of AFC is lost during the acetone precipitation process.

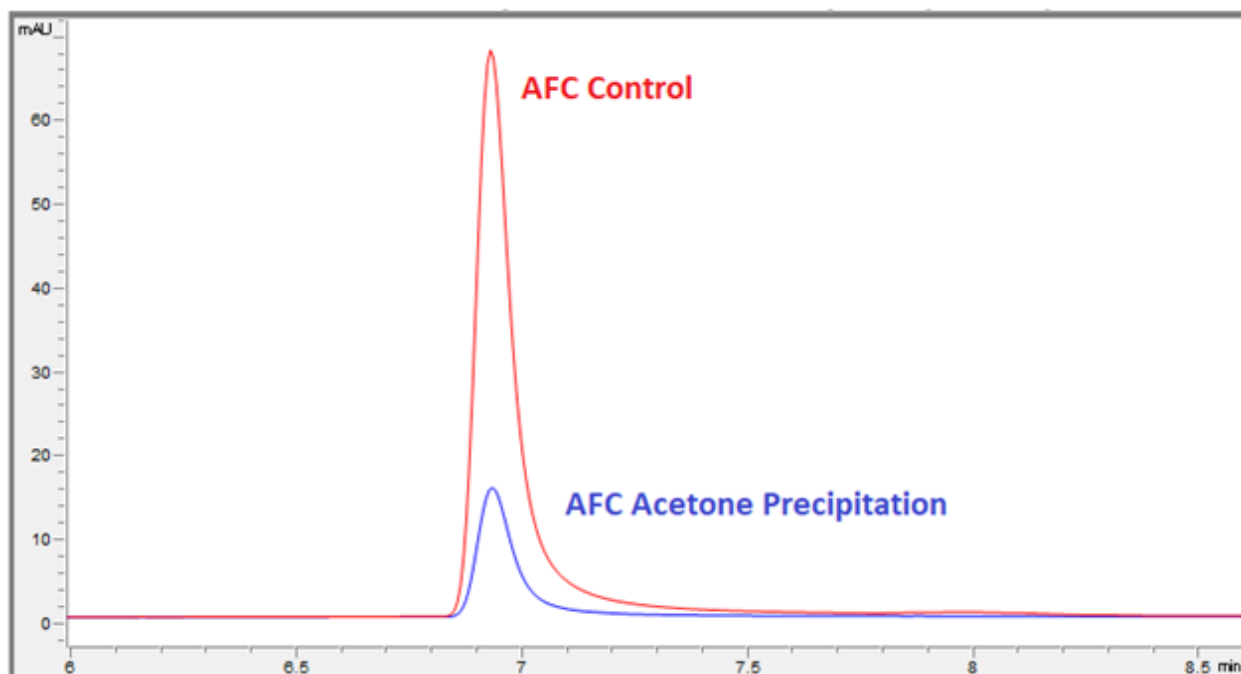


**Figure 3.23:** HPLC chromatogram of AFC at 378 nm before (red) and after (blue) acetone precipitation suggests that significant amount of AFC is lost during the precipitation process.

The acetone precipitated AFC standard was then used to confirm the identity of the suspected AFC peak from the Peptide Specificity Experiment (Figures 3.20, 3.22, and 3.23). While the retention time was the same between the AFC standard and the suspected AFC peak, a difference in signal behavior was observed. As summarized in Figure 3.24, the AFC standard has a higher signal at 378 nm compared to the signal measured at 338 nm. However, the reverse is true for the peak observed in the LNCaP + HSSKLQ-AFC. In fact, the same behavior is shared with the intact HSSKLQ-AFC substrate. This supports the hypothesis that the incubation of HSSKLQ-AFC with FBS containing RPMI does not fluoresce despite cleavage due to the lack of

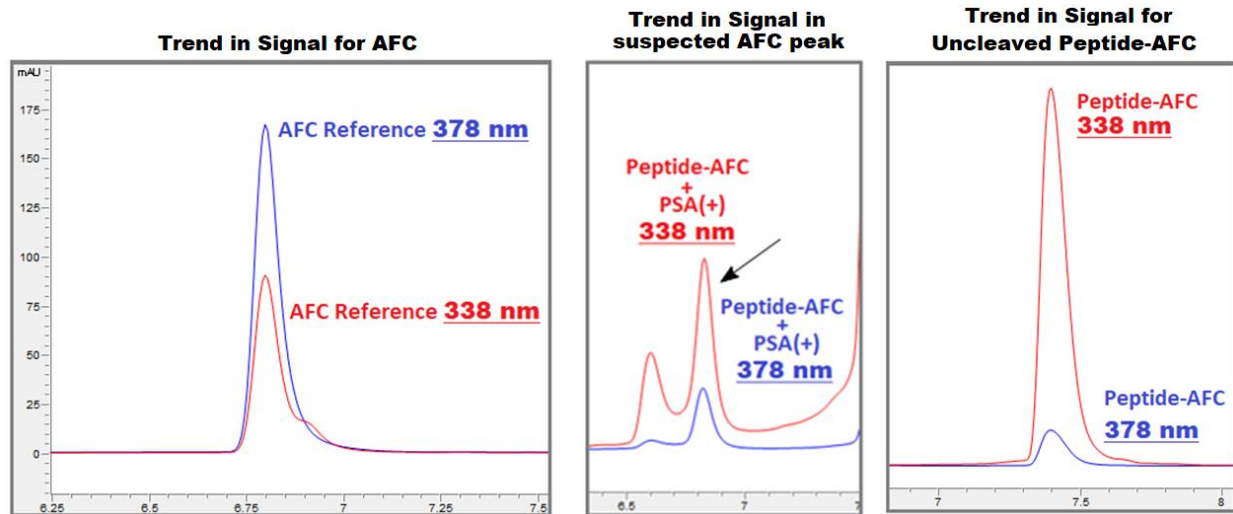


**Figure 3.24:** Comparison of the trends in signal between AFC standard, Suspected AFC peak, and Uncleaved Peptide-AFC show that the trend in signal is similar between the suspected AFC peak and the uncleaved peptide-AFC (338 nm > 378 nm signal) but different from the AFC standard (378 nm > 337 nm signal).

released free AFC. If you can recall, the cleavage of the aryl-amide bond to release free AFC is what causes the fluorescence. Thus, non-specific cleavage by FBS to release AFC-bound peptide fragments would not be detected in the fluorescent measurements. The identity of the suspected AFC peak could be an AFC-bound peptide fragment that coincidentally has the same retention time as free AFC. I also believe the drastic change in spectral properties following the release of free AFC is reflected in the change in signal behavior previously observed. Hence, all together, I believe that the loss of AFC during the precipitation process as well as the non-specific cleavage of the HSSKLQ-AFC peptide explains the disconnect between the PSA Detection Experiment and the Peptide Specificity Experiment. However, this suggests that the HSSKLQ sequence is also not specific towards PSA due to the non-specific cleavage by FBS. Thus, I have decided to move forward by testing the in vivo stability to see if the sequences are specific enough to remain stable in absence of a tumor. Between RSSYYSL and HSSKLQ, RSSYYSL was chosen based on the significantly faster kinetics (Figure 3.25). Thus, RSSYYSL will remain the focus of my investigation due to practicality.

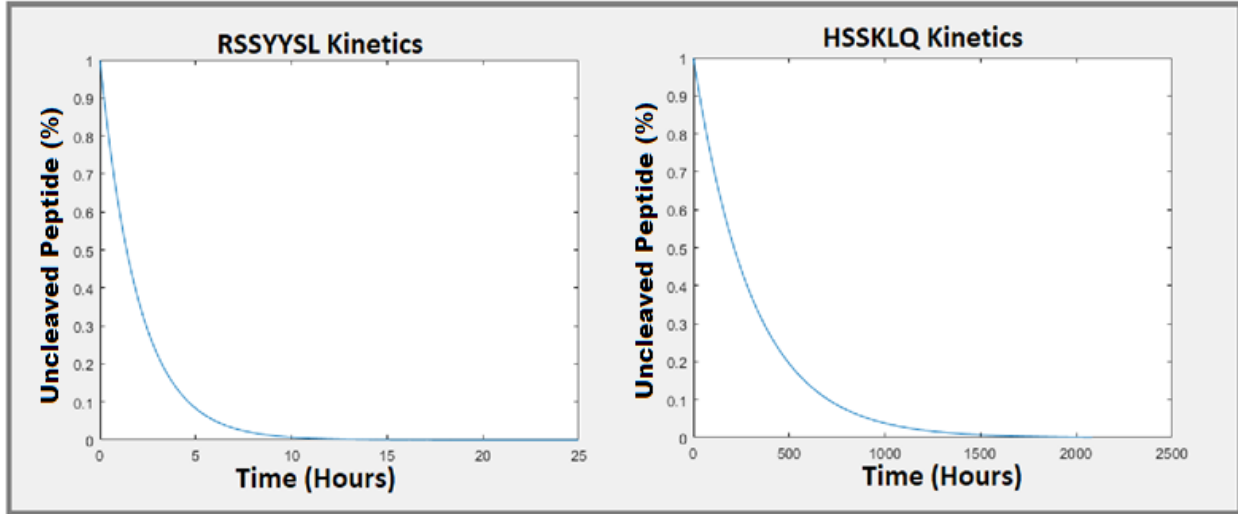


**Figure 3.25:** Comparison of kinetics between RSSYYSL [4] and HSKLQ [5] using simple Michaelis-Menten kinetics and literature reported kinetic parameters shows that RSSYYSL is cleaved significantly faster than HSKLQ at 45 nM of PSA. Matlab code found in Appendix B.

### 3.2. References

- 1) Peptide Design. (n.d.). Retrieved from <https://www.thermofisher.com/us/en/home/life-science/protein-biology/protein-biology-learning-center/protein-biology-resource-library/pierce-protein-methods/peptide-design.html>
- 2) Smith, R., Bissell, E., Mitchell, A., & Pearson, K. (1980). Direct photometric or fluorometric assay of proteinases using substrates containing 7-amino-4-trifluoromethylcoumarin. *Thrombosis Research*, 17(3-4), 393-402. doi:10.1016/0049-3848(80)90074-2
- 3) Jobling, J. W., Eggstein, A. A., & Petersen, W. (1915). Serum Proteases and Mechanism of Abderhalden Reaction. *Southern Medical Journal*, 8(11), 967. doi:10.1097/00007611-191511000-00020
- 4) Coombs, G. S., Bergstrom, R. C., Pellequer, J. L., Baker, S. I., Navre, M., Smith M. M., Tainer J. A., Madison E. L., Corey, David. R. (1998). Substrate specificity of prostate-specific antigen (PSA). *Cell Chemical Biology*, 5(9), 475-488. doi:https://doi.org/10.1016/S1074-5521(98)90004-7
- 5) Denmeade, S. R., Lou, W., Lövgren, J., Malm, J., Lilja, H., & Issacs, J. T. (1997). Specific and Efficient Peptide Substrates for Assaying the Proteolytic Activity of Prostate-specific Antigen. *Cancer Research*, 57(21). Retrieved October, 2017.

## Chapter 4: Peptide + Alginate Analysis

### 4.1. Results and Discussion

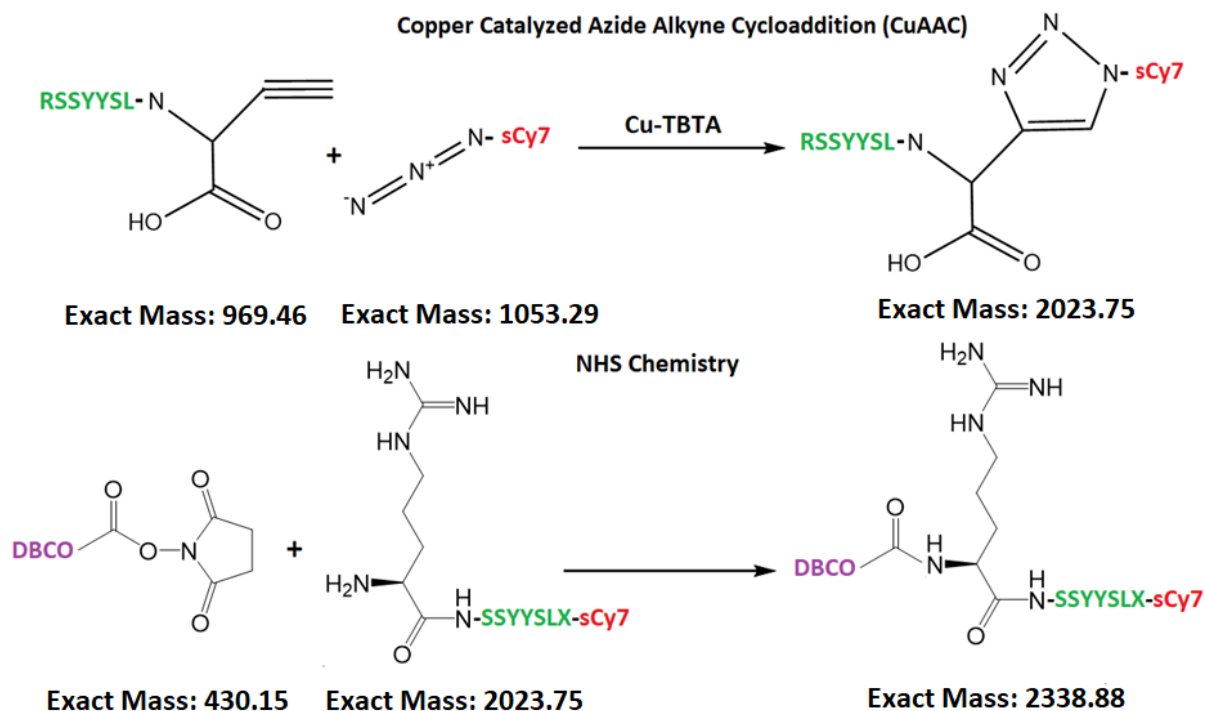


**Figure 4.1:** Synthesis plan for DBCO-RSSYYSLX-Cy7. CuAAC with TBTA will be first used to conjugate the sCy7 while on the other side, the N-terminus will be conjugated with DBCO using NHS chemistry.

In order to start in vivo work, a stronger fluorescing dye and a DBCO click chemistry moiety to interact with the azide-modified alginate are needed. Hence, synthesis of DBCO-RSSYYSLX-sCy7 was attempted with a copper catalyzed click chemistry reaction on the propargylglycine and an NHS reaction on the N terminus (Figure 4.1).

The sCy7-azide was successfully conjugated (Figure 4.2) but the NHS reaction encountered difficulties. Initially, the NHS reaction was performed right after the click chemistry reaction, but the expected product mass did not show up on the LCMS. This may have been due to the interference with the chemicals already present from the click chemistry reaction, specifically the Cu:TBTA complex which is known to be a strong oxidizing agent [1]. Therefore,

the NHS reaction was repeated with preparatory HPLC purified RSSYSLX-sCy7 but while the mass was observed on the LCMS, the yield was very low (Figure 4.3).

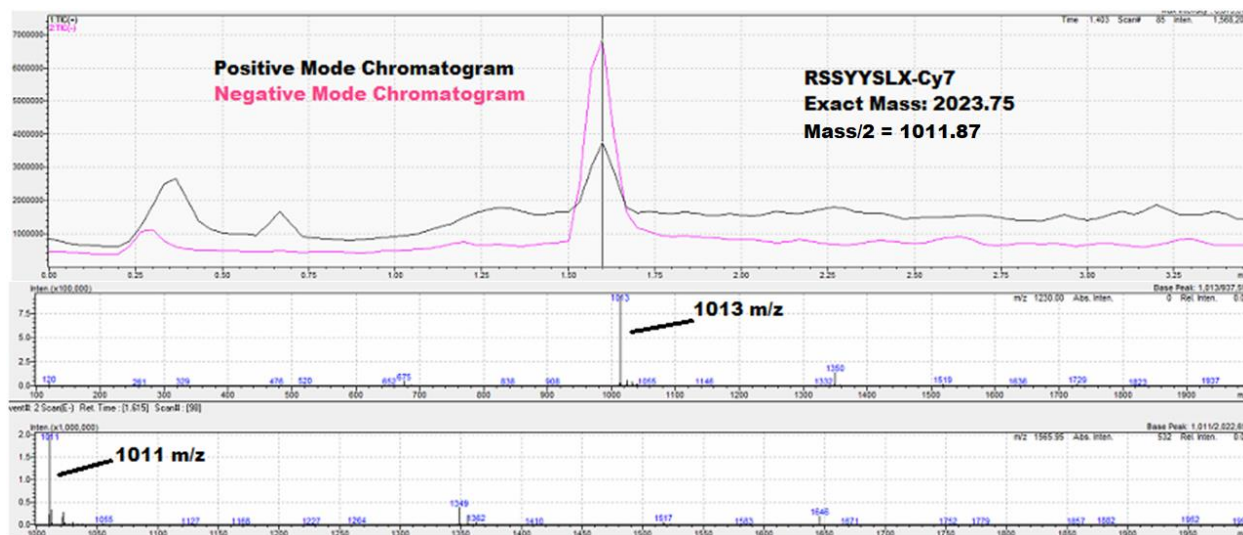


**Figure 4.2:** LCMS of the RSSYSLX-Cy7 after preparatory HPLC purification shows successful collection of my molecule in both positive (1013 m/z) and negative (1011 m/z) modes. Both ESI modes are shown in the LCMS where top is the positive mode and the bottom is the negative mode.

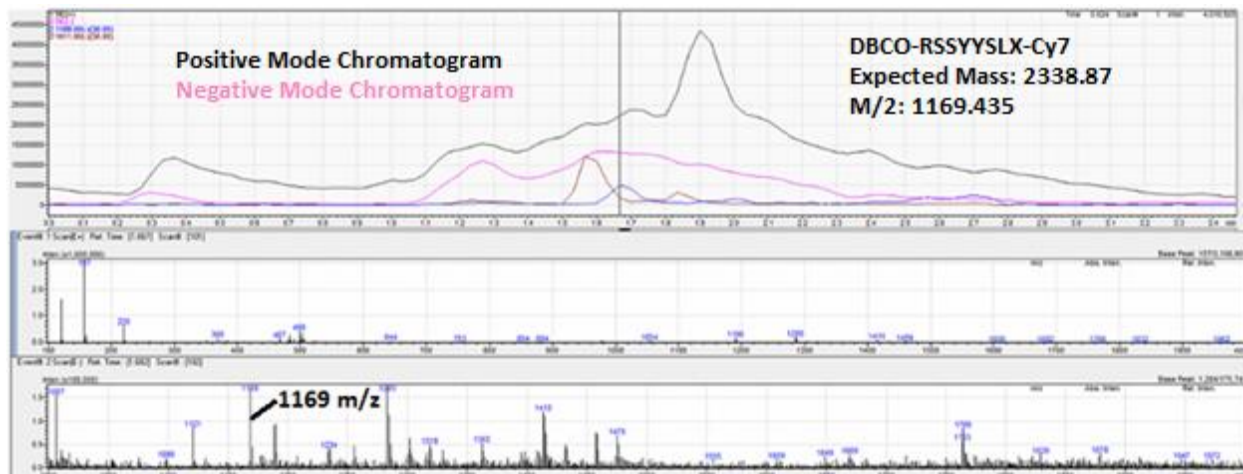


**Figure 4.3:** LCMS analysis of the DBCO-RSSYSLX-Cy7 reaction shows a small peak of the expected product mass in the negative mode with a slight deviation (DBCO-RSSYSLX-Cy7 M/2 = 1169.435). Both ESI modes are shown in the LCMS where top is the positive mode and the bottom is the negative mode.

Thus, an alternative strategy with RSSYYSLC was attempted with a maleimide reaction to attach sCy5 followed by NHS chemistry to attach the DBCO on the N-terminus of the peptide (Figure 4.4). The reaction and purification proceeded smoothly and a 30.7% yield of the DBCO-RSSYYSLC-sCy5 molecule (DPC) was measured (Figures 4.5 and 4.6). Using a method similar to the shake flask method, a solubility of 51.07  $\mu\text{M}$  was observed for DPC (Figure 4.7).

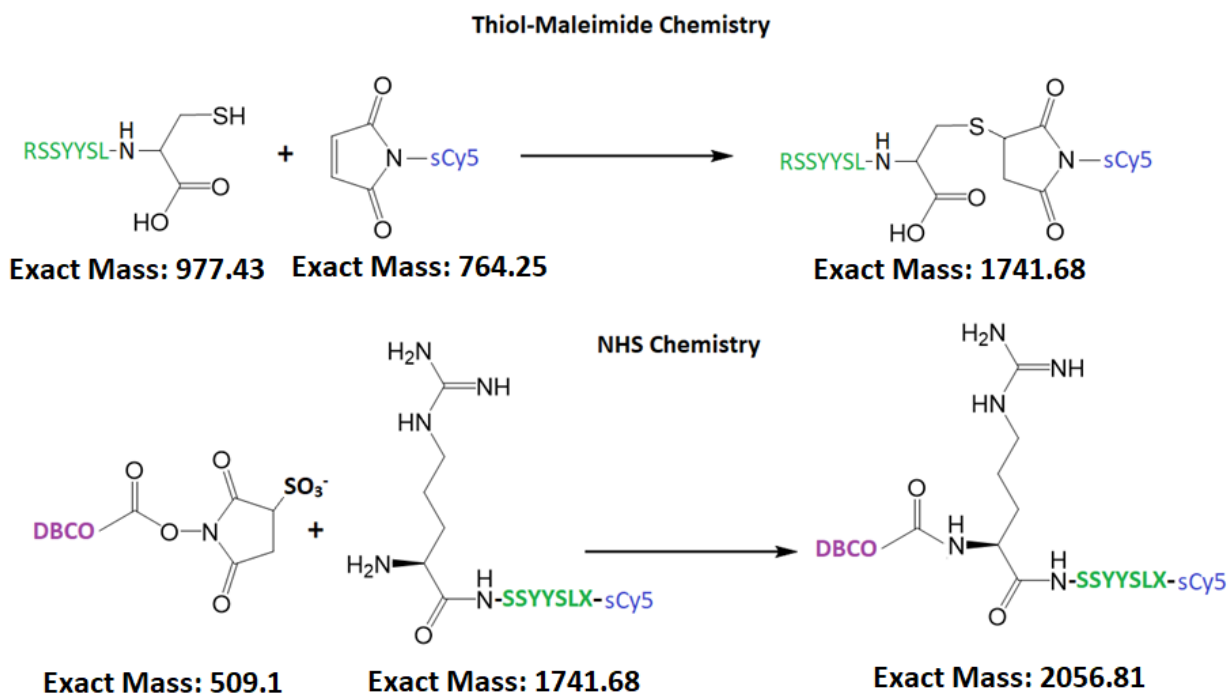


**Figure 4.4:** Strategy for the synthesis of DBCO-RSSYYSLC-sCy5. Thiol-Maleimide chemistry will be first used to attach sCy5 onto the C-terminal end while the N-terminal amine will be conjugated to DBCO using NHS chemistry.

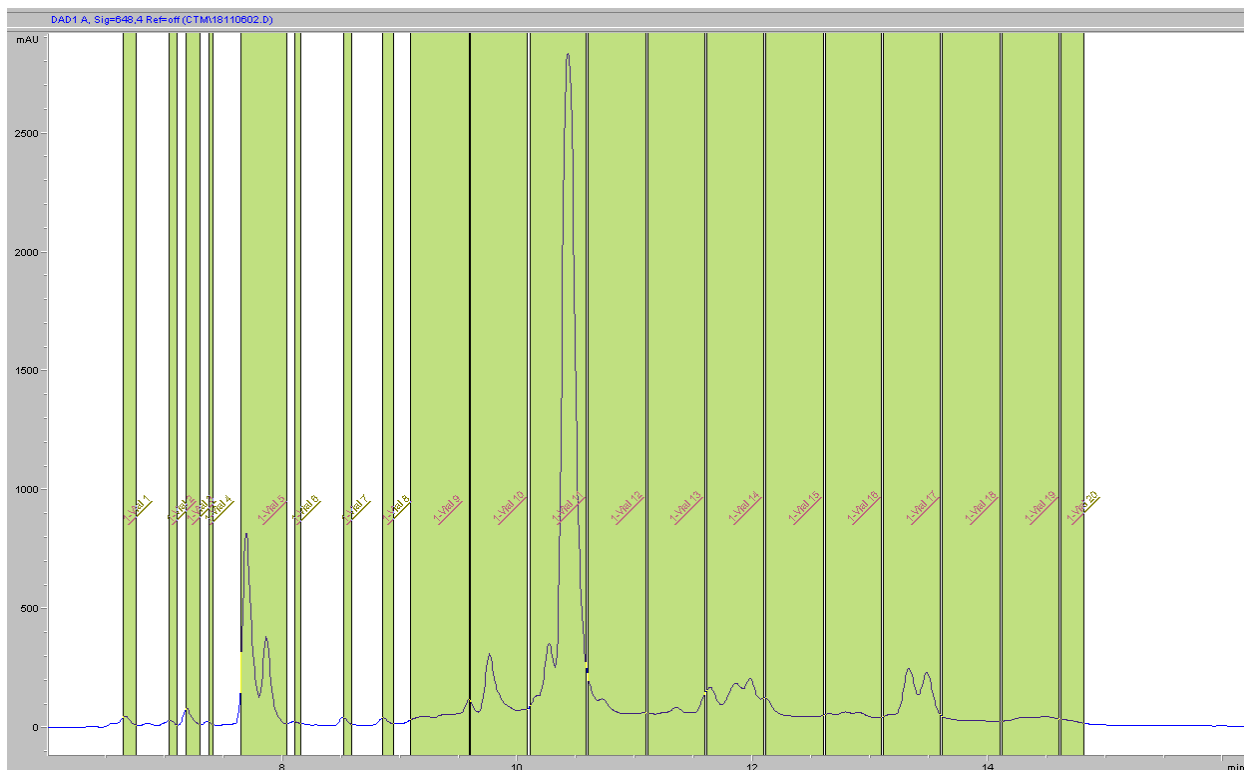


**Figure 4.5:** Chromatogram of the purification and fraction collection of DBCO-RSSYYSLC-sCy5 using preparatory HPLC using a peak based method at 648 nm. The peak with 11-minute retention time was collected.

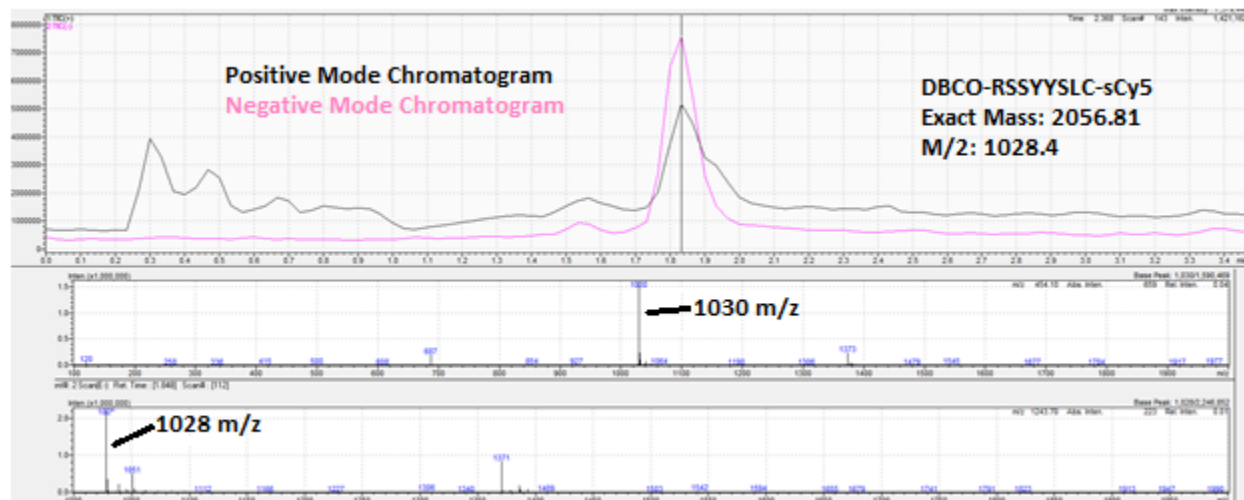


**Figure 4.6:** LCMS analysis of DPC after purification shows successful collection and relative purity of the molecule in both the positive and negative mode. Both ESI modes are shown in the LCMS where top is the positive mode and the bottom is the negative mode.

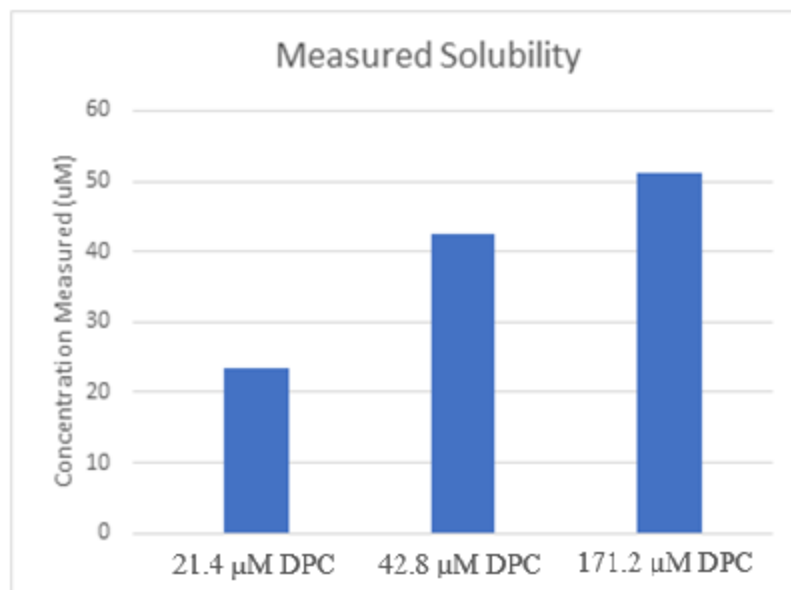


**Figure 4.7:** Solubility for DPC measured at PBS:DMSO (9:1) using a method based on the shake flask method yielded a solubility of 51.04  $\mu\text{M}$ .

Azide-modified alginate were then synthesized by using EDC/NHS chemistry to modify the carboxylic acid groups with azides (Figure 4.8). The alginate was designed to have approximately 40 azides per alginate strand as my fellow lab mate has experienced optimal calcium crosslinking at 40 azides per alginate strand. The resulting synthesis yielded ~37 azides per alginate strand. With the alginate, the Peptide Specificity Experiment was then reattempted with no serum RPMI. Calcium crosslinked alginate gels were incubated with cell culture media where the fluorescence of the supernatant was measured to detect cleaved Cy5 containing molecules (Figure 4.9). The results of the experiment are shown in Figure 4.10.

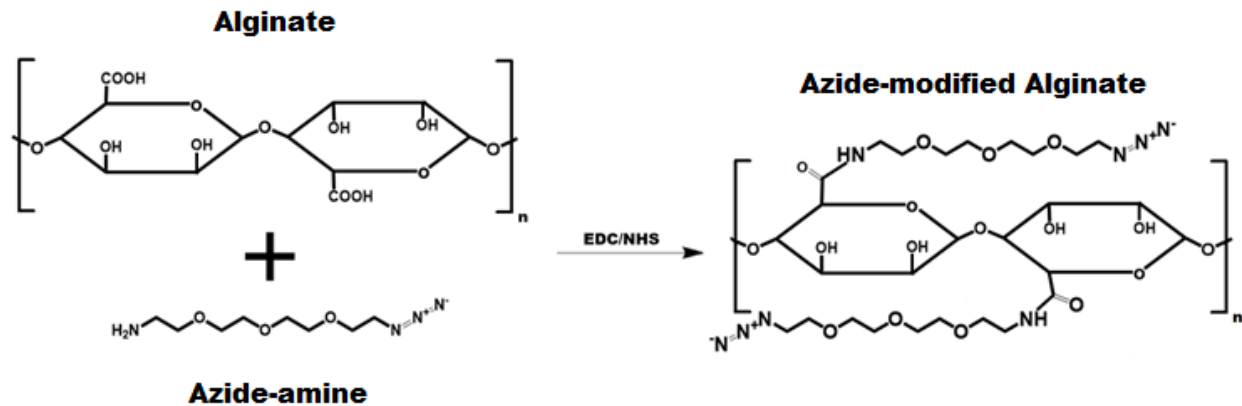


**Figure 4.8:** Schematic of the modification of alginate with azide-amine through EDC/NHS chemistry by targeting the carboxylic acid groups on the alginate strands.

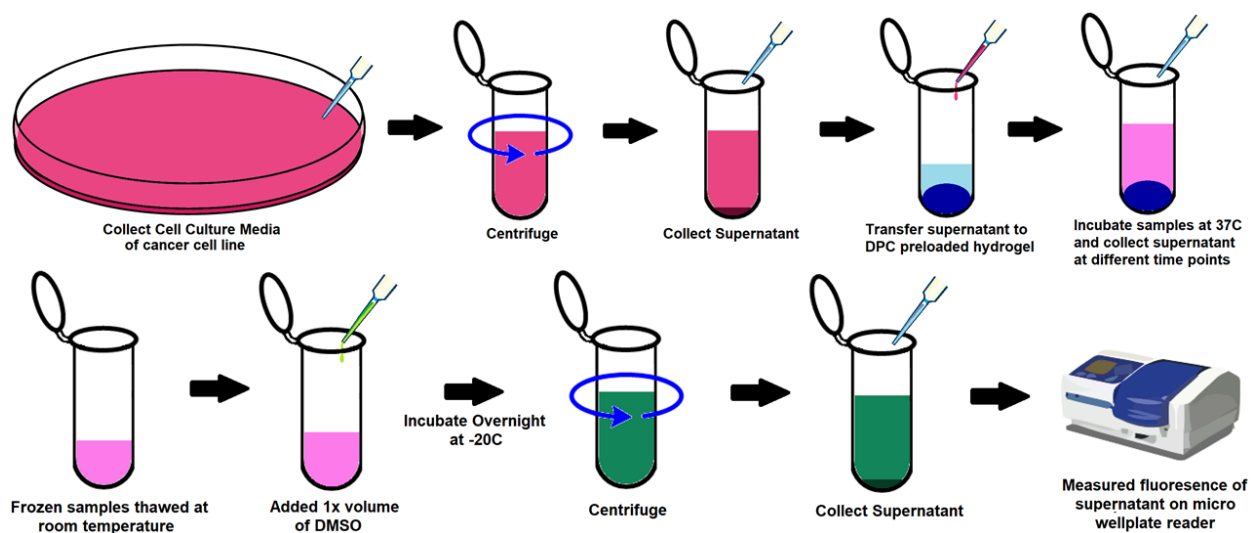


**Figure 4.9:** Schematic for the Peptide Specificity Experiment with crosslinked DPC preloaded alginate hydrogel. Cell culture media supernatant were collected and incubated with the crosslinked DPC preloaded alginate hydrogel at 37°C. The supernatant was collected at time points and were stored at -80°C. Samples were thawed together at room temperature after collection of the last time point, whereupon the sample was precipitated with DMSO and the fluorescence of the supernatant measured on the micro well plate reader.

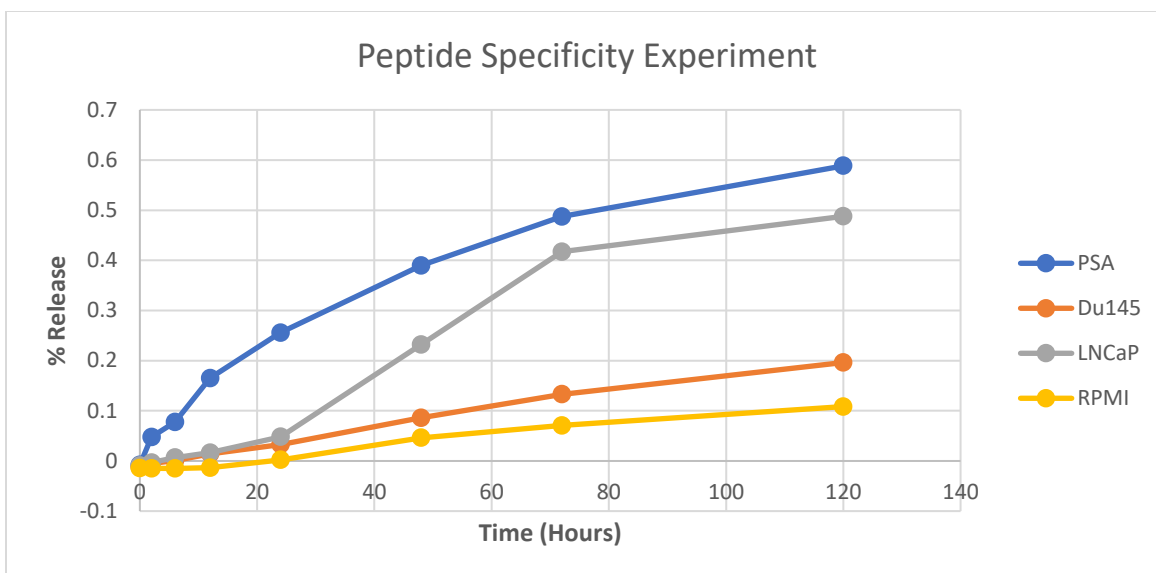


**Figure 4.10:** Peptide Specificity Experiment results with preloaded calcium crosslinked hydrogels show significant cleavage by LNCaP cell culture supernatant during incubation with the preloaded hydrogels. The difference between Du145 and LNCaP groups were statistically significant ( $p < 0.05$ ). The difference between Du145 and RPMI was also statistically significant ( $p < 0.05$ ), suggesting that the Du145 is cleaving the peptide linkers to release Cy5, albeit at a much slower rate compared to LNCaP.

LNCaP showed a much higher release than that of the negative controls which was statistically significant ( $p < 0.05$ ). However, some signal was measured in the RPMI control, presumably the passive release of unbound DPC. In addition, Du145 is also releasing a bit more than the RPMI control, suggesting some cleavage of my peptide by the Du145 extracellular media.

The loading efficiency of DPC onto azide-modified alginate was then measured. The procedure was done by loading DPC onto the azide-modified alginate, followed by fluorescence measurement of the supernatant after precipitation of the alginate (Figure 4.11). It is assumed that the measured fluorescence represents unbound DPC molecules, and that the amount calculated by subtracting the measured amount from how much was initially added is equal to the amount of DPC bound onto the alginate strands. The results in Figure 4.12 show about 60% loading efficiency after 24 hours of incubation with loading concentrations between 0.27 to 4.44  $\mu\text{M}$ . Thus, it is implied that 40% of the DPC are unbound which helps support the hypothesis

that the signal in RPMI control was due to unbound DPC. A loading efficiency of ~3% was measured for the unmodified control alginate which may have been due to some DPC being stuck in the precipitated alginate pellet.

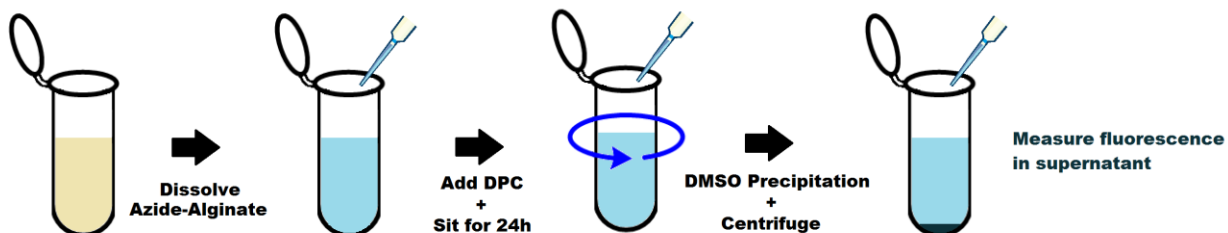


**Figure 4.11:** Schematic for the measurement of the loading efficiency. Alginate was loaded onto the alginate strands for 24 hours before DMSO precipitation and subsequent analysis of the fluorescence in the supernatant. The calculated value was subtracted from the added amount to calculate the amount of DPC loaded onto the alginate.

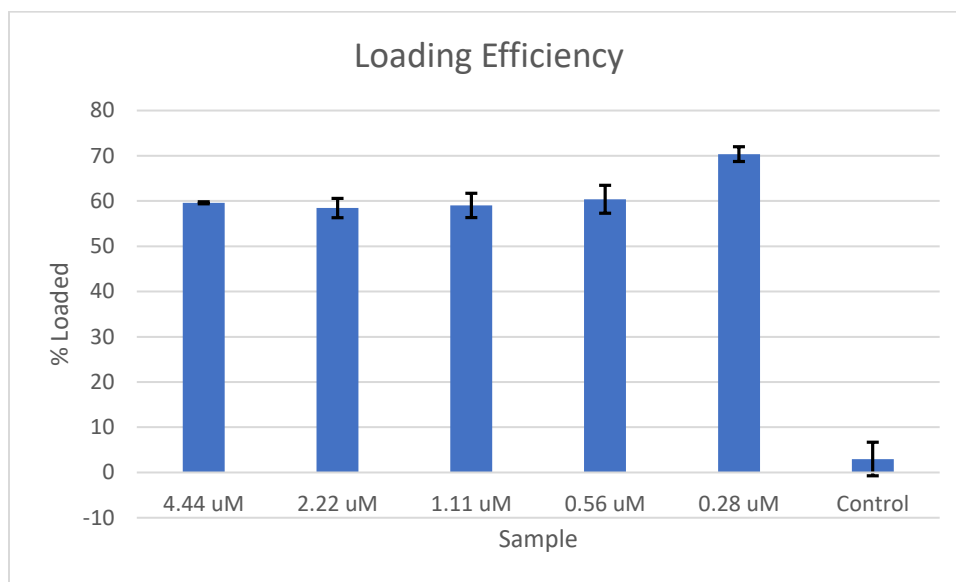


**Figure 4.12:** Summary of the loading efficiency measurements show about 60% loading efficiency at different concentrations. The control unmodified alginate measured about 3% loading efficiency which was deemed insignificant. Error bars represent the standard deviation of the samples.

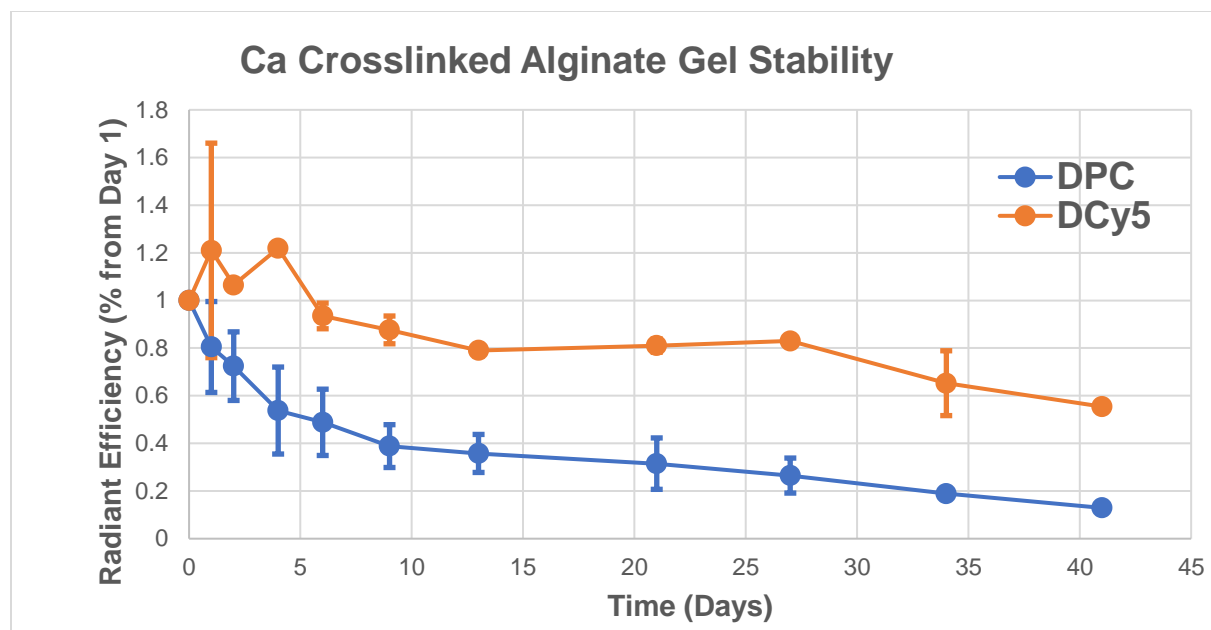


**Figure 4.13:** Fluorescent measurements for the In vivo stability experiment with preloaded calcium crosslinked gels (n=2). Alginate were preloaded with DPC for 24 hours before crosslinking with calcium followed by subcutaneous injection into the subcutaneous space in male CD1 mice. The fluorescence measurement results show instability of the device in vivo for both DPC and DCy5 preloaded gels.

The calcium crosslinked preloaded gels were then injected in vivo in male CD1 mice to test the stability of the device in absence of a tumor in the subcutaneous space. The gels were preloaded with either DCy5 (control) or DPC (experimental) before crosslinking and subsequent injection into the mice. The fluorescence was measured over time and the measured signal was background subtracted and taken as a percentage of the initial measurement. It was reasoned that the large drop in signal from Day 0 to Day 1 was due to release of unbound DPC and alginate strands dissociating from the bulk gel due to incomplete crosslinking. Hence, the initial measurement was assumed to be representative at Day 1, 24 hours after the initial injection at Day 0. The results are summarized below in Figure 4.13 and suggest poor stability of both DPC and DCy5 preloaded gels. On a related note, during the Peptide Specificity Experiment with the calcium crosslinked preloaded alginate hydrogels, it was observed that the calcium and alginate strands seem to dissociate from the gel by the 5<sup>th</sup> day. Taken together, it was concluded that the decrease in fluorescence observed in vivo isn't necessarily due to cleavage of the peptide but

possibly due to potential instability of calcium-crosslinked alginate gels. Therefore, an alternative crosslinker may be ideal.

Tetra-BCN was considered as an alternative crosslinker for the alginate gel. T-BCN is a molecule with four BCN arms that crosslinks azide-modified alginate by using the BCN arms to directly bind onto the azide-groups to connect strands of alginate together (Figure 4.14).

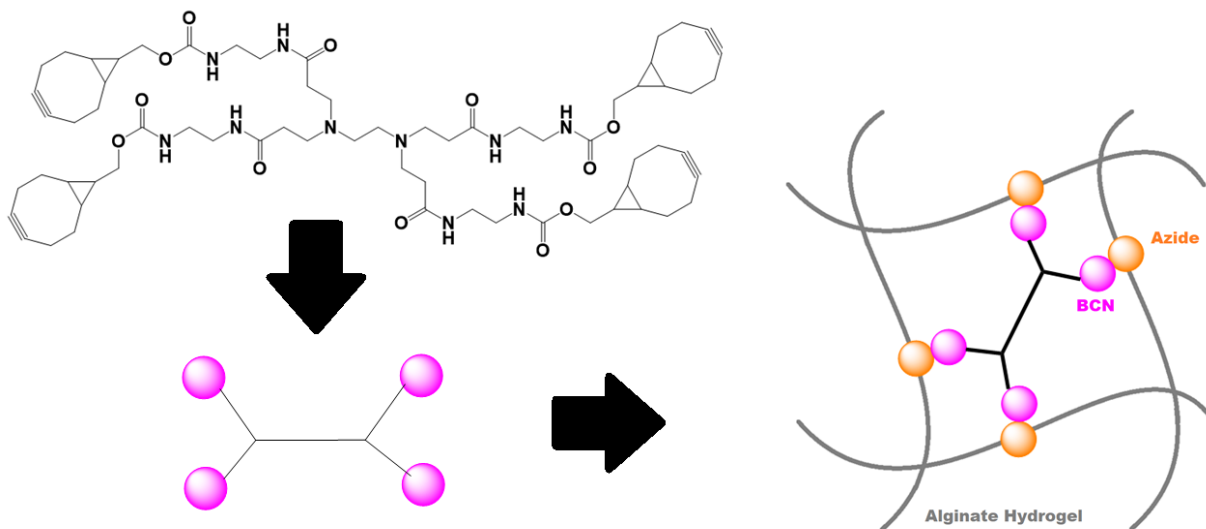


**Figure 4.14:** Schematic for T-BCN crosslinking of azide-modified alginate strands to create a hydrogel.

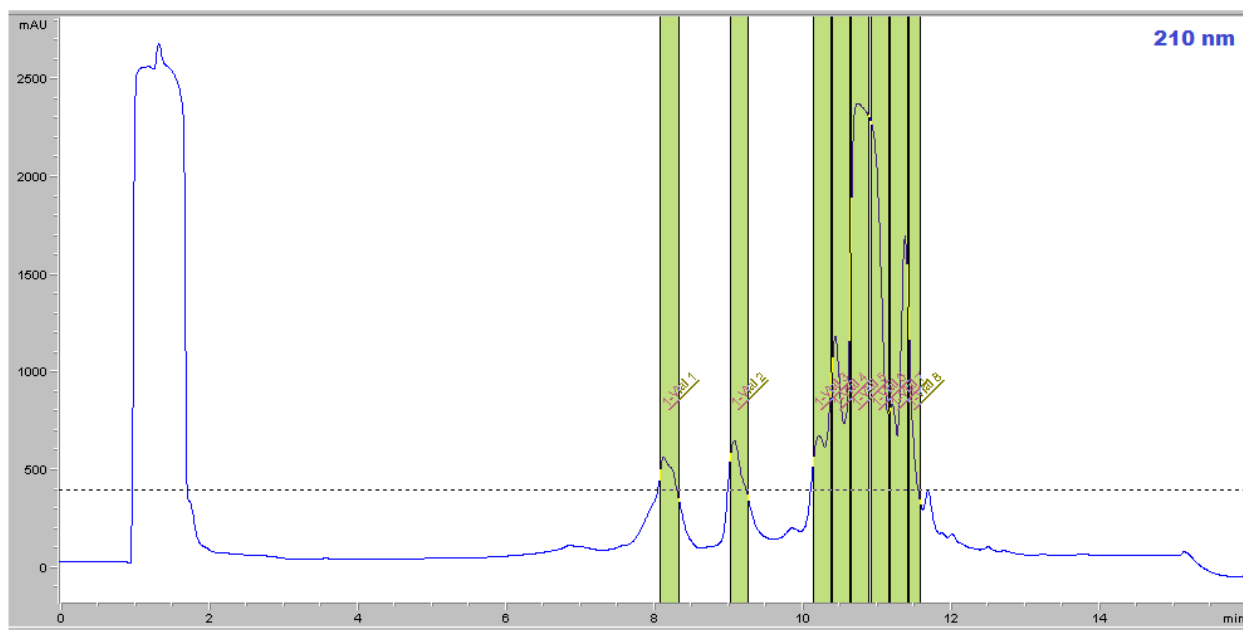


**Figure 4.15:** Chromatogram at 210 nm for the preparatory HPLC purification and fraction collection of T-BCN using a peak based method at 210 nm. Peak with 10.9-minute retention time was collected.

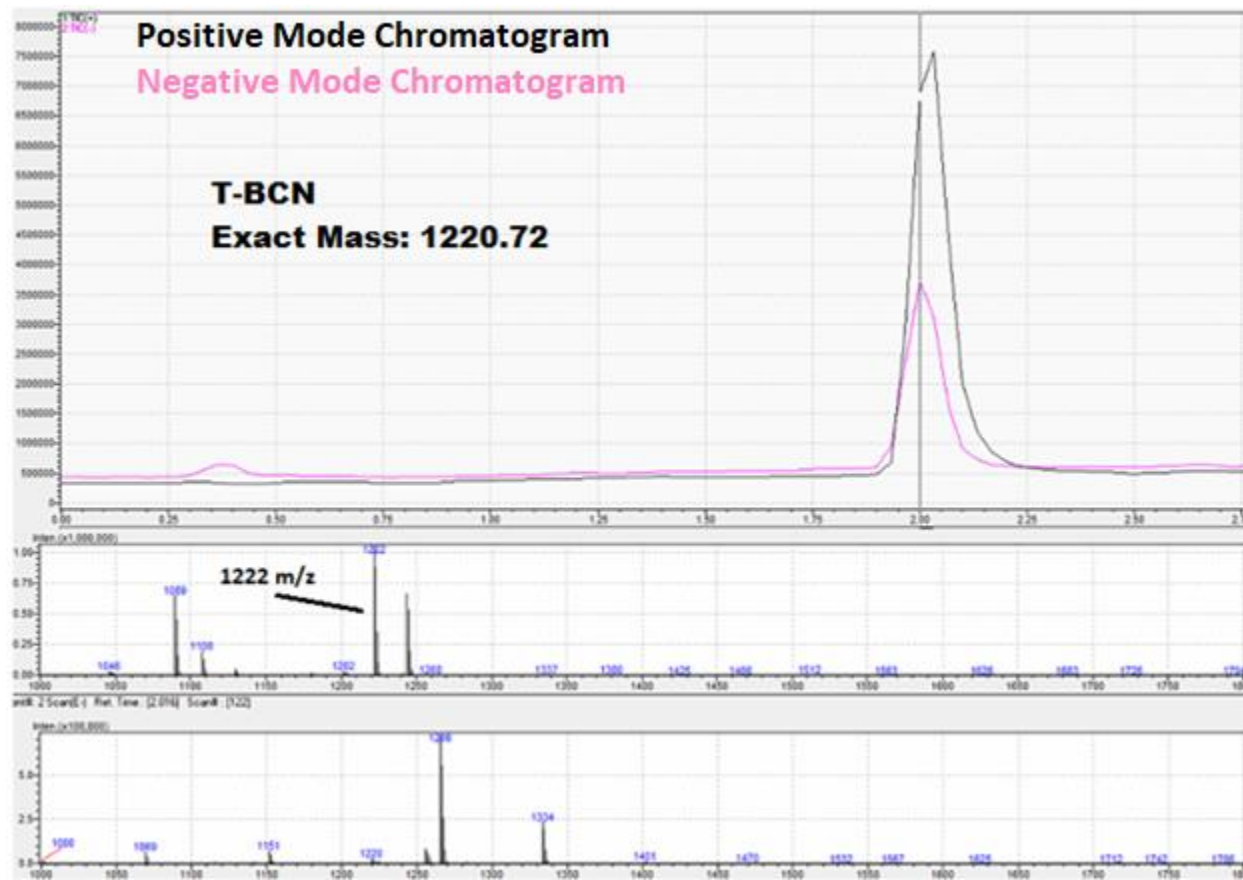


**Figure 4.16:** LCMS of the preparatory HPLC purified T-BCN shows successful collection of the product with detection of 1222 m/z in the positive mode ( $1221 + [H]^+$  m/z). Both ESI modes are shown in the LCMS where top is the positive mode and the bottom is the negative mode.

T-BCN was synthesized with NHS chemistry and a ~97% yield was attained (Figures 4.15 and 4.16). The T-BCN was then used to repeat the In Vivo Stability Experiment. DPC or DCy5 preloaded alginate were crosslinked with T-BCN and injected into male CD1 mice (Figure 4.17). Compared to what was observed in the calcium crosslinked hydrogel, the T-BCN crosslinked hydrogel seemed to have a much more stable signal in both the DPC and DCy5 groups, suggesting better stability of the hydrogel. While the difference between DPC and Cy5 were found to be almost statistically significant (calculated p-value of 0.06196), the plateau in the fluorescence measurement seems to suggest some potential for long-term stability but further measurement will be needed for a definitive conclusion.

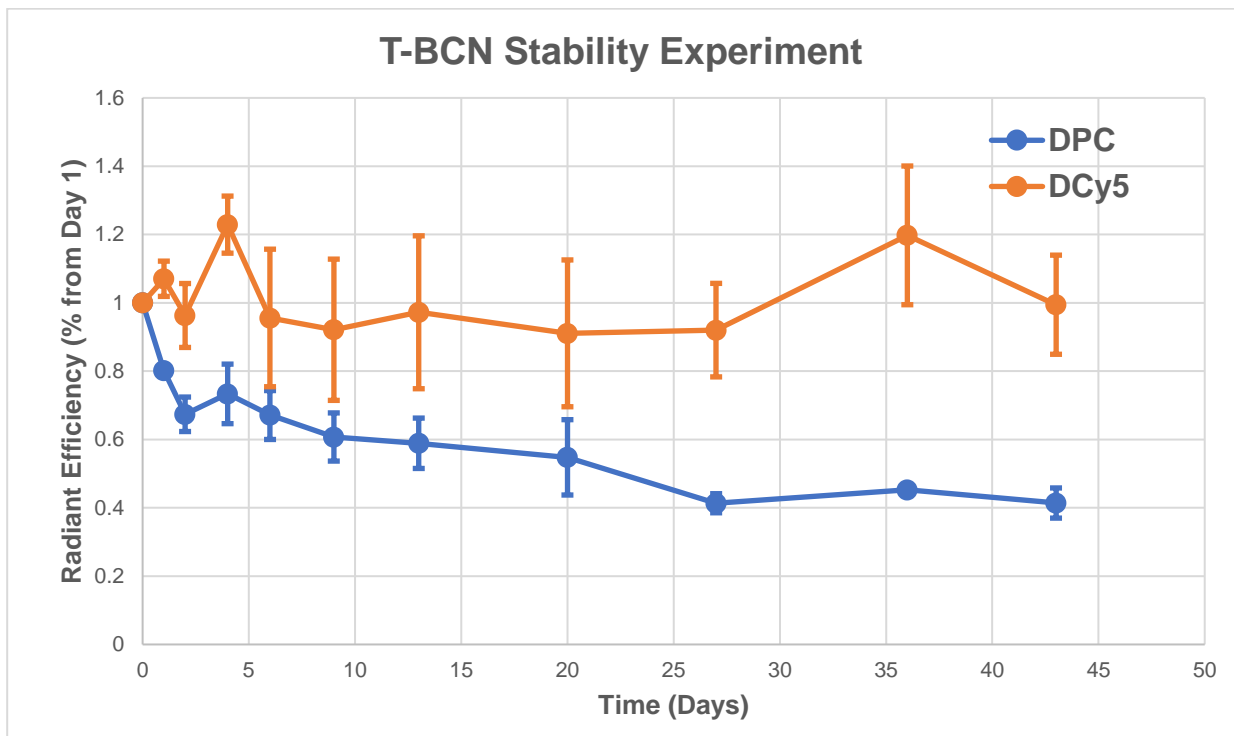


**Figure 4.17:** In vivo stability experiment repeated with preloaded T-BCN crosslinked alginate gels (n=2). Alginate gels were preloaded with DPC for 24 hours before crosslinking with T-BCN for 30 minutes, followed by subcutaneous injection into male CD1 mice. The fluorescence measurements show higher stability with both DPC and DCy5 compared to that of the calcium crosslinked counterpart.

The Peptide Specificity Experiment was then repeated with the T-BCN crosslinker (Figure 4.18). The results showed no difference between the groups outside the positive control. However, there was some promise shown towards the end where the fluorescence in the LNCaP group sharply increased.

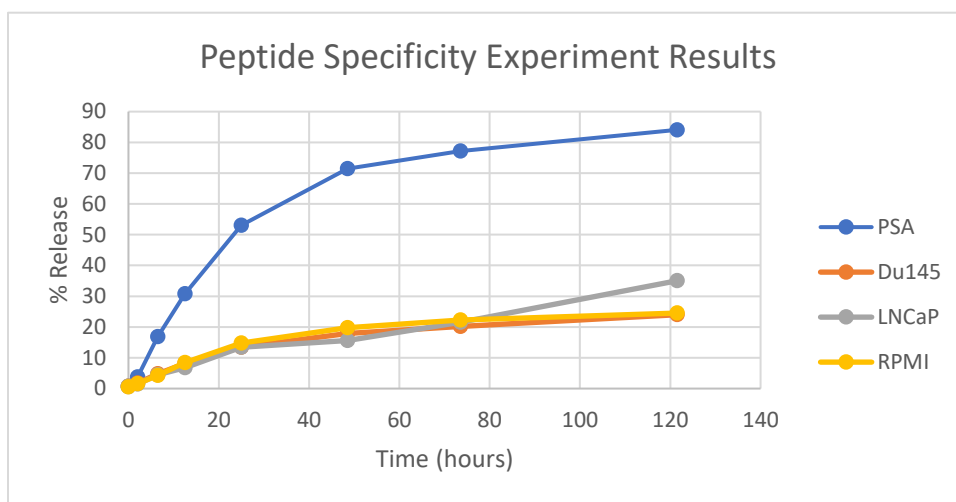


**Figure 4.18:** Peptide Specificity Experiment results with DPC preloaded T-BCN crosslinked alginate gels. DPC preloaded gels were crosslinked with T-BCN overnight before addition of cell culture media. Fluorescence measurements of the supernatant show inconclusive results that were very different from the calcium crosslinked version (Figure 4.10).

During the experiment, the hydrogel was observed to expand over time. It was also noticed that normally, the hydrogel layer is hard to see due to the transparency of the material. However, in the Du145 and LNCaP samples, the hydrogel surface acquired a faint grey-brown color allowing for easy identification, presumably due to the miscellaneous extracellular secretions by the cells in culture. With this in consideration, a possible explanation could be that the surface of the hydrogel becomes blocked by all these miscellaneous materials, limiting the diffusion of PSA inwards. Thus, it is possible that the increased signal observed in the LNCaP group was due to the hydrogel expanding enough so that the PSA can access and cleave the peptide to release the fluorophore. In summary, the experimental result was inconclusive, and the

experiment would need to be repeated with preloaded hydrogels that were given time to swell prior to starting the experiment.

The kinetics were then measured for DPC while bound onto the alginate hydrogel. Complications arose when attempting to measure the proper Michaelis-Menten parameters, mainly not having enough azides on the gel for the required concentrations. Proper methodology for measuring  $k_{cat}$  and  $K_m$  requires a large range of concentrations centered around the  $K_m$  which was not feasible due to the limited amount of azides per alginate strand [2]. The azide per alginate strand ratio could be increased for future studies but from a fellow lab member's experience, the properties of the alginate change as more azides are added, presumably due to the loss of the carboxylic acid groups. Thus, proper care and consideration would be needed in that regard. Nonetheless, for the current limitation, an assumption that the concentration of substrate will always be much lower than that of the  $K_m$  ( $270 \times 10^{-6}$  M for SSYYSG [3]). The assumption allows one to calculate  $k_{cat}/K_m$  by measuring the velocity of the reaction with any substrate concentration, assuming the substrate is detectable at the chosen concentration. The reaction rate was measured at a concentration range between 0.27 and 4.44  $\mu$ M with a good linearity (Figure 4.20). The time at which to stop and measure the reaction was estimated through the peptide specificity data based on the initial linear region where the reaction velocity is at its maximum. A  $k_{cat}/K_m$  value of  $160 \text{ s}^{-1}\text{M}^{-1}$  was observed which was quite different from the literature reported value of  $3100 \text{ s}^{-1}\text{M}^{-1}$  for SSYYSG [3]. However, this isn't too surprising since DBCO-RSSYYSLC-sCy5 is quite different to that of SSYYSG. For instance, the lowered kinetics could possibly be due to the sCy5 hindering the enzymatic cleavage. In addition, the lower reaction

rate can reasonably be explained by the limited accessibility of the enzyme to the bound substrate in the hydrogel matrix.

$$V = \frac{k_{cat} * [E] * [S]}{K_m + [S]}$$

$$K_m \gg [S] : V = \frac{k_{cat} * [E] * [S]}{K_m}$$

**Figure 4.19:** Michaelis Menten Kinetics Equation. With the assumption that  $K_m \gg [S]$ , we can easily measure  $k_{cat}/K_m$ .

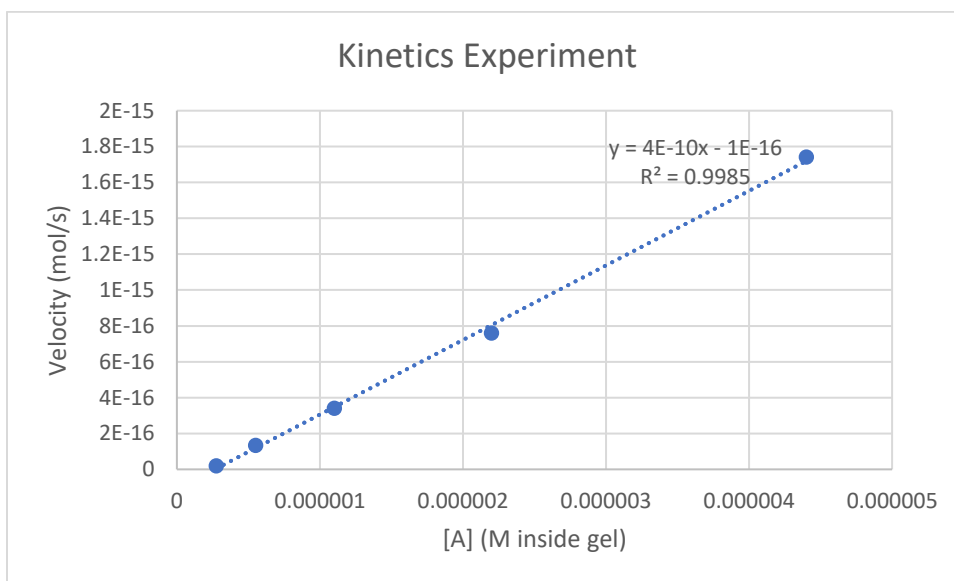


**Figure 4.20:** Result from the kinetics experiment after 7 hours reaction of the DPC preloaded T-BCN crosslinked alginate gel. The fluorescence of the supernatant was measured and the reaction velocity (mol/s) was calculated using a standard curve. The slope was used to calculate a  $k_{cat}/K_m$  value of  $160 \text{ s}^{-1}\text{M}^{-1}$ .

Finally, a tumor experiment was done to determine the functionality of the device. An initial experiment was done where LNCaP cells and DPC preloaded T-BCN crosslinked alginate gels were injected together on the right flank whereas the same gel was crosslinked alone on the left flank as a control (Figure 4.21). There was a significant decrease in signal after the tumor started visibly growing at Day 22 that was almost statistically significant at Day 33 (pvalue = 0.0558). However, there is the possibility that the decrease in signal isn't due to cleavage of the peptide but due to the tumor mass growing around the hydrogel and blocking the signal.

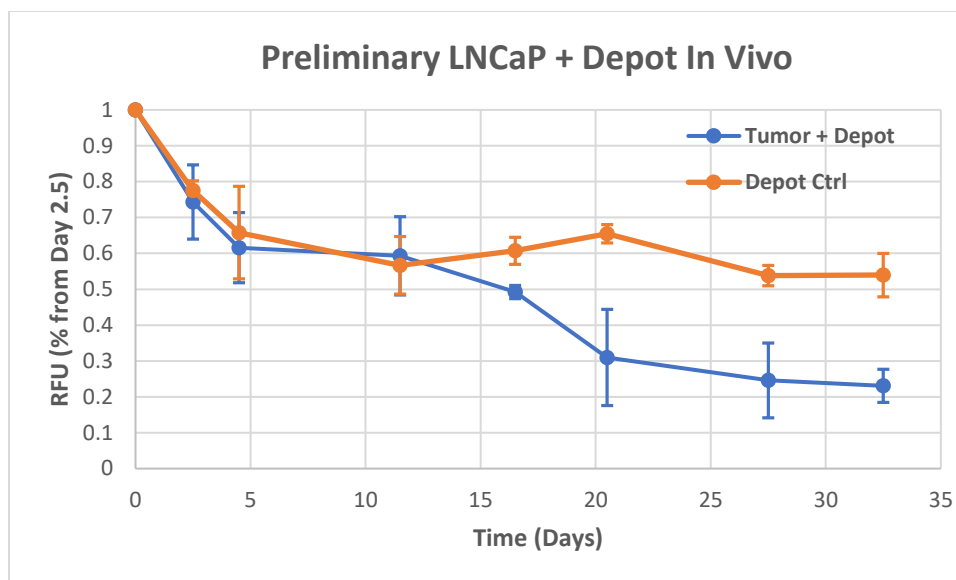


**Figure 4.21:** Result from In Vivo Tumor Experiment with DPC preloaded T-BCN crosslinked alginate gels (n=2). Alginate gels were preloaded with DPC for 24 hours before 30 minutes of T-BCN crosslinking followed by co-injection of the gel and the LNCaP tumor cells in Matrigel (3 million cells). The preliminary results suggest increased reduction in signal by the PSA (+) LNCaP tumor starting at around 15 days. Calculated p-value = 0.0558 at the last time point. The error bars are standard error mean.

The tumor experiment was repeated where the preloaded T-BCN crosslinked gels were injected 24 hours after the initial Matrigel/Tumor injection at the same location marked the day before. In addition to the DPC preloaded gels, DCy5 preloaded gels were also injected at the tumor site as a separate control. The results are summarized in Figure 4.22. While the DPC depot + LNCaP showed decreased fluorescent signal compared to the DPC depot + Matrigel control, the difference was not found to be statistically significant (pvalue = 0.1568 at Day 30). The DCy5 depot + LNCaP control seems to suggest some influence on the measured fluorescence by the tumor. It was also observed that by injecting the depot 24 hours after the initial tumor inoculation, the resulting tumor growth pushed the hydrogel depot away from the initial injection site, contrary to the preliminary experiment where co-injection resulted in tumor growth around the depot. This tumor growth induced jostling seemed to affect the orientation of the gel, increasing or decreasing the fluorescent signal based on the random tumor growth in an inconsistent manner. The result of this interaction can be seen by the large error bars observed in

both tumor groups. Thus, it is difficult to say whether the PSA expressing LNCaP tumors cleaved the peptide linkers to release fluorophore if at all. However, even if cleavage activity by PSA was present in the experiment, the kinetics are a lot slower than expected based on the Peptide Specificity Experiment results with the calcium-crosslinked alginate gels (Figure 4.10). Thus, the key goal for future work is to analyze the Peptide Specificity Experiment results with the T-BCN-crosslinked alginate gels and investigate why the abnormal release curve observed during incubation with LNCaP.

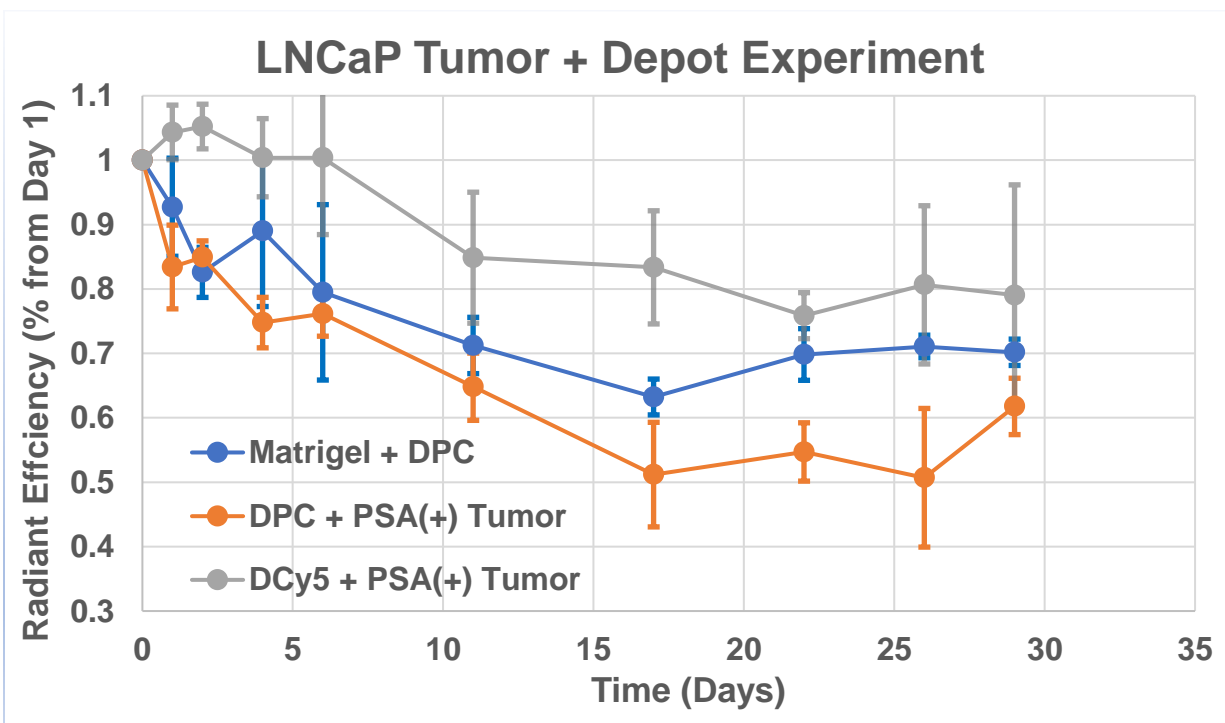


**Figure 4.22:** Results from the LNCaP Tumor + Depot Experiment (n=3). Alginate were preloaded with DPC or DCy5 for 24 hours before 30-minute crosslinking with T-BCN. The gel was then injected subcutaneously with either Matrigel or the LNCaP tumor cell mixture (3 million cells). The resulting measurements show inconclusive results (pvalue = 0.1568 at Day 30 between DPC + LNCaP and DPC + Matrigel) with large variability within the tumor containing groups. The error bars are standard error mean.

## 4.2. References

- 1) Hein, J. E., & Fokin, V. V. (2010). ChemInform Abstract: Copper-Catalyzed Azide-Alkyne Cycloaddition (CuAAC) and Beyond: New Reactivity of Copper(I) Acetylides. ChemInform, 41(28). doi:10.1002/chin.201028218
- 2) Bisswanger, H. (2013). Practical Enzymology. Hoboken: Wiley.
- 3) Coombs, G. S., Bergstrom, R. C., Pellequer, J. L., Baker, S. I., Navre, M., Smith M. M., Tainer J. A., Madison E. L., Corey, David. R. (1998). Substrate specificity of prostate-specific antigen (PSA). Cell Chemical Biology, 5(9), 475-488.

## Chapter 5: Conclusion

### 5.2. Conclusion

There is currently a lack of devices that have high selectivity towards tumors, that can wait in the extracellular space for long periods of time and remain effective upon sensing a tumor. This dissertation seeks to demonstrate the possibility of such a device through achieving two goals: to demonstrate negligible release in absence of a tumor and to show rapid release in response to a tumor. Of the two, the dissertation showed a strong support for the former. The results in the *in vivo* stability experiment show a plateauing release curve after an initial drop, suggesting a potentially stable device. Further testing for longer periods of time are required to determine whether this plateauing behavior will continue for months to prove the long-term stability of the device. On the other hand, the dissertation was not able to demonstrate a fast, preferential release towards a PSA expressing tumor. The tumor experiment was inconclusive with the seemingly slow release in response to the tumor and the random tumor growth resulting in inconsistent measurements. The key for future work lies in the analysis of the cleavage of DPC in T-BCN-crosslinked alginate gels by PSA in a variety of conditions to better understand the underlying mechanisms. Future work would also need to be done to show the potential application of the device as either a diagnostic or therapeutic in a local tumor recurrence model. A critical additional step in the realization of the device is to demonstrate the refillability of the device. With a refillable device, some non-specific release is tolerable, as long as an effective concentration of active agent remains over the scale of months. Thus, with a refill every couple of months, one can achieve a device that remains effective for years on end. In theory, the current design of the device should allow for refillability through systemic injection but complications had arisen and due to lack of time, the refillability was not properly investigated

and was consequently not addressed in this dissertation. Altogether, further work would need to be done to determine whether the presented device can prove the possibility of creating a long-term sentinel gel for early tumor recurrence detection.

## APPENDICES

## Appendix A

### List of Abbreviations

ACN	Acetonitrile
BCN	bicyclo[6.1.0]nonyne
BMP	Bone morphogenic protein
CREKA	Cys-Arg-Glu-Lys-Ala peptide amino acid sequence
Cu	Copper
CuAAC	Copper Catalyzed Azide-Alkyne Cycloaddition
Cy5.5	Cyanine 5.5
DBCO	Dibenzocyclooctyne
DCM	Dichloromethane
DIPEA	N,N-Diisopropylethylamine
DMF	Dimethylformamide
DMSO	dimethyl sulfoxide
Dox	Doxorubicin
DPC	DBCO-RSSYYSLC-Cy5
EDC	1-ethyl-3-(3-dimethylaminopropyl)carbodiimide
EDTA	Ethylenediaminetetraacetic acid
FBS	Fetal Bovine Serum
FITC	6-fam
Fmoc	Fluorenylmethyloxycarbonyl
HPLC	High performance liquid chromatography
HPMA	N-(2-hydroxypropyl)methacrylamide
LCMS	liquid chromatography mass spectroscopy
MMP	Matrix metalloproteinase
MTBE	methyl tert-butyl ether
NHS	N-hydroxysuccinimide
PBS	phosphate buffered saline
PEG	polyethylene glycol
PLL	poly-L-lysine
PSA	Prostate Specific Antigen
RGD	Arg-Gly-Asp peptide amino acid sequence
RSSYYSL	Arg-Ser-Ser-Tyr-Tyr-Ser-Leu peptide amino acid sequence
sCy5	sulfo-Cyanine5.5
sCy7	sulfo-Cy7
sNHS	sulfo-N-hydroxysuccinimide
SPAAC	strain promoted azide alkyne cycloaddition
T-BCN	Tetra-bicyclo[6.1.0]nonyne
TBTA	Tris(benzyltriazolylmethyl)amine
TIS	Triisopropyl silane
UNC	University of North Carolina Chapel Hill

## Appendix B

### Matlab Code for Comparison of Kinetics Between RSSYYSL and HSSKLQ

Assumption: Kinetics were evaluated using 45 nM enzyme concentration based on the measured extracellular PSA concentration in LNCaP xenografts [1]. The kinetic parameters for RSSYYSL [2] and HSSKLQ [3] were obtained from literature.

RSSYYSL:

```
kcat = 0.83;  
Km = 270*10^-6;  
SC = 1.11*10^-6;  
Smax = 1.11*10^-6;  
EC=45*10^-9;  
t=2;  
TF = 30;
```

```
Cm = [0];  
Tm = [0];  
SCm = [SC];
```

```
while(t<3000)  
    v = kcat*EC*SC/(SC+Km);  
    SC = SC-v*TF;  
    Tm = [Tm,t-1];  
    SCm = [SCm,SC];  
    t=t+1  
end
```

```
TmHours = Tm/(2 *60)  
plot(TmHours,SCm/Smax)  
title('RSSYYSL Kinetics')  
xlabel('Time (Hours)'),ylabel('Uncleaved Peptide (%)')
```

HSSKLQ:

```
kcat = 0.0096;  
Km = 475*10^-6;  
SC = 1.11*10^-6;  
Smax = 1.11*10^-6;  
EC=45*10^-9;  
t=2;  
TF = 30;
```

```
Cm = [0];  
Tm = [0];  
SCm = [SC];
```

```
while(t<25000)  
    v = kcat*EC*SC/(SC+Km);  
    SC = SC-v*TF;  
    Tm = [Tm,t-1];  
    SCm = [SCm,SC];  
    t=t+1  
end
```

```
TmHours = Tm/(2 *60)  
plot(TmHours,SCm/Smax)  
title('HSSKLQ Kinetics')  
xlabel('Time (Hours)'),ylabel('Uncleaved Peptide (%)')
```

## References:

- 1) Denmeade, S. R., Sokoll, L. J., Chan, D. W., Khan, S. R., & Isaacs, J. T. (2001). Concentration of enzymatically active prostate-specific antigen (PSA) in the extracellular fluid of primary human prostate cancers and human prostate cancer xenograft models. *The Prostate*, 48(1), 1-6. doi:10.1002/pros.1075
- 2) Coombs, G. S., Bergstrom, R. C., Pellequer, J. L., Baker, S. I., Navre, M., Smith M. M., Tainer J. A., Madison E. L., Corey, David. R. (1998). Substrate specificity of prostate-specific antigen (PSA). *Cell Chemical Biology*, 5(9), 475-488.  
doi:[https://doi.org/10.1016/S1074-5521\(98\)90004-7](https://doi.org/10.1016/S1074-5521(98)90004-7)
- 3) Denmeade, S. R., Lou, W., Lövgren, J., Malm, J., Lilja, H., & Issacs, J. T. (1997). Specific and Efficient Peptide Substrates for Assaying the Proteolytic Activity of Prostate-specific Antigen. *Cancer Research*, 57(21). Retrieved October, 2017.